Dissertation zur Erlangung des Doktorgrades

der Fakultät für Chemie und Pharmazie

der Ludwig-Maximilians-Universität München

Experimental and Molecular Dynamics Studies on Protein Aggregation at Compressible Interfaces

Tim Maximilian Sarter

aus

Annweiler am Trifels, Deutschland

2025

Erklärung

Diese Dissertation wurde im Sinne von § 7 der Promotionsordnung vom 28. November 2011 von Herrn Prof. Dr. Wolfgang Frieß betreut.

Eidesstattliche Versicherung

Diese Dissertation wurde eigenständig und ohne unerlaubte Hilfe erarbeitet.

Mannheim, den 20.11.2025 ……

Tim Maximilian Sarter

Dissertation eingereicht am:	21.11.2025
1. Gutachter:	Prof. Dr. Wolfgang Frieß
2. Gutachterin:	Prof. Dr. Olivia Merkel
Mündliche Prüfung am:	29.01.2026

Per aspera ad astra

– nach Seneca

Acknowledgments

First and foremost, I would like to thank my supervisor Prof. Dr. Wolfgang Frieß. I am grateful for his ideas, his guidance, and for challenging me throughout the years, both scientifically and during Singstar duels.

Many thanks to our chair Prof. Dr. Olivia Merkel for being the co-referee of this thesis and making our institute a great place to work. I further want to thank Prof. Dr. Gerhard Winter for his former role of chair of the institute and the opportunity of getting to know the field of pharmaceutical technology during my practical year.

I thank my student interns for their valuable contributions to this work, namely Katharina Sommer, Katja Gimmler, Maja Zehak, Antonia Engelhard, Gabrielle Langenfeld, Robert Pakocs, Hannah Lichtmannegger, Johanna Modrack, Athanasia Karavalasi, Chiara Rampf, and Lisa Schorre.

A big thank you to all Technos for the often-quoted nice working atmosphere. The skiing trips, visits to the Starkbierfest, Frühlingsfest, and Wiesn, the summer, winter, and Christmas parties, and all the events in between made my time at the institute truly memorable (although some memories may have the occasional gap). A special thanks to my fellow Solidaten, prost-doc Prüßi, Schlagergartensquad Kathi and Stina, satellite and Bermudadreieck member Leonie, and my brother-in-Laim Joschka.

I want to thank "dem besten AK aller Zeiten"[1] for being not only wonderful colleagues, but also great friends. It is impossible to break your contributions to my time in Munich down to one sentence, but I will try nonetheless. I thank Imke for being the heart, soul, and memory of AKF; Ken for being the senior scientist of our hearts inside and outside the lab; Elena for many counseling sessions in the Kiosk; my short-term labmate Eleni for shaping the Bermudadreieck into its dangerous form; Ricci for always reminding us of the importance of a morning coffee break and puns; Düsi for being a great companion in pub quizzes and daily life; Jobi for always being there when you need him; Lasse for being an integral part of my academic and personal development for the past nine years; Anian for being a certified high-performer in only the best ways; Paul for taking over Elena's role as counselor; and our newest members Caro and Theresa for the short but memorable time together.

[1] Frieß, W. Christmas Party 2023.

I am especially thankful to my parents for always supporting me on my path to the person I am today. In the end, I want to express my deepest gratitude to Ioana for her continuous support, encouragement, and many fruitful discussions throughout the years.

Table of Contents

Chapter I: General Introduction

1.1 Protein Stability

Protein-based therapeutics have emerged as one of the most successful drug classes in recent decades.[1–3] Yet, they are prone to instabilities, which not only limit shelf life and therapeutic efficacy but may also trigger adverse immunogenic responses.[4–6] Protein instabilities are generally classified into four main categories: chemical instability, conformational instability, colloidal instability, and instability at interfaces.[7]

1.1.1 Chemical Stability

Proteins are susceptible to various chemical degradation pathways. Oxidation leads to the chemical modification of both amino acid side chains and, in some cases, the peptide backbone.[8] Although many residues can be oxidized, methionine and tryptophan are the most prone. Oxidation is promoted by the presence of metal ions, which could be mitigated by the addition of chelating agents. Direct exposure to oxygen and light also accelerates the process. Methionine is a commonly used excipient to mitigate oxidation.[8] Oxidative modifications are typically analyzed by HPLC-based methods, including LC-MS, RP-, or Protein A chromatography.[9]

Deamidation refers to the hydrolysis of the amide side chains of asparagine and glutamine to aspartate and glutamate. The rate of deamidation is strongly pH-dependent, with acidic conditions slowing the reaction down.[8] Deamidation products can be detected by ion-exchange chromatography[10] and capillary gel electrophoresis.[11]

Hydrolysis or proteolysis describes the nonenzymatic cleavage of an amide bond within the polypeptide chain.[8] In monoclonal antibodies (mAbs), this reaction often occurs in the hinge region and is influenced by metal ions, buffer composition, and pH. The resulting fragments can be characterized by size-exclusion chromatography[12] and capillary gel electrophoresis.[13]

1.1.2 Conformational Stability

Conformational stability describes the Gibbs free energy change associated with the transition from the native, folded state to the unfolded state.[7] The free energy of folding arises from multiple forces, including hydrophobic interactions, hydrogen bonding, van der Waals interactions, and electrostatic contributions.[14,15] Experimental assessment often relies on the apparent melting temperature as a surrogate for conformational stability, which can

be determined by differential scanning calorimetry or fluorimetry. Thermal transitions in secondary structure can, for example, be monitored by circular dichroism and Fourier-transform infrared spectroscopy.[16] Isothermal methods include chemical denaturation using denaturants such as guanidine hydrochloride.[17] Fluorimetric measurements then provide stability-indicating characteristics such as the Gibbs free energy change of unfolding.[18]

Conformational stability depends on the intrinsic properties of the protein as well as on temperature and solution conditions such as pH and excipients.[15] Chemical denaturants like urea decrease stability by preferentially binding to the unfolded state. In contrast, stabilizers such as sucrose are preferentially excluded from the protein surface, thereby shifting the equilibrium toward native ensembles with less solvent exposure.[16,19]

1.1.3 Colloidal Stability

Colloidal stability describes the protein–protein interactions (PPIs) between individual protein molecules.[7] These interactions impact protein solution viscosity, solubility, and aggregation.[8] The overall balance of PPIs, dominated by electrostatic forces and van der Waals interactions, can be quantified by the second osmotic virial coefficient, A_2.[16] A positive A_2 indicates net repulsive interactions, whereas a negative A_2 reflects net attractive interactions.[20,21] Experimental methods commonly used to determine A_2 are static light scattering and analytical ultracentrifugation.[8] An alternative used to characterize PPIs is the diffusion interaction parameter k_D, which can be more easily obtained by dynamic light scattering. A correlation between k_D and A_2 values has been established.[22–24]

The most important factor influencing colloidal stability is solution pH. When proteins carry a high net charge, electrostatic repulsion between molecules increases colloidal stability. Near the isoelectric point, the colloidal stability of the solution is often decreased.[16,25] The charge interaction is additionally modulated by ions in solution. Often, added salts screen surface charges, thus reducing electrostatic repulsion and decreasing colloidal stability.[23,26,27]

1.1.4 Interfacial Stability

Due to their amphiphilic nature, proteins adsorb to interfaces, forming a film.[8,28] Such interfaces occur at many stages of drug processing, storage, and clinical use. These include i) solid–liquid interfaces such as columns, filters, containers, or tubing during transfer and filling operations, ii) air–liquid interfaces during mixing, storage, and shipping, iii) ice–

liquid interfaces during freezing and thawing, and iv) liquid–liquid interfaces in siliconized cartridges.[29–31]

Proteins may unfold at interfaces.[31–38] Proteins with high structural stability at interfaces are often termed “hard” proteins, such as lysozyme,[36] whereas those with lower structural stability are referred to as “soft” proteins, such as BSA[34,36] or HSA.[33] For mAbs, numerous studies have reported no detectable changes in secondary or tertiary structure after interfacial interaction.[39–42] However, detecting small populations of only partially unfolded species remains challenging.[37,43]

Dynamic interfaces that can compress and expand are more detrimental to protein stability than static ones. This effect e.g. occurs when a vial containing a protein solution is agitated. The interfacial compression compacts the already highly concentrated protein layer, followed by relaxation of the interface. Protein aggregates formed in this process are released into the bulk solution.[40,44–47]

Similarly, particle formation has been observed upon pumping of protein solutions.[48–50] For peristaltic pumping, the particle formation follows the same principle: formation of a protein film on the tubing surface, stretching and compression of the film induced by roller movement, and release of film fragments into the bulk solution.[51–53] Typically, surfactants are added to mitigate interfacial stress, which compete with protein molecules for interfacial adsorption.[54]

1.1.5 Protein Aggregation

Protein aggregation in biopharmaceutical solutions does not necessarily stop on dimer or oligomer level but can lead to subvisible and visible particles, resulting in failure to meet regulatory requirements and an increased risk of immunogenicity.[55–58] All the aforementioned protein instabilities can expedite aggregation. As aggregation involves the association of protein molecules into higher-molecular-weight species, colloidal interactions play a central role.[16] Low conformational stability, leading to partial unfolding, can also initiate aggregation.[59] Nevertheless, aggregates often contain a substantial fraction of protein molecules retaining native-like structure.[40–42] Furthermore, deamidation has been shown to reduce the colloidal stability of a mAb, thereby increasing its aggregation propensity.[60] Enhanced aggregation has likewise been observed for oxidized antibodies.[61] As mentioned before, compressible interfaces promote protein aggregation by compacting the protein film adsorbed to the interface.

1.2 Computational Methods

1.2.1 Computational Methods for Assessing Protein Aggregation

In this regard, computational methods are increasingly being explored for assessing protein self-interaction and aggregation propensity, as they allow for fast *in silico* analysis without material consumption. Various computational descriptors exist, which mainly identify aggregation-prone spots and suggest point mutations to mitigate aggregation.[58,62] Most of the *in silico* algorithms are based on the amino acid sequence of the protein.[63] Examples include Aggrescan, which estimates the aggregation propensity on amino acid level based on data derived from measurements of amyloidogenic proteins.[64] The TANGO algorithm predicts the probability that a peptide segment will form β-strand-mediated aggregates.[65] Other algorithms take the three-dimensional structure of the protein molecule into account. AggScore analyzes the distribution of certain surface patches on the protein that drive aggregation.[66] The spatial aggregation propensity algorithm even employs short Molecular Dynamics (MD) simulations of complete mAbs to determine the effective hydrophobicity that is dynamically exposed on specific surface regions,[67] highlighting the potential of MD as a tool for protein stability optimization.

1.2.2 MD Simulations

MD is a simulation technique that predicts the movement of atoms over time. It has gained importance in investigating protein molecules, elucidating the mechanisms of protein folding,[68–70] optimizing drug discovery,[71–75] designing proteins of enhanced stability,[76–78] and even optimizing biopharmaceutical formulation development.

MD simulations are based on Newton's equations of motion. By knowing the potential energy and the forces acting on all atoms, the new atomic positions can be computed, which is repeated iteratively for every simulation step. To perform these calculations, a force field is required, which calculates the interatomic interactions and the potential energy of the system using the atomic coordinates.[79] Potential functions are typically divided into two interaction types. Bonded interactions include bond stretching, angle bending, dihedral, and improper dihedral potentials. Nonbonded interactions consist of a Lennard–Jones component and Coulomb electrostatics.[80]

To prevent energy drifts resulting from numerical integration errors and to reproduce experimental conditions, the system is typically coupled to a thermostat, which adjusts velocities during integration to keep the temperature constant.[81] In a similar way, the

pressure of the system can be controlled by rescaling the dimensions of the simulation box, resulting in an NPT ensemble.[79] Alternatively, simulations can be carried out in a canonical (NVT) ensemble, where the volume and temperature are kept constant.[82]

1.2.3 Coarse-Grained MD Simulations

All-atom MD simulations can reproduce properties of biomolecules with high accuracy, but are limited by their heavy computational cost. Coarse-grained (CG) force fields have been developed as an alternative, in which groups of atoms are represented by beads, i.e., interacting mass points that correspond to a group of atoms. This reduces the number of particles and interactions that must be computed, while allowing for larger integration time steps. Coarse-graining thereby accelerates simulations while preserving essential structural and thermodynamic properties.[83–85] After the mapping step, in which parts of the molecule are grouped into a single bead, a force field must be parameterized to describe the interactions between beads. Different methodologies exist for force field development. Bottom–up approaches derive CG potentials directly from atomistic simulations, thereby preserving structural and thermodynamic properties. Top–down approaches, by contrast, are calibrated against macroscopic parameters such as density or partition coefficient, thereby improving their correspondence with experimental data.[86–89]

The Martini force field, one of the best–known top–down models, employs a four–to–one mapping scheme and parameterizes nonbonded interactions against experimental thermodynamic data on oil/water partitioning.[90] The model aims for broad applicability across biomolecules, including lipids, proteins, and polymers, without the need for reparametrization.[91–93] This is, however, not always the case, as certain shortcomings of the force field have been identified. These include, for example, the overestimation of protein-protein interactions.[94–96]

1.2.4 MD Simulations in Protein Formulation Development

MD simulations are increasingly utilized in formulation development, particularly to gain insights into protein stabilization mechanisms at the molecular level. For example, CG MD simulations of mAbs illustrate the electrostatic network formation leading to high viscosity at high protein concentration.[97] A common focus of MD simulations in formulation development is the effect of formulation parameters, such as buffer components, on protein aggregation.[98–101] Other excipients studied for their impact on protein stability include surfactants,[102] sugars and polyols,[103,104] amino acids, and salts such as NaCl.[105,106] More recently, MD has even been employed to quantitatively predict the aggregation kinetics of

mAbs in their respective formulations.[107,108] Although previous research provided insights into stabilization mechanisms at the molecular level, there remains a need for systematic investigations across a broader range of pH values and additives which are supported by suitable experimental verification. Additionally, none of these studies included an interface.

1.2.5 MD Simulations at Interfaces

Previous work focussed on the molecular interactions between low-molecular-weight proteins and solid interfaces as well as the associated conformational changes.[109–113] Protein aggregation upon adsorption to interfaces was also addressed, including all-atom and CG MD simulations of low-molecular-weight proteins at air–liquid and silica–liquid interfaces.[114–117] These studies, however, focused on the specific protein regions and microstructures driving adsorption and aggregation rather than general aggregation mechanisms, and were limited to static interfaces.

Pugnaloni et al. considered a dynamic, compressible interface. They conducted Brownian dynamics simulations to investigate the compression and expansion of proteins, represented as uniform, monodisperse spheres with predefined interparticle interactions, adsorbed to an interface.[118] Both PPI and adsorption strength influenced the film properties and protein desorption upon interfacial compression and relaxation. The approach did not capture realistic interactions arising from the protein structure or formulation conditions, and protein aggregation was not quantified.

In summary, numerous MD studies have explored protein adsorption to interfaces. Only a few have also addressed protein aggregation, while none took different dynamic interfaces and formulation parameters into account. Additionally, these approaches were limited to MD simulations without comparison to experimental data. Research investigating protein adsorption and aggregation at different compressible interfaces on a molecular level, while also considering formulation conditions and quantitative experimental verification, is lacking. These are, however, essential to gain a better understanding of the mechanisms driving protein aggregation at these interfaces.

1.3 References

(1) Ebrahimi, S. B.; Samanta, D. Engineering Protein-Based Therapeutics through Structural and Chemical Design. *Nat. Commun.* **2023**, *14* (1), 2411.

(2) Walsh, G. Biopharmaceutical Benchmarks 2014. *Nat. Biotechnol.* **2014**, *32* (10), 992–1000.

(3) Leader, B.; Baca, Q. J.; Golan, D. E. Protein Therapeutics: A Summary and Pharmacological Classification. *Nat. Rev. Drug Discov.* **2008**, *7* (1), 21–39.

(4) Wang, W.; Singh, S. K.; Li, N.; Toler, M. R.; King, K. R.; Nema, S. Immunogenicity of Protein Aggregates—Concerns and Realities. *Int. J. Pharm.* **2012**, *431* (1–2), 1–11.

(5) Frokjaer, S.; Otzen, D. E. Protein Drug Stability: A Formulation Challenge. *Nat. Rev. Drug Discov.* **2005**, *4* (4), 298–306.

(6) Bye, J. W.; Platts, L.; Falconer, R. J. Biopharmaceutical Liquid Formulation: A Review of the Science of Protein Stability and Solubility in Aqueous Environments. *Biotechnol. Lett.* **2014**, *36* (5), 869–875.

(7) Manning, M. C.; Holcomb, R. E.; Payne, R. W.; Stillahn, J. M.; Connolly, B. D.; Katayama, D. S.; Liu, H.; Matsuura, J. E.; Murphy, B. M.; Henry, C. S.; et al. Stability of Protein Pharmaceuticals: Recent Advances. *Pharm. Res.* **2024**, 1–67.

(8) Manning, M. C.; Liu, J.; Li, T.; Holcomb, R. E. Rational Design of Liquid Formulations of Proteins. *Adv. Protein Chem. Struct. Biol.* **2018**, *112*, 1–59.

(9) Loew, C.; Knoblich, C.; Fichtl, J.; Alt, N.; Diepold, K.; Bulau, P.; Goldbach, P.; Adler, M.; Mahler, H.; Grauschopf, U. Analytical Protein A Chromatography as a Quantitative Tool for the Screening of Methionine Oxidation in Monoclonal Antibodies. *J. Pharm. Sci.* **2012**, *101* (11), 4248–4257.

(10) Leblanc, Y.; Faid, V.; Lauber, M. A.; Wang, Q.; Bihoreau, N.; Chevreux, G. A Generic Method for Intact and Subunit Level Characterization of mAb Charge Variants by Native Mass Spectrometry. *J. Chromatogr. B* **2019**, *1133*, 121814.

(11) Gervais, D. Protein Deamidation in Biopharmaceutical Manufacture: Understanding, Control and Impact. *J. Chem. Technol. Biotechnol.* **2016**, *91* (3), 569–575.

(12) Salinas, B. A.; Sathish, H. A.; Shah, A. U.; Carpenter, J. F.; Randolph, T. W. Buffer-dependent Fragmentation of a Humanized Full-length Monoclonal Antibody. *J. Pharm. Sci.* **2010**, *99* (7), 2962–2974.

(13) Vlasak, J.; Ionescu, R. Fragmentation of Monoclonal Antibodies. *mAbs* **2011**, *3* (3), 253–263.

(14) Dill, K. A. Dominant Forces in Protein Folding. *Biochemistry* **1990**, *29* (31), 7133–7155.

(15) Wang, W. Instability, Stabilization, and Formulation of Liquid Protein Pharmaceuticals. *Int. J. Pharm.* **1999**, *185* (2), 129–188.

(16) Chi, E. Y.; Krishnan, S.; Randolph, T. W.; Carpenter, J. F. Physical Stability of Proteins in Aqueous Solution: Mechanism and Driving Forces in Nonnative Protein Aggregation. *Pharm. Res.* **2003**, *20* (9), 1325–1336.

(17) Freire, E.; Schön, A.; Hutchins, B. M.; Brown, R. K. Chemical Denaturation as a Tool in the Formulation Optimization of Biologics. *Drug Discov. Today* **2013**, *18* (19–20), 1007–1013.

(18) Svilenov, H.; Markoja, U.; Winter, G. Isothermal Chemical Denaturation as a Complementary Tool to Overcome Limitations of Thermal Differential Scanning Fluorimetry in Predicting Physical Stability of Protein Formulations. *Eur. J. Pharm. Biopharm.* **2018**, *125*, 106–113.

(19) Arakawa, T.; Timasheff, S. N. The Stabilization of Proteins by Osmolytes. *Biophys. J.* **1985**, *47* (3), 411–414.

(20) Yadav, S.; Shire, S. J.; Kalonia, D. S. Factors Affecting the Viscosity in High Concentration Solutions of Different Monoclonal Antibodies. *J. Pharm. Sci.* **2010**, *99* (12), 4812–4829.

(21) Saito, S.; Hasegawa, J.; Kobayashi, N.; Kishi, N.; Uchiyama, S.; Fukui, K. Behavior of Monoclonal Antibodies: Relation Between the Second Virial Coefficient (B2) at Low

Concentrations and Aggregation Propensity and Viscosity at High Concentrations. *Pharm. Res.* **2012**, *29* (2), 397–410.

(22) Lehermayr, C.; Mahler, H.; Mäder, K.; Fischer, S. Assessment of Net Charge and Protein–Protein Interactions of Different Monoclonal Antibodies. *J. Pharm. Sci.* **2011**, *100* (7), 2551–2562.

(23) Menzen, T.; Friess, W. Temperature-Ramped Studies on the Aggregation, Unfolding, and Interaction of a Therapeutic Monoclonal Antibody. *J. Pharm. Sci.* **2014**, *103* (2), 445–455.

(24) Roberts, D.; Keeling, R.; Tracka, M.; Walle, C. F. van der; Uddin, S.; Warwicker, J.; Curtis, R. Specific Ion and Buffer Effects on Protein–Protein Interactions of a Monoclonal Antibody. *Mol. Pharm.* **2015**, *12* (1), 179–193.

(25) Chi, E. Y.; Krishnan, S.; Kendrick, B. S.; Chang, B. S.; Carpenter, J. F.; Randolph, T. W. Roles of Conformational Stability and Colloidal Stability in the Aggregation of Recombinant Human Granulocyte Colony-stimulating Factor. *Protein Sci.* **2003**, *12* (5), 903–913.

(26) Chou, D. K.; Krishnamurthy, R.; Manning, M. C.; Randolph, T. W.; Carpenter, J. F. Physical Stability of Albinterferon-α2b in Aqueous Solution: Effects of Conformational Stability and Colloidal Stability on Aggregation. *J. Pharm. Sci.* **2012**, *101* (8), 2702–2719.

(27) Zhang, F.; Skoda, M. W. A.; Jacobs, R. M. J.; Martin, R. A.; Martin, C. M.; Schreiber, F. Protein Interactions Studied by SAXS: Effect of Ionic Strength and Protein Concentration for BSA in Aqueous Solutions. *J. Phys. Chem. B* **2007**, *111* (1), 251–259.

(28) Nakanishi, K.; Sakiyama, T.; Imamura, K. On the Adsorption of Proteins on Solid Surfaces, a Common but Very Complicated Phenomenon. *J. Biosci. Bioeng.* **2001**, *91* (3), 233–244.

(29) Thirumangalathu, R.; Krishnan, S.; Ricci, M. S.; Brems, D. N.; Randolph, T. W.; Carpenter, J. F. Silicone Oil- and Agitation-induced Aggregation of a Monoclonal Antibody in Aqueous Solution. *J. Pharm. Sci.* **2009**, *98* (9), 3167–3181.

(30) Mehta, S. B.; Carpenter, J. F.; Randolph, T. W. Colloidal Instability Fosters Agglomeration of Subvisible Particles Created by Rupture of Gels of a Monoclonal Antibody Formed at Silicone Oil-Water Interfaces. *J. Pharm. Sci.* **2016**, *105* (8), 2338–2348.

(31) Li, J.; Krause, M. E.; Chen, X.; Cheng, Y.; Dai, W.; Hill, J. J.; Huang, M.; Jordan, S.; LaCasse, D.; Narhi, L.; et al. Interfacial Stress in the Development of Biologics: Fundamental Understanding, Current Practice, and Future Perspective. *Aaps J* **2019**, *21* (3), 44.

(32) Zoungrana, T.; Findenegg, G. H.; Norde, W. Structure, Stability, and Activity of Adsorbed Enzymes. *J. Colloid Interface Sci.* **1997**, *190* (2), 437–448.

(33) Norde, W. Energy and Entropy of Protein Adsorption. *J. Disper. Sci. Technol.* **2007**, *13* (4), 363–377.

(34) Norde, W.; Giacomelli, C. E. BSA Structural Changes during Homomolecular Exchange between the Adsorbed and the Dissolved States. *J. Biotechnol.* **2000**, *79* (3), 259–268.

(35) Norde, W.; Zoungrana, T. Surface-induced Changes in the Structure and Activity of Enzymes Physically Immobilized at Solid/Liquid Interfaces. *Biotechnol. Appl. Bioc.* **1998**, *28* (2), 133–143.

(36) Norde, W.; Favier, J. P. Structure of Adsorbed and Desorbed Proteins. *Colloids Surf.* **1992**, *64* (1), 87–93.

(37) Kopp, M. R. G.; Grigolato, F.; Zürcher, D.; Das, T. K.; Chou, D.; Wuchner, K.; Arosio, P. Surface-Induced Protein Aggregation and Particle Formation in Biologics: Current Understanding of Mechanisms, Detection and Mitigation Strategies. *J. Pharm. Sci.* **2022**.

(38) Manning, M. C.; Chou, D. K.; Murphy, B. M.; Payne, R. W.; Katayama, D. S. Stability of Protein Pharmaceuticals: An Update. *Pharm. Res.* **2010**, *27* (4), 544–575.

(39) Bee, J. S.; Chiu, D.; Sawicki, S.; Stevenson, J. L.; Chatterjee, K.; Freund, E.; Carpenter, J. F.; Randolph, T. W. Monoclonal Antibody Interactions with Micro- and Nanoparticles: Adsorption, Aggregation, and Accelerated Stress Studies. *J. Pharm. Sci.* **2009**, *98* (9), 3218–3238.

(40) Koepf, E.; Eisele, S.; Schroeder, R.; Brezesinski, G.; Friess, W. Notorious but Not Understood: How Liquid-Air Interfacial Stress Triggers Protein Aggregation. *Int. J. Pharmaceut.* **2018**, *537* (1–2), 202–212.

(41) Telikepalli, S. N.; Kumru, O. S.; Kalonia, C.; Esfandiary, R.; Joshi, S. B.; Middaugh, C. R.; Volkin, D. B. Structural Characterization of IgG1 mAb Aggregates and Particles Generated Under Various Stress Conditions. *J. Pharm. Sci.* **2014**, *103* (3), 796–809.

(42) Brych, S. R.; Gokarn, Y. R.; Hultgen, H.; Stevenson, R. J.; Rajan, R.; Matsumura, M. Characterization of Antibody Aggregation: Role of Buried, Unpaired Cysteines in Particle Formation. *J. Pharm. Sci.* **2010**, *99* (2), 764–781.

(43) Das, T. K.; Chou, D. K.; Jiskoot, W.; Arosio, P. Nucleation in Protein Aggregation in Biotherapeutic Development: A Look into the Heart of the Event. *J. Pharm. Sci.* **2022**, *111* (4), 951–959.

(44) Koepf, E.; Schroeder, R.; Brezesinski, G.; Friess, W. The Missing Piece in the Puzzle: Prediction of Aggregation via the Protein-Protein Interaction Parameter A∗ 2. *Eur. J. Pharm. Biopharm.* **2018**, *128*, 200–209.

(45) Bee, J. S.; Schwartz, D. K.; Trabelsi, S.; Freund, E.; Stevenson, J. L.; Carpenter, J. F.; Randolph, T. W. Production of Particles of Therapeutic Proteins at the Air–Water Interface during Compression/Dilation Cycles. *Soft Matter* **2012**, *8* (40), 10329–10335.

(46) Lin, G. L.; Pathak, J. A.; Kim, D. H.; Carlson, M.; Riguero, V.; Kim, Y. J.; Buff, J. S.; Fuller, G. G. Interfacial Dilatational Deformation Accelerates Particle Formation in Monoclonal Antibody Solutions. *Soft Matter* **2016**, *12* (14), 3293–3302.

(47) Ghazvini, S.; Kalonia, C.; Volkin, D. B.; Dhar, P. Evaluating the Role of the Air-Solution Interface on the Mechanism of Subvisible Particle Formation Caused by Mechanical Agitation for an IgG1 mAb. *J. Pharm. Sci.* **2016**, *105* (5), 1643–1656.

(48) Kalonia, C. K.; Heinrich, F.; Curtis, J. E.; Raman, S.; Miller, M. A.; Hudson, S. D. Protein Adsorption and Layer Formation at the Stainless Steel–Solution Interface Mediates Shear-Induced Particle Formation for an IgG1 Monoclonal Antibody. *Mol. Pharm.* **2018**, *15* (3), 1319–1331.

(49) Her, C.; Carpenter, J. F. Effects of Tubing Type, Formulation, and Postpumping Agitation on Nanoparticle and Microparticle Formation in Intravenous Immunoglobulin Solutions Processed With a Peristaltic Filling Pump. *J. Pharm. Sci* **2020**, *109* (1), 739–749.

(50) Her, C.; Tanenbaum, L. M.; Bandi, S.; Randolph, T. W.; Thirumangalathu, R.; Mallela, K. M. G.; Carpenter, J. F.; Elias, Y. Effects of Tubing Type, Operating Parameters, and Surfactants on Particle Formation During Peristaltic Filling Pump Processing of a mAb Formulation. *J. Pharm. Sci.* **2020**, *109* (4), 1439–1448.

(51) Deiringer, N.; Aleshkevich, S.; Müller, C.; Friess, W. Modification of Tubings for Peristaltic Pumping of Biopharmaceutics. *J. Pharm. Sci.* **2022**, *111* (12), 3251–3260.

(52) Deiringer, N.; Friess, W. Proteins on the Rack: Mechanistic Studies on Protein Particle Formation during Peristaltic Pumping. *J. Pharm. Sci* **2022**, *111* (5), 1370–1378.

(53) Deiringer, N.; Frieß, W. Reaching the Breaking Point: Effect of Tubing Characteristics on Protein Particle Formation during Peristaltic Pumping. *Int. J. Pharmaceut.* **2022**, *627*, 122216.

(54) Kanthe, A. D.; Krause, M.; Zheng, S.; Ilott, A.; Li, J.; Bu, W.; Bera, M. K.; Lin, B.; Maldarelli, C.; Tu, R. S. Armoring the Interface with Surfactants to Prevent the Adsorption of Monoclonal Antibodies. *ACS Appl. Mater. Interfaces* **2020**, *12* (8), 9977–9988.

(55) Schellekens, H. Immunogenicity of Therapeutic Proteins: Clinical Implications and Future Prospects. *Clin. Ther.* **2002**, *24* (11), 1720–1740.

(56) Rosenberg, A. S. Effects of Protein Aggregates: An Immunologic Perspective. *AAPS J.* **2006**, *8* (3), E501–E507.

(57) Mahler, H.; Friess, W.; Grauschopf, U.; Kiese, S. Protein Aggregation: Pathways, Induction Factors and Analysis. *J. Pharm. Sci.* **2009**, *98* (9), 2909–2934.

(58) Khetan, R.; Curtis, R.; Deane, C. M.; Hadsund, J. T.; Kar, U.; Krawczyk, K.; Kuroda, D.; Robinson, S. A.; Sormanni, P.; Tsumoto, K.; et al. Current Advances in Biopharmaceutical Informatics: Guidelines, Impact and Challenges in the Computational Developability Assessment of Antibody Therapeutics. *mAbs* **2022**, *14* (1), 2020082.

(59) Philo, J.; Arakawa, T. Mechanisms of Protein Aggregation. *Curr. Pharm. Biotechnol.* **2009**, *10* (4), 348–351.

(60) Alam, M. E.; Barnett, G. V.; Slaney, T. R.; Starr, C. G.; Das, T. K.; Tessier, P. M. Deamidation Can Compromise Antibody Colloidal Stability and Enhance Aggregation in a pH-Dependent Manner. *Mol. Pharm.* **2019**, *16* (5), 1939–1949.

(61) Klair, N.; Kim, M. T.; Lee, A.; Xiao, N. J.; Patel, A. R. Stress Temperature Studies in Small Scale Hastelloy® Drug Substance Containers Lead to Increased Extent of and Increased Variability in Antibody-Drug Conjugate and Monoclonal Antibody Aggregation: Evidence for Novel Oxidation-Induced Crosslinking in Monoclonal Antibodies. *J. Pharm. Sci.* **2021**, *110* (4), 1615–1624.

(62) Pérez, A.-M. W.; Lorenzen, N.; Vendruscolo, M.; Sormanni, P. Therapeutic Antibodies, Methods and Protocols. *Methods Mol. Biol.* **2021**, *2313*, 57–113.

(63) Prabakaran, R.; Rawat, P.; Thangakani, A. M.; Kumar, S.; Gromiha, M. M. Protein Aggregation: In Silico Algorithms and Applications. *Biophys. Rev.* **2021**, *13* (1), 71–89.

(64) Conchillo-Solé, O.; Groot, N. S. de; Avilés, F. X.; Vendrell, J.; Daura, X.; Ventura, S. AGGRESCAN: A Server for the Prediction and Evaluation of "Hot Spots" of Aggregation in Polypeptides. *BMC Bioinform.* **2007**, *8* (1), 65.

(65) Fernandez-Escamilla, A.-M.; Rousseau, F.; Schymkowitz, J.; Serrano, L. Prediction of Sequence-Dependent and Mutational Effects on the Aggregation of Peptides and Proteins. *Nat. Biotechnol.* **2004**, *22* (10), 1302–1306.

(66) Sankar, K.; Krystek, S. R.; Carl, S. M.; Day, T.; Maier, J. K. X. AggScore: Prediction of Aggregation-prone Regions in Proteins Based on the Distribution of Surface Patches. *Proteins: Struct., Funct., Bioinform.* **2018**, *86* (11), 1147–1156.

(67) Chennamsetty, N.; Voynov, V.; Kayser, V.; Helk, B.; Trout, B. L. Design of Therapeutic Proteins with Enhanced Stability. *Proc. Natl. Acad. Sci.* **2009**, *106* (29), 11937–11942.

(68) Lindorff-Larsen, K.; Piana, S.; Dror, R. O.; Shaw, D. E. How Fast-Folding Proteins Fold. *Science* **2011**, *334* (6055), 517–520.

(69) Daggett, V.; Fersht, A. The Present View of the Mechanism of Protein Folding. *Nat. Rev. Mol. Cell Biol.* **2003**, *4* (6), 497–502.

(70) Piana, S.; Lindorff-Larsen, K.; Shaw, D. E. Protein Folding Kinetics and Thermodynamics from Atomistic Simulation. *Proc. Natl. Acad. Sci.* **2012**, *109* (44), 17845–17850.

(71) Dodani, S. C.; Kiss, G.; Cahn, J. K. B.; Su, Y.; Pande, V. S.; Arnold, F. H. Discovery of a Regioselectivity Switch in Nitrating P450s Guided by Molecular Dynamics Simulations and Markov Models. *Nat. Chem.* **2016**, *8* (5), 419–425.

(72) Tamamis, P.; Pierou, P.; Mytidou, C.; Floudas, C. A.; Morikis, D.; Archontis, G. Design of a Modified Mouse Protein with Ligand Binding Properties of Its Human Analog by Molecular Dynamics Simulations: The Case of C3 Inhibition by Compstatin. *Proteins: Struct., Funct., Bioinform.* **2011**, *79* (11), 3166–3179.

(73) Michielssens, S.; Peters, J. H.; Ban, D.; Pratihar, S.; Seeliger, D.; Sharma, M.; Giller, K.; Sabo, T. M.; Becker, S.; Lee, D.; et al. A Designed Conformational Shift To Control Protein Binding Specificity. *Angew. Chem. Int. Ed.* **2014**, *53* (39), 10367–10371.

(74) Shan, Y.; Kim, E. T.; Eastwood, M. P.; Dror, R. O.; Seeliger, M. A.; Shaw, D. E. How Does a Drug Molecule Find Its Target Binding Site? *J. Am. Chem. Soc.* **2011**, *133* (24), 9181–9183.

(75) Guvench, O.; MacKerell, A. D. Computational Fragment-Based Binding Site Identification by Ligand Competitive Saturation. *PLoS Comput. Biol.* **2009**, *5* (7), e1000435.

(76) Childers, M. C.; Daggett, V. Insights from Molecular Dynamics Simulations for Computational Protein Design. *Mol. Syst. Des. Eng.* **2017**, *2* (1), 9–33.

(77) Chao, S.-H.; Matthews, S. S.; Paxman, R.; Aksimentiev, A.; Gruebele, M.; Price, J. L. Two Structural Scenarios for Protein Stabilization by PEG. *J. Phys. Chem. B* **2014**, *118* (28), 8388–8395.

(78) Pikkemaat, M. G.; Linssen, A. B. M.; Berendsen, H. J. C.; Janssen, D. B. Molecular Dynamics Simulations as a Tool for Improving Protein Stability. *Protein Eng.* **2002**, *15* (3), 185–192.

(79) Lindahl, E. R. Molecular Modeling of Proteins. *Methods Mol. Biol.* **2008**, *443*, 3–23.

(80) Vanommeslaeghe, K.; Guvench, O.; MacKerell, A. D. Molecular Mechanics. *Curr. Pharm. Des.* **2014**, *20* (20), 3281–3292.

(81) Hünenberger, P. H. Advanced Computer Simulation, Approaches for Soft Matter Sciences I. *Adv. Polym. Sci.* **2005**, 105–149.

(82) Tuckerman, M. E.; Martyna, G. J. Understanding Modern Molecular Dynamics: Techniques and Applications. *J. Phys. Chem. B* **2000**, *104* (2), 159–178.

(83) Joshi, S. Y.; Deshmukh, S. A. A Review of Advancements in Coarse-Grained Molecular Dynamics Simulations. *Mol. Simul.* **2021**, *47* (10–11), 786–803.

(84) Bond, P. J.; Holyoake, J.; Ivetac, A.; Khalid, S.; Sansom, M. S. P. Coarse-Grained Molecular Dynamics Simulations of Membrane Proteins and Peptides. *J. Struct. Biol.* **2007**, *157* (3), 593–605.

(85) Nielsen, S. O.; Lopez, C. F.; Srinivas, G.; Klein, M. L. Coarse Grain Models and the Computer Simulation of Soft Materials. *J. Phys.: Condens. Matter* **2004**, *16* (15), R481.

(86) Noid, W. G. Perspective: Coarse-Grained Models for Biomolecular Systems. *J. Chem. Phys.* **2013**, *139* (9), 090901.

(87) Jarin, Z.; Newhouse, J.; Voth, G. A. Coarse-Grained Force Fields from the Perspective of Statistical Mechanics: Better Understanding of the Origins of a MARTINI Hangover. *J. Chem. Theory Comput.* **2021**, *17* (2), 1170–1180.

(88) Souza, P. C. T.; Alessandri, R.; Barnoud, J.; Thallmair, S.; Faustino, I.; Grünewald, F.; Patmanidis, I.; Abdizadeh, H.; Bruininks, B. M. H.; Wassenaar, T. A.; et al. Martini 3: A General Purpose Force Field for Coarse-Grained Molecular Dynamics. *Nat. Methods* **2021**, *18* (4), 382–388.

(89) Sun, T.; Minhas, V.; Korolev, N.; Mirzoev, A.; Lyubartsev, A. P.; Nordenskiöld, L. Bottom-Up Coarse-Grained Modeling of DNA. *Front. Mol. Biosci.* **2021**, *8*, 645527.

(90) Jong, D. H. de; Singh, G.; Bennett, W. F. D.; Arnarez, C.; Wassenaar, T. A.; Schäfer, L. V.; Periole, X.; Tieleman, D. P.; Marrink, S. J. Improved Parameters for the Martini Coarse-Grained Protein Force Field. *J. Chem. Theory Comput.* **2013**, *9* (1), 687–697.

(91) Marrink, S. J.; Risselada, H. J.; Yefimov, S.; Tieleman, D. P.; Vries, A. H. de. The MARTINI Force Field: Coarse Grained Model for Biomolecular Simulations. *J. Phys. Chem. B* **2007**, *111* (27), 7812–7824.

(92) Grünewald, F.; Alessandri, R.; Kroon, P. C.; Monticelli, L.; Souza, P. C. T.; Marrink, S. J. Polyply; a Python Suite for Facilitating Simulations of Macromolecules and Nanomaterials. *Nat. Commun.* **2022**, *13* (1), 68.

(93) Baoukina, S.; Monticelli, L.; Risselada, H. J.; Marrink, S. J.; Tieleman, D. P. The Molecular Mechanism of Lipid Monolayer Collapse. *Proc. National Acad. Sci.* **2008**, *105* (31), 10803–10808.

(94) Thomasen, F. E.; Pesce, F.; Roesgaard, M. A.; Tesei, G.; Lindorff-Larsen, K. Improving Martini 3 for Disordered and Multidomain Proteins. *J. Chem. Theory Comput.* **2022**, *18* (4), 2033–2041.

(95) Thomasen, F. E.; Skaalum, T.; Kumar, A.; Srinivasan, S.; Vanni, S.; Lindorff-Larsen, K. Rescaling Protein-Protein Interactions Improves Martini 3 for Flexible Proteins in Solution. *Nat. Commun.* **2024**, *15* (1), 6645.

(96) Binder, J.; Zalar, M.; Huelsmeyer, M.; Siedler, M.; Curtis, R.; Friess, W. Enhancing Martini3 for Protein Self-Interaction Simulations. *Eur. J. Pharm. Sci.* **2025**, 107068.

(97) Buck, P. M.; Chaudhri, A.; Kumar, S.; Singh, S. K. Highly Viscous Antibody Solutions Are a Consequence of Network Formation Caused by Domain–Domain Electrostatic Complementarities: Insights from Coarse-Grained Simulations. *Mol. Pharm.* **2015**, *12* (1), 127–139.

(98) Saurabh, S.; Kalonia, C.; Li, Z.; Hollowell, P.; Waigh, T.; Li, P.; Webster, J.; Seddon, J. M.; Lu, J. R.; Bresme, F. Understanding the Stabilizing Effect of Histidine on mAb Aggregation: A Molecular Dynamics Study. *Mol. Pharm.* **2022**, *19* (9), 3288–3303.

(99) Saurabh, S.; Zhang, Q.; Seddon, J. M.; Lu, J. R.; Kalonia, C.; Bresme, F. Unraveling the Microscopic Mechanism of Molecular Ion Interaction with Monoclonal Antibodies: Impact on Protein Aggregation. *Mol. Pharm.* **2024**, *21* (3), 1285–1299.

(100) Berner, C. Application of Molecular Dynamics Simulations for Developability Assessment and Formulation Development of Biologics. **2023**.

(101) Ko, S. K.; Berner, C.; Kulakova, A.; Schneider, M.; Antes, I.; Winter, G.; Harris, P.; Peters, G. H. J. Investigation of the pH-Dependent Aggregation Mechanisms of GCSF Using

Low Resolution Protein Characterization Techniques and Advanced Molecular Dynamics Simulations. *Comput. Struct. Biotechnol. J.* **2022**, *20*, 1439–1455.

(102) Lou, H.; Wu, Y.; Kuczera, K.; Schöneich, C. Coarse-Grained Molecular Dynamics Simulation of Heterogeneous Polysorbate 80 Surfactants and Their Interactions with Small Molecules and Proteins. *Mol. Pharm.* **2024**, *21* (10), 5041–5052.

(103) Arsiccio, A.; Paladini, A.; Pattarino, F.; Pisano, R. Designing the Optimal Formulation for Biopharmaceuticals: A New Approach Combining Molecular Dynamics and Experiments. *J. Pharm. Sci.* **2019**, *108* (1), 431–438.

(104) Cloutier, T.; Sudrik, C.; Mody, N.; Sathish, H. A.; Trout, B. L. Molecular Computations of Preferential Interaction Coefficients of IgG1 Monoclonal Antibodies with Sorbitol, Sucrose, and Trehalose and the Impact of These Excipients on Aggregation and Viscosity. *Mol. Pharm.* **2019**, *16* (8), 3657–3664.

(105) Cloutier, T. K.; Sudrik, C.; Mody, N.; Hasige, S. A.; Trout, B. L. Molecular Computations of Preferential Interactions of Proline, Arginine.HCl, and NaCl with IgG1 Antibodies and Their Impact on Aggregation and Viscosity. *mAbs* **2020**, *12* (1), 1816312.

(106) Pandya, A.; Zhang, C.; Barata, T. S.; Brocchini, S.; Howard, M. J.; Zloh, M.; Dalby, P. A. Molecular Dynamics Simulations Reveal How Competing Protein–Surface Interactions for Glycine, Citrate, and Water Modulate Stability in Antibody Fragment Formulations. *Mol. Pharm.* **2024**, *21* (11), 5497–5509.

(107) Wang, Y.; Williams, H. D.; Dikicioglu, D.; Dalby, P. A. Predictive Model Building for Aggregation Kinetics Based on Molecular Dynamics Simulations of an Antibody Fragment. *Mol. Pharm.* **2024**, *21* (11), 5827–5841.

(108) Lai, P.-K.; Fernando, A.; Cloutier, T. K.; Kingsbury, J. S.; Gokarn, Y.; Halloran, K. T.; Calero-Rubio, C.; Trout, B. L. Machine Learning Feature Selection for Predicting High Concentration Therapeutic Antibody Aggregation. *J. Pharm. Sci.* **2021**, *110* (4), 1583–1591.

(109) Mücksch, C.; Urbassek, H. M. Accelerated Molecular Dynamics Study of the Effects of Surface Hydrophilicity on Protein Adsorption. *Langmuir* **2016**, *32* (36), 9156–9162.

(110) Kubiak-Ossowska, K.; Jachimska, B.; Mulheran, P. A. How Negatively Charged Proteins Adsorb to Negatively Charged Surfaces: A Molecular Dynamics Study of BSA Adsorption on Silica. *J. Phys. Chem. B* **2016**, *120* (40), 10463–10468.

(111) Shen, J.-W.; Wu, T.; Wang, Q.; Pan, H.-H. Molecular Simulation of Protein Adsorption and Desorption on Hydroxyapatite Surfaces. *Biomaterials* **2008**, *29* (5), 513–532.

(112) Ozboyaci, M.; Kokh, D. B.; Corni, S.; Wade, R. C. Modeling and Simulation of Protein–Surface Interactions: Achievements and Challenges. *Q Rev Biophys* **2016**, *49*, e4.

(113) Raffaini, G.; Ganazzoli, F. Protein Adsorption on a Hydrophobic Surface: A Molecular Dynamics Study of Lysozyme on Graphite. *Langmuir* **2010**, *26* (8), 5679–5689.

(114) Itoh, S. G.; Yagi-Utsumi, M.; Kato, K.; Okumura, H. Effects of a Hydrophilic/Hydrophobic Interface on Amyloid-β Peptides Studied by Molecular Dynamics Simulations and NMR Experiments. *J. Phys. Chem. B* **2019**, *123* (1), 160–169.

(115) Okumura, H. Perspective for Molecular Dynamics Simulation Studies of Amyloid-β Aggregates. *J. Phys. Chem. B* **2023**, *127* (51), 10931–10940.

(116) Kubiak-Ossowska, K.; Mulheran, P. A. Multiprotein Interactions during Surface Adsorption: A Molecular Dynamics Study of Lysozyme Aggregation at a Charged Solid Surface. *J. Phys. Chem. B* **2011**, *115* (28), 8891–8900.

(117) Simone, A. D.; Kitchen, C.; Kwan, A. H.; Sunde, M.; Dobson, C. M.; Frenkel, D. Intrinsic Disorder Modulates Protein Self-Assembly and Aggregation. *Proc. Natl. Acad. Sci.* **2012**, *109* (18), 6951–6956.

(118) Pugnaloni, L. A.; Ettelaie, R.; Dickinson, E. Brownian Dynamics Simulation of Adsorbed Layers of Interacting Particles Subjected to Large Extensional Deformation. *J. Colloid Interf. Sci.* **2005**, *287* (2), 401–414.

Chapter II: Aim and Outline of the Thesis

The aim of this thesis is to contribute to a deeper understanding of the impact of process and formulation parameters on protein aggregation at different compressible interfaces by combining molecular dynamics (MD) simulations and experiments. Throughout processing and handling of biopharmaceuticals, protein molecules adsorb to various dynamic interfaces such as the silicone–liquid interface during pumping or the air–liquid interface upon vial agitation. Compression and relaxation of these interfaces upon mechanical stress promote protein aggregation, impacting product quality and safety, yet, the underlying mechanisms and influencing factors are not fully understood.

In this study, coarse-grained MD models are developed to describe the phenomena at compressible silicone–liquid and air–liquid interfaces. These models are verified and complemented by suitable experimental setups, providing insights into the mechanisms and the influence of formulation parameters on protein aggregation during pumping and shaking on a molecular level.

First, an MD setup for protein aggregation at a moving silicone–liquid interface, imitating tubing, is generated. Verification by experimental data on protein particle formation is needed to give a better understanding of the mechanism and impact of process parameters on protein aggregation during pumping (**Chapter III**). Afterward, an improved model is used to identify how exactly pH, ionic strength, and protein type influence protein particle formation upon mechanical interfacial stress (**Chapter IV**). Our model of protein aggregation at the silicone–liquid interface is then transferred to the air–liquid interface. By combining MD with experimental setups designed to isolate and precisely control interfacial compression and decompression stress, the mechanisms of particle formation at different compressible interfaces can be compared directly (**Chapter V**). Finally, the model is extended to full monoclonal antibodies in different formulations. Correlation of simulation results with experimental data on protein particle formation upon shaking allows to estimate the aggregation propensity of mAbs during formulation development (**Chapter VI**).

Overall, this thesis should demonstrate the value of combining experiments and MD to gain insights into interfacial protein aggregation on a molecular level, ultimately supporting biopharmaceutical process and formulation development.

Chapter III: Molecular Dynamics Study of Protein Aggregation at Moving Interfaces

This chapter is published as:

Sarter, T., & Friess, W.

Molecular Dynamics Study of Protein Aggregation at Moving Interfaces.

Molecular Pharmaceutics, 2024, 21(3), 1214-1221.

Department of Pharmacy, Pharmaceutical Technology and Biopharmaceutics, Ludwig-Maximilians-Universität München, 81377 Munich, Germany

Note from the authors:

The version included in this thesis is identical with the published article apart from minor changes.

The published article can be assessed online via:

https://doi.org/10.1021/acs.molpharmaceut.3c00865

Keywords:

Molecular Dynamics; Protein Aggregation; Interface; Pumping; Protein Film

1. Abstract

Repeated compression and dilation of a protein film adsorbed to an interface leads to aggregation and entry of film fragments into the bulk. This is a major mechanism for protein aggregate formation in drug product upon mechanical stress like shaking or pumping. To gain better understanding of these events we developed a Molecular Dynamics (MD) setup, which would in a later stage allow for *in silico* formulation optimization. In contrast to previous approaches, the molecules of our model protein human growth hormone displayed realistic shapes, surfaces, and interactions with each other and the interface. This enabled a quantitative assessment of protein cluster formation. Simulation outcomes aligned with experimental data on subvisible particles and turbidity, thereby validating the model. Computational and experimental results indicated that compression speed does not affect the aggregation behavior of pre-formed protein films, but rather their regeneration. Protein clusters that formed during compression disassembled upon relaxation, suggesting that particles originate from a partly compressed state. Desorption studies via Steered MD revealed that proteins from compressed systems are more likely to detach as clusters, implying that compression effects at the interface translate into aggregates present in the bulk solution. With the possibility to study the impact of different variables upon compression and dilation at the interface on a molecular level, our model contributes to the understanding of the mechanisms of protein aggregation at moving interfaces**.** It also enables further studies changing formulation parameters, interfaces, or proteins.

Graphical Abstract

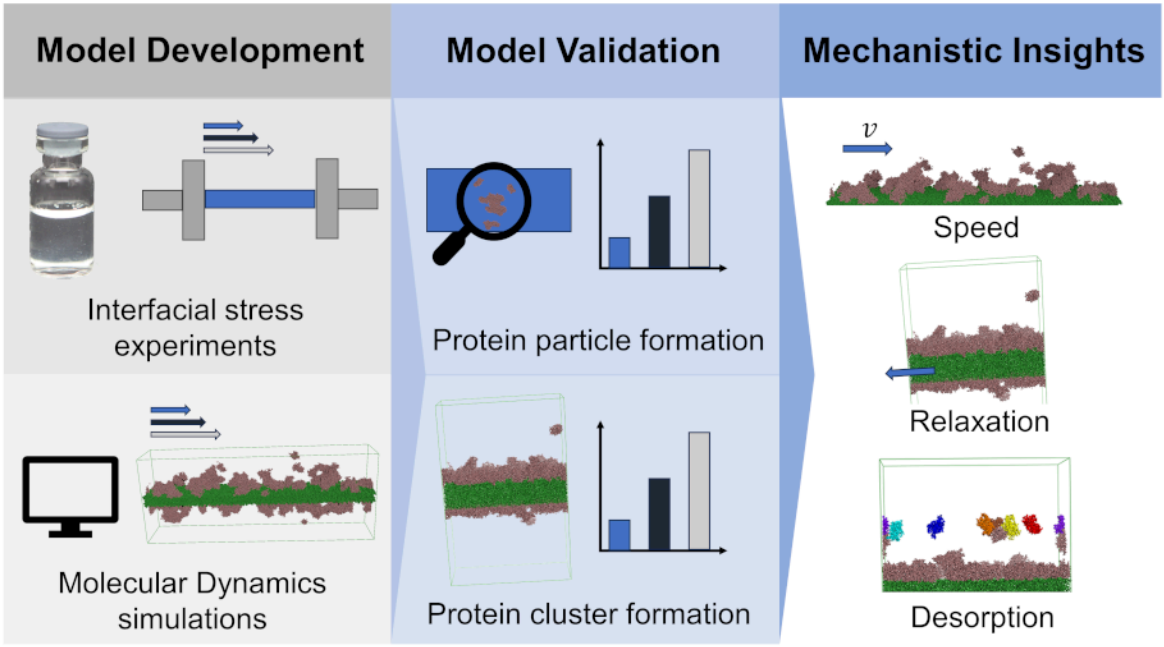

2. Introduction

The presence of protein aggregates, particularly protein particles, poses a substantial risk to biopharmaceuticals. It can result in the loss of active protein, non-compliance with regulatory standards, and an elevated risk of immunogenicity.[1–4] Interfaces are known to be major stress factors that promote protein aggregation during processing of protein solutions.[5,6] Proteins are amphiphilic molecules and therefore adsorb to interfaces and form a protein film.[7–10] Interfaces include for example air–liquid interfaces in form of vial headspace or air bubbles.[11] Compression and dilation cycles of said film formed at the air–liquid interface then lead to protein aggregation, layer collapse and detachment of fragments into the bulk.[8,12,13] Solid interfaces in form of tubing during peristaltic pumping are widely used in industry for transfer and filling operations.[9,14,15] It has been found that the particles observed in peristaltic pumping are the result of a similar mechanism: The formation of a protein film on the tubing surface, stretching and compression of the film during roller movement, and the subsequent entry of film fragments into the bulk solution.[9]

To further elucidate the mechanism, isolate it from competing phenomena, and dissect the influence of individual factors on protein aggregation at interfaces, computational tools can be employed. Such tools include Molecular Dynamics (MD), where the motions of particles in a system are simulated.[16] Baoukina et al. used an early version of the Martini coarse grained forcefield[17] to simulate the collapse of a lipid, not protein, monolayer at the air–liquid interface.[18] Pugnaloni et al. performed Brownian Dynamics simulations of compression and expansion of adsorbed particles mimicking protein and surfactant molecules.[19] Proteins were modeled as monodisperse spheres with uniform, arbitrarily set interparticle interactions. Thus, this approach does not account for realistic interactions that arise from the protein structure as well as from the conditions in the bulk solution, such as pH and ionic strength. The observations were limited to area function and stress response and did not consider protein aggregation. Most importantly, quantitative comparisons between simulations and experiments were not possible due to the model's simplicity.

In this study we built a new MD model to verify the current concept of protein aggregation at moving solid interfaces such as tubing. This model should form the basis to examine the influence of individual factors on temporary protein oligomerization and enable predictions. Compared to previous studies, a more accurate description of the interactions between the protein molecules as well as between protein molecules and the interface was needed. Therefore, proteins were modeled on an individual amino acid level with realistic shapes

and surfaces, although changes in secondary structures could not be captured. The interface imitated the commonly used tubing material poly(dimethylsiloxane) (PDMS). After establishing the model, we studied the impact of compression factor and speed on protein aggregation and desorption. Furthermore, we mimicked multiple pumping cycles to investigate the influence of repeated compression–dilation cycles as they occur for example upon recycling a protein solution during diafiltration or ultrafiltration. Importantly, the semiquantitative evaluation of our simulations was supported by experimental data analyzing protein aggregate formation at different size levels upon repeated compression and dilation.

3. Materials and Methods

3.1 Computational Details

3.1.1 Coarse-grained Models

The crystal structure 1HGU of human growth hormone (hGH) was obtained from RCSB and prepared via Schrödinger BioLuminate to fill in missing side chains and assign hydrogen bonds. A coarse-grained model was built from the atomistic structure via the martinize2 script.[20] To conserve the protein's structure, a Gō-like approach was chosen. The Lennard-Jones well depth was set to 9.4124 kJ/mol, which has been shown to correspond well with all-atom simulations.[21] To mimic the tubing interface, a polymer slab imitating the properties of PDMS[22] was generated via Schrödinger BioLuminate and the Polyply python suite.[23] Both structures were energy minimized using a steepest descent algorithm.

3.1.2 Simulation Details

The simulations were performed with the GROMACS simulation package versions 2020.4 and 2021.4[24–26] and the open-source PLUMED library[27] version 2.8.0.[28] For all simulations, the Verlet cutoff scheme with a buffer tolerance of 0.005 kJ/mol was used. Coulomb interactions were treated with the reaction-field method and a cutoff of 1.1 nm, whilst Van-der-Waals interactions were treated with the cutoff scheme using a cutoff distance of 1.1 nm as previously suggested.[29,30]

The systems were prepared with an initial size of 85 x 35 x 18 nm. This size was chosen to strike a balance between a sufficiently large sample of a tubing section and managing computational expenditure, as well as to prevent self-interaction with periodic images. After the initial preparation, the system was equilibrated in the NPT ensemble for temperature, pressure, density, and root mean square deviation (RMSD) of hGH C_α atoms to stabilize. The temperature was set to 298 K and controlled by the stochastic velocity rescaling thermostat.[31] For the adsorption step, harmonic restraints with a target x-dimensional distance of zero between the protein monomers' center of mass and the polymer slab's center of mass were applied, followed by an additional equilibration step of 400 ns.

For compression and decompression runs, the simulation box was deformed with a velocity of 0.04 m/s. Anisotropic pressure coupling using the Parrinello-Rahman barostat[32] and a compressibility of zero in all but one dimension was used. Positional restraints of 100 kJ/mol were applied on the polymer. If not stated otherwise, 30 systems per condition were

analyzed. For the desorption step, harmonic restraints between the protein monomer center of mass and the polymer slab center of mass were applied to increase their x-dimensional distance. Ten monomers each in ten different systems were pulled. For cluster analysis, the average number of monomers per cluster using a cutoff distance of 0.53 nm, equaling twice the van der Waals radius of a standard Martini bead,[29] was determined.

3.2 Experimental Details

3.2.1 Materials

Human growth hormone (isoelectric point of 5.1[33]) in 10 mM sodium phosphate pH 7.0 was used as the model protein. Buffer components were dissolved in highly purified water obtained from an Arium pro DI Ultrapure Water System (Sartorius Stedim Biotech GmbH, Goettingen, Germany). The pH of the buffers was adjusted using either hydrochloric acid (VWR, Darmstadt, Germany) or sodium hydroxide (Bernd Kraft GmbH, Duisburg, Germany). Prior to use, the buffers were filtered through 0.2 µm cellulose acetate filters (47 mm diameter, Sartorius Stedim Biotech GmbH), while the protein formulations were filtered through 0.22 µm poly(ether sulfone) membrane syringe filters (VWR, Darmstadt, Germany). Sodium dihydrogen phosphate and disodium hydrogen phosphate were obtained from Merck KGaA (Darmstadt, Germany).

3.2.2 Stretching Studies

Stretching studies were performed in triplicates as previously established.[9] Accusil silicone tubing pieces (Watson-Marlow, Falmouth, United Kingdom) of 130 mm length and 6.0 mm inner diameter were sealed with stoppers and filled with approximately 2.5 mL of 1 mg/mL hGH 10 mM sodium phosphate pH 7.0 solution. Stretching was performed by the TA.Xtplus Texture Analyser (Stable Micro Systems, Surrey, UK) at a speed of 5 mm/s for a total of 500 cycles. For speed studies, compression speeds of 5 mm/s, 10 mm/s, and 40 mm/s were used. After stretching, protein solution was removed and analyzed for particles.

3.2.3 Particle Analysis

Subvisible particle (SVP) analysis was conducted using light obscuration with a PAMAS SVSS particle counter equipped with a PAMAS HCB-LD-25/25 sensor (PAMAS Partikelmess- und Analysesysteme GmbH, Rutesheim, Germany), following the guidelines outlined in Ph. Eur. 2.9.19. Each sample was subjected to a pre-rinse of 0.3 mL, followed by three separate analyses using 0.4 mL of the sample each time.

Samples of 1.8 mL were analyzed for turbidity using a TL2360 turbidimeter (Hach Lange GmbH, Duesseldorf, Germany). Data is given in formazine nephelometric units (FNU).

Visible particles were investigated by visual inspection with photo-documentation (Nikon D5300 SLR digital camera, Nikon Corporation, Japan).

3.2.4 Size Exclusion Chromatography (SEC)

Samples were analyzed using an Agilent 1100 device (Agilent Technologies, Boeblingen, Germany) with a G1314A UV detector. 20 µg of sample were injected onto a 7.8 x 300 mm TSK Gel G3000 SWXL column (Tosoh Bioscience, Stuttgart, Germany) with 150 mM potassium phosphate buffer at pH 6.5 as the mobile phase.

4. Results and Discussion

4.1 An MD Setup to Study Protein Aggregation at Dynamic Interfaces

Our study was motivated by previous research, which suggests that a protein film initially forms, and through roller movement, compacts into aggregates that eventually enter the bulk solution.[9,15] In a first step, we therefore aimed to simulate this phenomenon **(Figure 1)**. To improve time efficiency and to allow us to simulate larger system sizes and timescales, a coarse-grained modeling approach was chosen. The Martini 3 forcefield, in which on average four heavy atoms are grouped into a bead,[29] has widely been used for simulations of biomolecules as well as for polymers.[23,34–36] We used an in-house reparametrized version of the Martini 3 forcefield, allowing for more accurate protein–protein interactions than the standard version of the forcefield. Although 4-1 mapping reduces the accuracy when compared to all-atom simulations, this is still a major improvement compared to previous studies[19] where proteins were modeled as monodisperse spheres with uniform, non-realistic interaction parameters.

The interface consisted of linear chains of a PDMS homopolymer, for which we assumed the same elastic modulus as for a Pt-cured silicone network. The lack of cross-linking, however, leads to a different response to mechanical stress in comparison to silicone tubing. While MD is a feasible method to study the mechanical behavior of polymers,[37] our primary focus was on mimicking the interactions of the surface with the protein molecules and not on the mechanical properties of the tubing. We therefore explicitly specified compression factor and speed while maintaining a realistic representation of the protein–polymer interactions. The forces required for specific compression levels cannot be depicted in our model.

The polymer layer was placed in the center of a box with monomers of the hydrophobic and aggregation-prone cytokine hGH[38] at pH 7.0 being inserted around it in random orientations. The thickness of the layer is sufficient to avoid interaction between proteins attached to different sides of the layer. Although the bulk concentration of protein in the experiments is substantially lower, the high protein concentration of about 80 g/L in this setup enabled a quick realization of the highly enriched hGH phase at the tubing surface. In our simulations, we reached about one third of the experimentally determined ≈3.5 mg/m^2 adsorbed at pH 7.[9]

We employed the technique of Steered Molecular Dynamics (SMD) to generate the protein film. In this approach, proteins are artificially pulled toward the interface allowing us to save

computational time. To ensure the accuracy of our simulation, we included an additional equilibration step. This step aimed to guarantee that the proteins were not merely pressed against the interface as in previous studies,[19] but were given the possibility to reorient. Furthermore, it allowed for initial cluster formation, resulting from the high protein concentration at the interface, to converge. Afterward, the simulation box was compressed with different velocities. Compressing the entire box instead of compressing the interface only ensures that periodic boundary conditions apply to the polymer interface and the associated protein molecules. To accelerate the reduction of the interfacial area available for protein, the compression was only permitted in dimension of tubing length and not width. Expansion perpendicular to the interface was permitted to keep the box volume constant. Relaxation was performed by redeformation in the opposite direction. Positional restraints on the polymer ensured that the polymer took up its initial conformation in the relaxation step instead of coiling up due to hydrophobic interactions, therefore imitating the restoring forces of the elastic polymer. SVPs consist of thousands to millions of monomers,[39] but MD is only feasible in much smaller scales. To assess the level of aggregation and compare it to real-life SVP formation, we characterized the clusters formed at the interface based on the number of monomers they contain.

Thus, in contrast to previous approaches,[19] we built an MD model of proteins at moving, solid interfaces, where proteins were modeled in a more realistic way. They consisted of individual amino acids, had their characteristic surface and shape, as well as realistic interactions with each other and the interface. The aggregation behavior could be analyzed quantitatively. To validate our model and verify the prevailing theories of protein aggregation at moving interfaces, we compared the results of our simulations to experimental data.

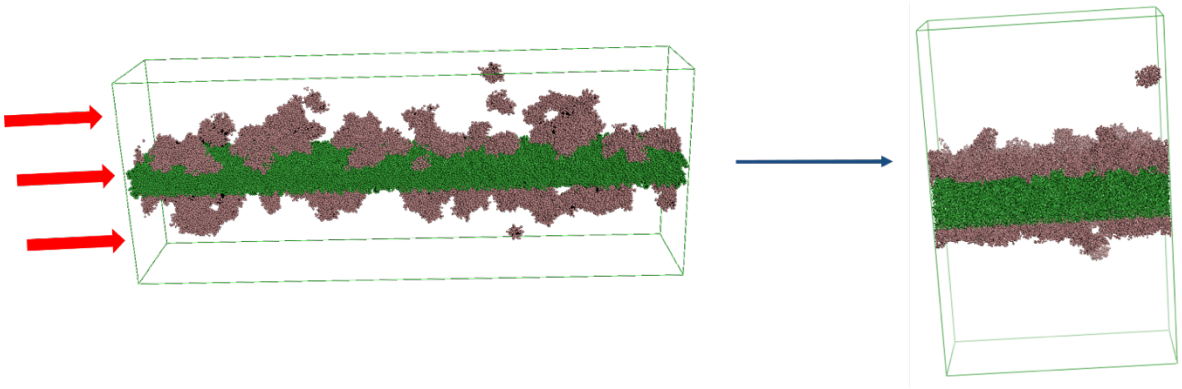

Figure 1: Simulation box with proteins (purple) adsorbed to the polymer slab (dark green) on both sides. After adsorption, the box gets deformed by external forces (left), resulting in a dense protein film with aggregate formation (right).

4.2 Comparison of Cluster size in Simulations and Particles found Experimentally for Increasing Compression Factors

A dependence of particle count on the compression factor was observed at the air–liquid as well as at the tubing–liquid interface. In the initial validation step of our model, the influence of this factor was investigated in simulations and compared to experimental results. We define compression factor c_f as the ratio of maximum and minimum length, or, in terms of compressive strain ε, as $c_f = 1/(1-\varepsilon)$. In compression–relaxation cycles, we subjected the hGH formulation to different compression factors ranging from 1.0 to 1.5. Initially, the protein solution was clear and free from visible particles. Already at a compression factor of 1.1, we noticed marked visible particle formation which did not noticeably change when increasing the compression factor. As observed in prior studies, no soluble aggregates could be detected by SEC.[9,40] An increasing compression factor correlates with an increase in the SVP count **(Figure 2)** as well as in turbidity **(Fig S1)**, which agrees with previous studies on tubing interfaces.[15] For air–liquid interfaces, particle formation also increased with more compression.[8,13] In our simulations, the system was compressed once and the average number of monomers per cluster at the interface was determined. A stronger contraction led to an increase in cluster size. Our model can be understood as following the development of a protein monomer to a protein aggregate, increasing its probability to grow into an SVP later on. Accordingly, we compared the cluster size in our model with the number of SVPs in experiments. The trend of an increase in particle number/cluster size with increasing

compression was consistent in both experiment and simulation. However, absolute numerical values cannot be compared directly due to differences in the overall setups between experiment and simulation. Additionally, comparing the size levels of SVPs to our cluster sizes is not expedient as all SVPs are on a size level far beyond our simulations. Simulations show a plateau in aggregate formation, while experiments indicate the onset of a similar trend at comparable compression factors. The simulations show an interaction amongst almost all protein molecules on one side of the interface under high compression, which accounts for the observed plateau at high compression factors. In tubing the association of a large share of proteins within a tubing segment might therefore account for the plateau formation. This is similar to the particle formation at air–liquid interfaces, where a plateau formation has also been observed.[8]

Previous simulation studies at moving interfaces did not look at protein aggregation and lacked supporting experimental data. We now established that increasing compression of an interface loaded with proteins led to higher degrees of protein cluster formation in the model as well as to an increasing turbidity and number of SVPs found in bulk solution experimentally. Experiments therefore support our model and vice versa, which shows protein film formation and subsequent compression as mode of aggregation and allows for a semi-quantitative statement about the extent of protein aggregation.

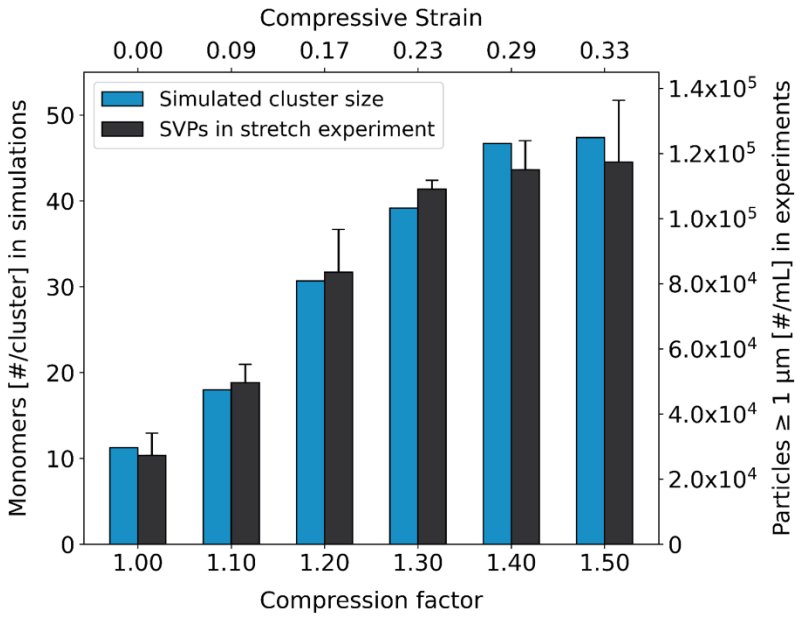

Figure 2: Average number of monomers per cluster in simulations and subvisible particle formation in stretch–relax experiments for compression factors ranging from 1.00 to 1.50.

4.3 Influence of Compression Speed on Protein Aggregation

To assess the influence of compression speed on protein aggregation, our MD system was compressed with a speed of 20 mm/s as well as 40 mm/s. Virtually no differences in the sizes of the clusters formed at the interface could be observed **(Figure 3a)**. The differences between the two speeds were minor with no clear trend visible. Similarly, stretch–relaxation experiments on tubing at 5 mm/s and 10 mm/s compression speed yielded no significant difference in SVP formation. In contrast, employing a markedly higher speed of 40 mm/s resulted in fewer particles **(Figure 3b)**. This phenomenon of higher particle count at lower speeds has previously been observed at the tubing interface. It has therefore been proposed, that at lower compression speeds, the protein film has more time to rebuild itself by interfacial adsorption.[9,15] In case of higher speeds, film formation may become incomplete, and the interfacial contraction does not render protein aggregates to the same extent. As we could not see a difference in protein aggregation in our simulations, where the protein film was already preformed, we also conclude that the lower particle count we observe experimentally at higher speeds most likely originates from the insufficient time for protein film formation, and not from the compression step itself.

The impact of the compression speed has also been observed Baoukina et al. who found more pronounced buckling of a lipid monolayer before folding at higher speed.[18] Pugnaloni et al. did not observe a difference in film wrinkling for weak protein–protein interactions, but more wrinkling in case of strong interactions at higher compression speed.[19]

(a) (b)

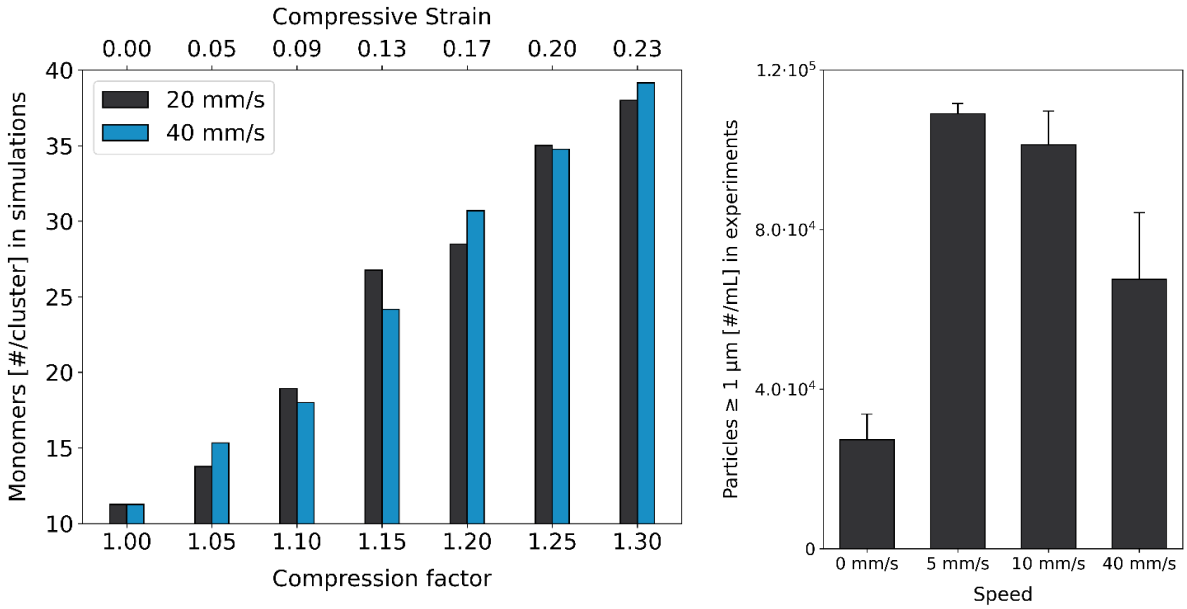

Figure 3: (a) Average number of monomers per cluster in simulations for two different compression speeds and compression factors ranging from 1.00 to 1.30. (b) Subvisible particle formation in stretch–relax experiments for different compression speeds at a compression factor of 1.30.

4.4 Cluster Formation Upon Multiple Compression–Relaxation Cycles

Three cycles of compression and subsequent relaxation were performed to imitate multiple pumping cycles **(Figure 4)**. As seen before, protein cluster size at the interface increased with increasing compression. During relaxation, the cluster size went back to approximately the starting level. The same holds true for the second and third cycle, where no significant difference to the first cycle could be observed. Clusters therefore form during compression and rather break up again in the relaxation step. This can likely be attributed to stronger protein–interfacial interactions compared to protein–protein interactions, leading to protein adhesion to the interface. This is contrary to observations at the air–liquid interface, where an increase in packing density during multiple cycles was reported[7]. However, the compression factor of 4 applied to the air–liquid interface is much higher than the ones applied in this study. This higher compression factor could lead to denser packing with stronger protein–protein interactions and therefore a decreased tendency for aggregates to break up.

Hence, the particles detected experimentally in the bulk solution are likely a result of desorption from the tubing interfaces in a partially compressed state, where proteins tend to be aggregated. Nonetheless, we cannot determine whether the detachment occurs during the compression or decompression phase. In previous simulations, displacement during compression, and not during relaxation was observed.[19] In experiments at the air–liquid interface protein desorption upon decompression, but not during compression was reported.[7] For smaller peptides, desorption upon compression and readsorption during extension has been reported.[41]

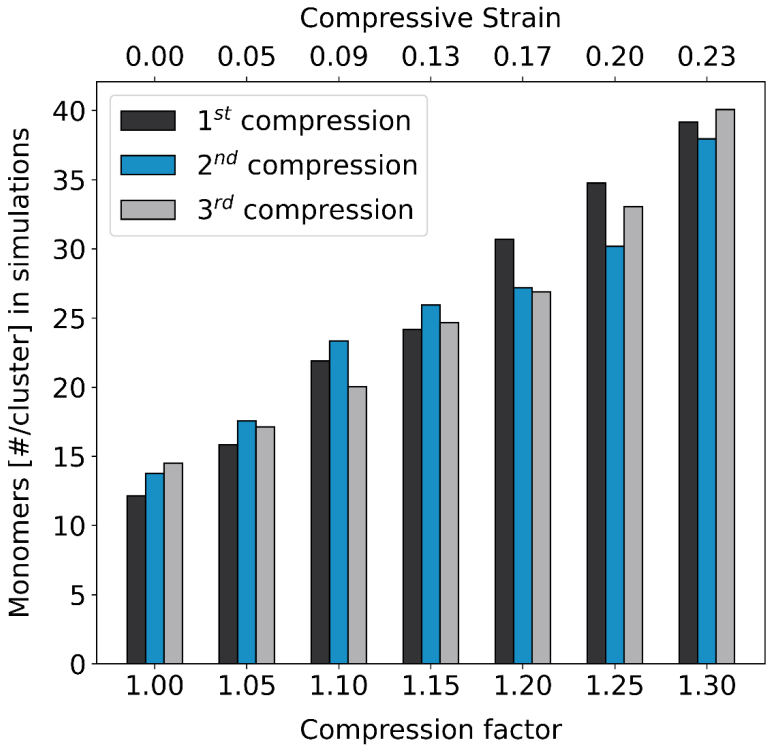

Figure 4: Average number of monomers per cluster in simulations over three cycles of compression and subsequent relaxation. In each case, the result after compression is shown.

4.5 Effects of Compression on Aggregates in Bulk Solution

In our simulations, we could not observe any protein detachment events taking place. This is likely due to the presence of strong protein–interfacial interactions and the formation of a viscoelastic film,[7,41] which kinetically hinders the desorption process. As a result, the dynamic equilibrium shifts toward the adsorbed state,[11,42] significantly limiting the occurrence of desorption events within the limited simulation time.[43] We therefore employed SMD techniques to induce protein desorption **(Figure 5a)**. We randomly selected ten

monomers from each system, subjected them to pulling forces, and analyzed whether they desorbed from the interface as individual monomers or as clusters. Under real-life conditions, it is reasonable to assume that detachment does not result from forces acting on individual monomers, but rather from other factors such as shear stress[44–46] or the reversible nature of the thermodynamic equilibrium.[47] Our approach was therefore not intended to perfectly replicate the desorption process, but rather to see, whether the effects of compression and subsequent aggregation observed directly at the interface also transferred into bulk solution.

When comparing the compressed to the non-compressed systems, proteins from compressed systems entered the bulk solution significantly more often as clusters **(Figure 5b)**. Higher compression therefore led to increased cluster formation not only at the interface but also in bulk after desorption, and these clusters mostly remained stable in the dilute phase.

In a much more simplistic model, individual particle detachment during compression has been described in case of weak interparticle interactions. In contrast, in case of stronger interactions proteins remained associated with the interface directly or via interaction with neighboring associated particles.[19] In our more realistic modeling of protein–interfacial and protein–protein interactions, no desorption could be observed. This may also be related to the smaller compression factors applied in our model of tubing deformation occurring upon peristaltic pumping as compared to previous compression studies at the air–liquid interface.

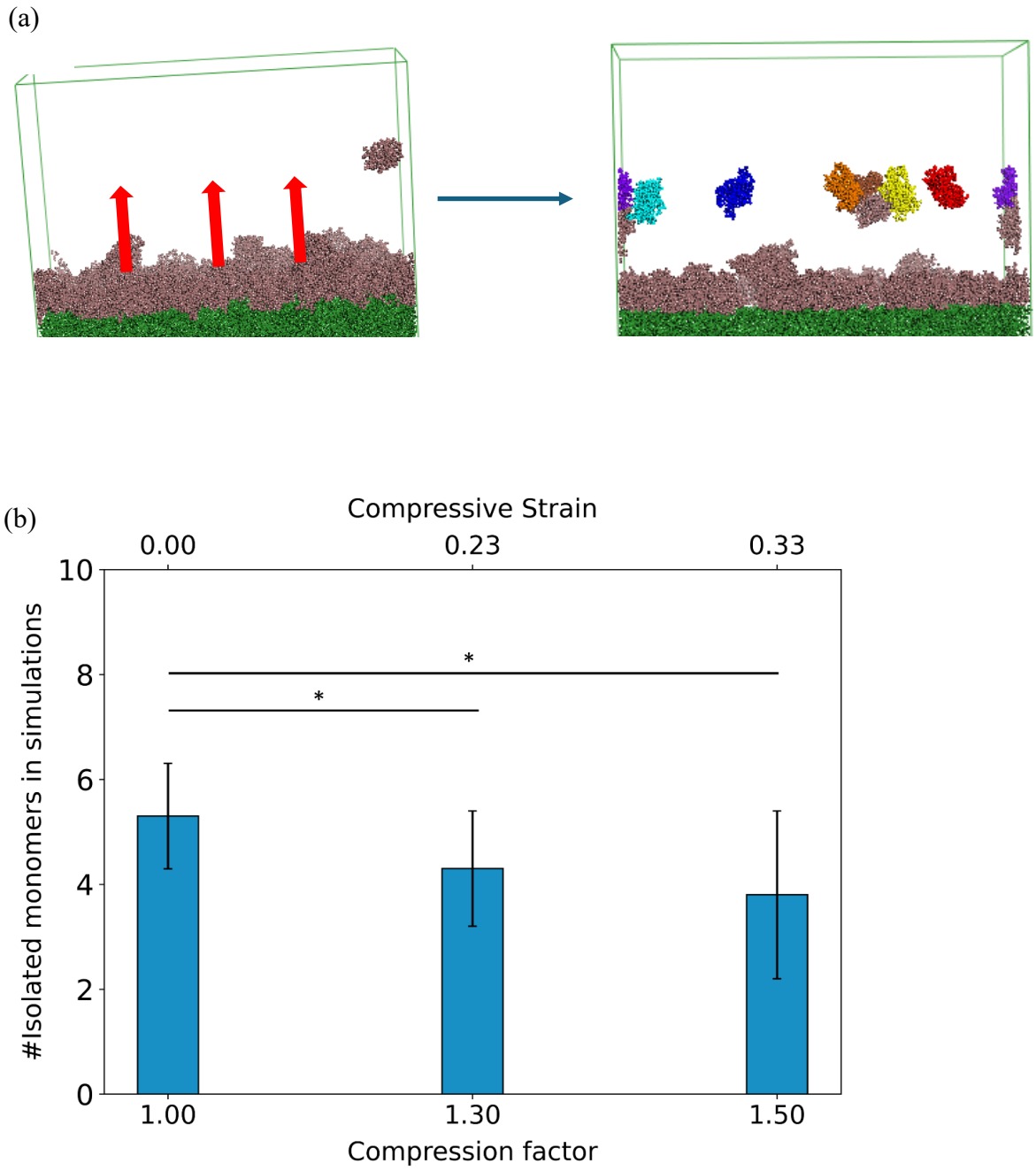

Figure 5: (a) Pulling on monomers leads to desorption of protein monomers or clusters. (b) Average number of proteins detached as isolated monomers as opposed to clusters in ten simulated systems of compression factors 1.3 and 1.5. A t-test was performed with * for $p \leq 0.05$.

5. Conclusions

In this study, we developed an MD setup to investigate protein aggregation at dynamic, solid interfaces. It has previously been found out that the particles observed during peristaltic pumping are the result of a mechanism similar to the particle formation at air–liquid interfaces. This mechanism includes protein film formation on the tubing surface, stretching and compression during roller movement, and film fragments entering the bulk.[9] Our MD model incorporates the structural and interactive properties of proteins, including their surface characteristics, shape, and interactions with both each other and the interface, albeit no changes in secondary structure. Experimental data supports our model, showing that increasing compression factors result in higher levels of protein cluster formation in the model and an increased turbidity as well as number of SVPs found in the bulk solution upon stretching and relaxing tubing filled with protein solution. We observed similar plateau formation in both simulations and experiments. Simulations demonstrate that the compression speed employed does not affect the aggregation tendency of the protein film. Instead, their main influence appears to be on the replenishment of the film. This is confirmed experimentally.[9,15] Simulations show that clusters form at the interface during compression but break up during relaxation. This suggests that particles in the bulk solution originate from detachment from tubing interfaces in the compressed state, where protein aggregation is more likely to occur. High compression results in a decrease in monomer content in the bulk solution after steered detachment, indicating that the effects observed at the interface can be transferred to the bulk phase.

Thus, our model confirms and complements the mechanism of protein aggregation at moving interfaces. It assesses the impact of individual factors on protein aggregation and provides a foundation for further studies. These could include exploring the impact of different pH values, by changing the initial protonation state of the proteins, or ionic strengths, adding sodium chloride, on the system. After appropriate parametrization, excipients like surfactants could be added to the simulation box. Furthermore, various interfaces (e.g., different tubing materials, air–liquid interfaces) or the behavior of different proteins could be studied. All these expansions could be of use in screening processes during formulation and process development. Additionally, further investigations are needed to determine the influence of structural changes on protein aggregation at moving interfaces.

6. Acknowledgments

The authors gratefully acknowledge the Leibniz Supercomputing Centre for funding this project by providing computing time on its Linux-Cluster.

7. References

(1) Schellekens, H. Immunogenicity of Therapeutic Proteins: Clinical Implications and Future Prospects. *Clin. Ther.* **2002**, *24* (11), 1720–1740.

(2) Rosenberg, A. S. Effects of Protein Aggregates: An Immunologic Perspective. *AAPS J.* **2006**, *8* (3), E501–E507.

(3) EP <2.9.19> Particulate Contamination: Sub-Visible Particles. In *European Pharmacopoeia*; European Directorate for the Quality of Medicines & HealthCare, 2011.

(4) USP <788> Particulate Matter in Injections. In *United States Pharmacopeia*; United States Pharmacopeial Convention, 2014.

(5) Kiese, S.; Papppenberger, A.; Friess, W.; Mahler, H. Shaken, Not Stirred: Mechanical Stress Testing of an IgG1 Antibody. *J. Pharm. Sci* **2008**, *97* (10), 4347–4366.

(6) Rudiuk, S.; Cohen-Tannoudji, L.; Huille, S.; Tribet, C. Importance of the Dynamics of Adsorption and of a Transient Interfacial Stress on the Formation of Aggregates of IgG Antibodies. *Soft Matter* **2012**, *8* (9), 2651–2661.

(7) Koepf, E.; Schroeder, R.; Brezesinski, G.; Friess, W. The Film Tells the Story: Physical-Chemical Characteristics of IgG at the Liquid-Air Interface. *Eur. J. Pharm. Biopharm.* **2017**, *119*, 396–407.

(8) Koepf, E.; Eisele, S.; Schroeder, R.; Brezesinski, G.; Friess, W. Notorious but Not Understood: How Liquid-Air Interfacial Stress Triggers Protein Aggregation. *Int. J. Pharmaceut.* **2018**, *537* (1–2), 202–212.

(9) Deiringer, N.; Friess, W. Proteins on the Rack: Mechanistic Studies on Protein Particle Formation during Peristaltic Pumping. *J. Pharm. Sci* **2022**, *111* (5), 1370–1378.

(10) Nakanishi, K.; Sakiyama, T.; Imamura, K. On the Adsorption of Proteins on Solid Surfaces, a Common but Very Complicated Phenomenon. *J. Biosci. Bioeng.* **2001**, *91* (3), 233–244.

(11) Fainerman, V. B.; Zholob, S. A.; Leser, M.; Michel, M.; Miller, R. Competitive Adsorption from Mixed Nonionic Surfactant/Protein Solutions. *J. Colloid Interface Sci.* **2004**, *274* (2), 496–501.

(12) Lin, G. L.; Pathak, J. A.; Kim, D. H.; Carlson, M.; Riguero, V.; Kim, Y. J.; Buff, J. S.; Fuller, G. G. Interfacial Dilatational Deformation Accelerates Particle Formation in Monoclonal Antibody Solutions. *Soft Matter* **2016**, *12* (14), 3293–3302.

(13) Bee, J. S.; Schwartz, D. K.; Trabelsi, S.; Freund, E.; Stevenson, J. L.; Carpenter, J. F.; Randolph, T. W. Production of Particles of Therapeutic Proteins at the Air–Water Interface during Compression/Dilation Cycles. *Soft Matter* **2012**, *8* (40), 10329–10335.

(14) Deiringer, N.; Aleshkevich, S.; Müller, C.; Friess, W. Modification of Tubings for Peristaltic Pumping of Biopharmaceutics. *J. Pharm. Sci.* **2022**, *111* (12), 3251–3260.

(15) Deiringer, N.; Frieß, W. Reaching the Breaking Point: Effect of Tubing Characteristics on Protein Particle Formation during Peristaltic Pumping. *Int. J. Pharmaceut.* **2022**, *627*, 122216.

(16) Karplus, M.; Petsko, G. A. Molecular Dynamics Simulations in Biology. *Nature* **1990**, *347* (6294), 631–639.

(17) Marrink, S. J.; Risselada, H. J.; Yefimov, S.; Tieleman, D. P.; Vries, A. H. de. The MARTINI Force Field: Coarse Grained Model for Biomolecular Simulations. *J. Phys. Chem. B* **2007**, *111* (27), 7812–7824.

(18) Baoukina, S.; Monticelli, L.; Risselada, H. J.; Marrink, S. J.; Tieleman, D. P. The Molecular Mechanism of Lipid Monolayer Collapse. *Proc. National Acad. Sci.* **2008**, *105* (31), 10803–10808.

(19) Pugnaloni, L. A.; Ettelaie, R.; Dickinson, E. Brownian Dynamics Simulation of Adsorbed Layers of Interacting Particles Subjected to Large Extensional Deformation. *J. Colloid Interf. Sci.* **2005**, *287* (2), 401–414.

(20) Kroon, P. C.; Grünewald, F.; Barnoud, J.; Tilburg, M. van; Souza, P. C.; Wassenaar, T. A.; Marrink, S.-J. Martinize2 and Vermouth: Unified Framework for Topology Generation. *arXiv preprint arXiv:2212.01191* **2022**.

(21) Poma, A. B.; Cieplak, M.; Theodorakis, P. E. Combining the MARTINI and Structure-Based Coarse-Grained Approaches for the Molecular Dynamics Studies of Conformational Transitions in Proteins. *J. Chem. Theory. Comput.* **2017**, *13* (3), 1366–1374.

(22) Cambiaso, S.; Rasera, F.; Rossi, G.; Bochicchio, D. Development of a Transferable Coarse-Grained Model of Polydimethylsiloxane. *Soft Matter* **2022**, *18* (40), 7887–7896.

(23) Grünewald, F.; Alessandri, R.; Kroon, P. C.; Monticelli, L.; Souza, P. C. T.; Marrink, S. J. Polyply; a Python Suite for Facilitating Simulations of Macromolecules and Nanomaterials. *Nat. Commun.* **2022**, *13* (1), 68.

(24) Spoel, D. V. D.; Lindahl, E.; Hess, B.; Groenhof, G.; Mark, A. E.; Berendsen, H. J. C. GROMACS: Fast, Flexible, and Free. *J. Comput. Chem.* **2005**, *26* (16), 1701–1718.

(25) Abraham, M. J.; Murtola, T.; Schulz, R.; Páll, S.; Smith, J. C.; Hess, B.; Lindahl, E. GROMACS: High Performance Molecular Simulations through Multi-Level Parallelism from Laptops to Supercomputers. *SoftwareX* **2015**, *1*, 19–25.

(26) Lindahl, E.; Hess, B.; Spoel, D. van der. GROMACS 3.0: A Package for Molecular Simulation and Trajectory Analysis. *Mol. Model. Annu.* **2001**, *7* (8), 306–317.

(27) Bonomi, M.; Bussi, G.; Camilloni, C.; Tribello, G. A.; Banáš, P.; Barducci, A.; Bernetti, M.; Bolhuis, P. G.; Bottaro, S.; Branduardi, D.; et al. Promoting Transparency and Reproducibility in Enhanced Molecular Simulations. *Nat. Methods* **2019**, *16* (8), 670–673.

(28) Tribello, G. A.; Bonomi, M.; Branduardi, D.; Camilloni, C.; Bussi, G. PLUMED 2: New Feathers for an Old Bird. *Comput. Phys. Commun.* **2014**, *185* (2), 604–613.

(29) Souza, P. C. T.; Alessandri, R.; Barnoud, J.; Thallmair, S.; Faustino, I.; Grünewald, F.; Patmanidis, I.; Abdizadeh, H.; Bruininks, B. M. H.; Wassenaar, T. A.; et al. Martini 3: A General Purpose Force Field for Coarse-Grained Molecular Dynamics. *Nat. Methods* **2021**, *18* (4), 382–388.

(30) Jong, D. H. de; Baoukina, S.; Ingólfsson, H. I.; Marrink, S. J. Martini Straight: Boosting Performance Using a Shorter Cutoff and GPUs. *Comput. Phys. Commun.* **2016**, *199*, 1–7.

(31) Bussi, G.; Donadio, D.; Parrinello, M. Canonical Sampling through Velocity Rescaling. *J. Chem. Phys.* **2007**, *126* (1), 014101.

(32) Parrinello, M.; Rahman, A. Polymorphic Transitions in Single Crystals: A New Molecular Dynamics Method. *J. Appl. Phys.* **1981**, *52* (12), 7182–7190.

(33) Ettori, C.; Righetti, P. G.; Chiesa, C.; Frigerio, F.; Galli, G.; Grandi, G. Purification of Recombinant Human Growth Hormone by Isoelectric Focusing in a Multicompartment Electrolyzer with Immobiline Membranes. *J. Biotechnol.* **1992**, *25* (3), 307–318.

(34) Alessandri, R.; Grünewald, F.; Marrink, S. J. The Martini Model in Materials Science. *Adv. Mater.* **2021**, *33* (24), 2008635.

(35) Grünewald, F.; Punt, M. H.; Jefferys, E. E.; Vainikka, P. A.; König, M.; Virtanen, V.; Meyer, T. A.; Pezeshkian, W.; Gormley, A. J.; Karonen, M.; et al. Martini 3 Coarse-Grained Force Field for Carbohydrates. *J. Chem. Theory Comput.* **2022**, *18* (12), 7555–7569.

(36) Lamprakis, C.; Andreadelis, I.; Manchester, J.; Velez-Vega, C.; Duca, J. S.; Cournia, Z. Evaluating the Efficiency of the Martini Force Field to Study Protein Dimerization in Aqueous and Membrane Environments. *J. Chem. Theory Comput.* **2021**, *17* (5), 3088–3102.

(37) Solar, M.; Meyer, H.; Gauthier, C.; Fond, C.; Benzerara, O.; Schirrer, R.; Baschnagel, J. Mechanical Behavior of Linear Amorphous Polymers: Comparison between Molecular Dynamics and Finite-Element Simulations. *Phys. Rev. E* **2012**, *85* (2), 021808.

(38) Oddone, I.; Arsiccio, A.; Duru, C.; Malik, K.; Ferguson, J.; Pisano, R.; Matejtschuk, P. Vacuum-Induced Surface Freezing for the Freeze-Drying of the Human Growth Hormone: How Does Nucleation Control Affect Protein Stability? *J. Pharm. Sci.* **2020**, *109* (1), 254–263.

(39) Carpenter, J. F.; Randolph, T. W.; Jiskoot, W.; Crommelin, D. J. A.; Middaugh, C. R.; Winter, G.; Fan, Y.-X.; Kirshner, S.; Verthelyi, D.; Kozlowski, S.; et al. Overlooking Subvisible Particles in Therapeutic Protein Products: Gaps That May Compromise Product Quality. *J. Pharm. Sci.* **2009**, *98* (4), 1201–1205.

(40) Kalonia, C. K.; Heinrich, F.; Curtis, J. E.; Raman, S.; Miller, M. A.; Hudson, S. D. Protein Adsorption and Layer Formation at the Stainless Steel–Solution Interface Mediates Shear-Induced Particle Formation for an IgG1 Monoclonal Antibody. *Mol. Pharmaceut.* **2018**, *15* (3), 1319–1331.

(41) Wang, L.; Atkinson, D.; Small, D. M. Interfacial Properties of an Amphipathic α-Helix Consensus Peptide of Exchangeable Apolipoproteins at Air/Water and Oil/Water Interfaces*. *J. Biol. Chem.* **2003**, *278* (39), 37480–37491.

(42) Norde, W.; Zoungrana, T. Surface-induced Changes in the Structure and Activity of Enzymes Physically Immobilized at Solid/Liquid Interfaces. *Biotechnol. Appl. Bioc.* **1998**, *28* (2), 133–143.

(43) Kotsmar, Cs.; Pradines, V.; Alahverdjieva, V. S.; Aksenenko, E. V.; Fainerman, V. B.; Kovalchuk, V. I.; Krägel, J.; Leser, M. E.; Noskov, B. A.; Miller, R. Thermodynamics,

Adsorption Kinetics and Rheology of Mixed Protein–Surfactant Interfacial Layers. *Adv. Colloid Interface Sci.* **2009**, *150* (1), 41–54.

(44) Koc, Y.; Mello, A. J. de; McHale, G.; Newton, M. I.; Roach, P.; Shirtcliffe, N. J. Nano-Scale Superhydrophobicity: Suppression of Protein Adsorption and Promotion of Flow-Induced Detachment. *Lab a Chip* **2008**, *8* (4), 582–586.

(45) Yeh, P.-Y. J.; Kizhakkedathu, J. N.; Madden, J. D.; Chiao, Mu. Electric Field and Vibration-Assisted Nanomolecule Desorption and Anti-Biofouling for Biosensor Applications. *Colloids Surf. B: Biointerfaces* **2007**, *59* (1), 67–73.

(46) Perevozchikova, T.; Nanda, H.; Nesta, D. P.; Roberts, C. J. Protein Adsorption, Desorption, and Aggregation Mediated by Solid-Liquid Interfaces. *J. Pharm. Sci.* **2015**, *104* (6), 1946–1959.

(47) Norde, W.; Giacomelli, C. E. BSA Structural Changes during Homomolecular Exchange between the Adsorbed and the Dissolved States. *J. Biotechnol.* **2000**, *79* (3), 259–268.

8. Supporting Information

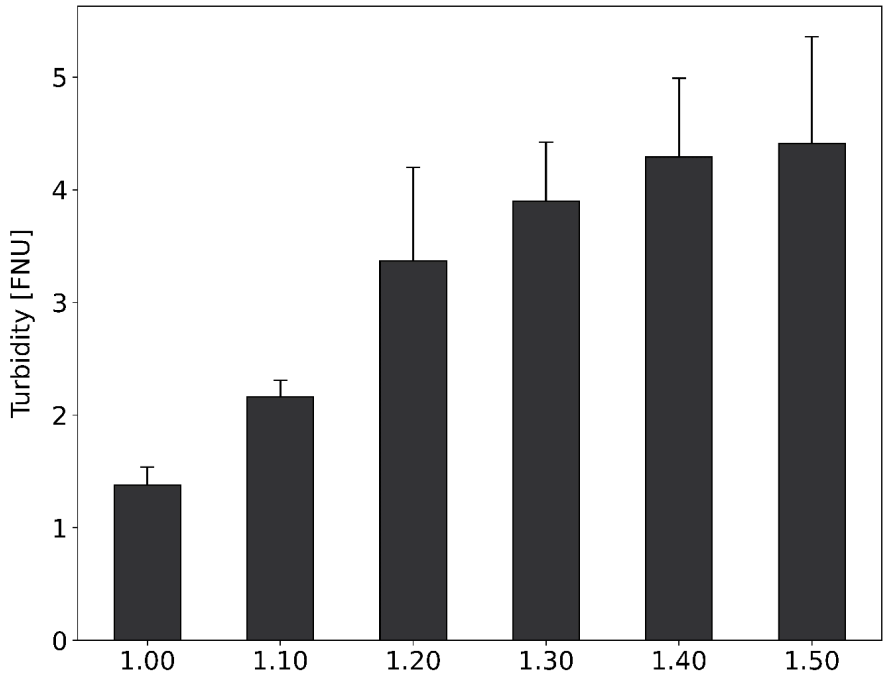

Figure S1: Turbidity in stretch–relax experiments for compression factors ranging from 1.00 to 1.50.

Chapter IV: Unraveling the Role of Formulation Parameters in Protein Particle Formation at Moving Interfaces Using Molecular Dynamics and Experiments

This chapter is published as:

Sarter, T., & Friess, W.

Unraveling the Role of Formulation Parameters in Protein Particle Formation at Moving Interfaces Using Molecular Dynamics and Experiments.

Molecular Pharmaceutics, 2025, 22(3), 4738-4746.

Department of Pharmacy, Pharmaceutical Technology and Biopharmaceutics, Ludwig-Maximilians-Universität München, 81377 Munich, Germany

Note from the authors:

The version included in this thesis is identical with the published article apart from minor changes.

The published article can be assessed online via:

https://doi.org/10.1021/acs.molpharmaceut.5c00330

Keywords:

Molecular Dynamics; Protein Aggregation; Interface; Protein Formulation; Pumping

1. Abstract

Interfacial stress during peristaltic pumping can lead to particle formation in biopharmaceutical solutions. Since the impact of formulation on protein particle formation is not fully understood, we combined Molecular Dynamics (MD) simulations with experimental methods to investigate and understand the effects of pH, ionic strength, and protein type during peristaltic pumping. Building on our previous work, we improved the MD model to provide a more accurate representation of a protein solution at a polymer interface. Our results indicate that the pH value affects aggregate formation in a human growth hormone solution, both while protein molecules are adsorbed to the interface and during the detachment of aggregates into the bulk. Both steps were also directly influenced by protein–protein interactions. Studies at high ionic strength suggest that when protein self-interaction is similar, the amount of protein molecules adsorbed to the interface can be decisive of the extent of particle formation. Additional studies employing lysozyme as a second protein confirmed that protein–protein interactions are the key factor in protein aggregation at interfaces, validating the MD model and our findings across different low-molecular-weight proteins. Our study uncovers the specific points of action through which formulation parameters influence protein particle formation upon mechanical interfacial stress. Furthermore, our model enables the prognosis of protein particle formation *in silico*, potentially saving resources in formulation and process development.

Graphical Abstract

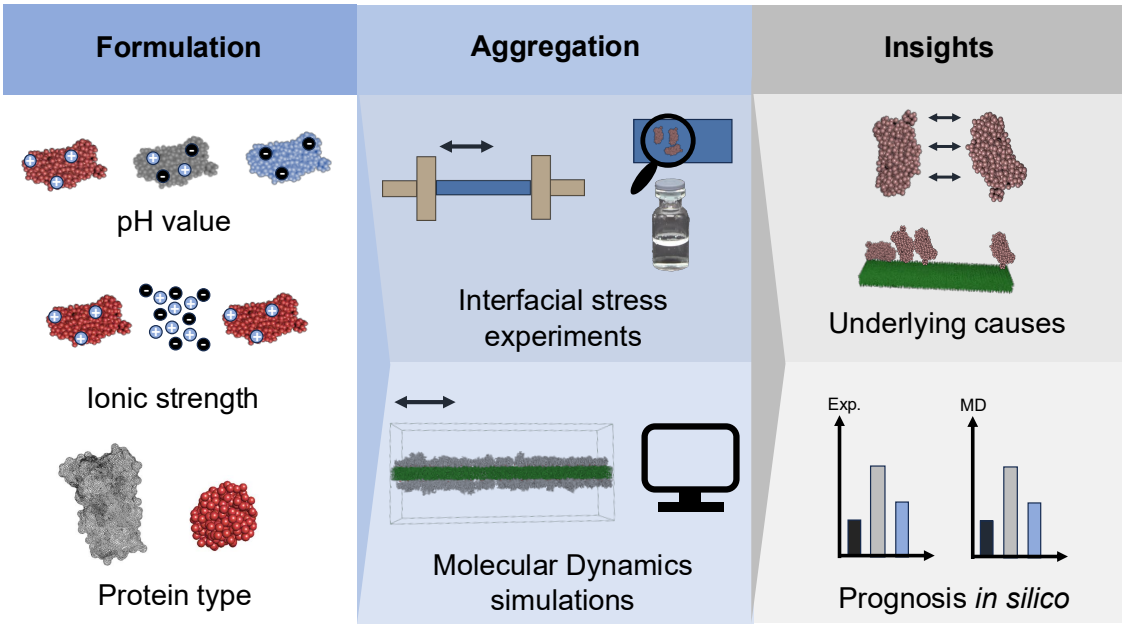

2. Introduction

Interfaces are known to promote particle formation in protein solutions, leading to loss of active protein, non-compliance with regulatory requirements, and an elevated risk of immunogenicity.[1–3] The particle formation observed during peristaltic pumping in transfer and filling operations of biopharmaceuticals results from such interfacial stress. Protein molecules adsorb to the tubing surface, the protein film stretches and compresses again during roller movement, and protein film fragments enter the bulk solution as aggregates.[4] Whereas studies on the influence of tubing material[5–7] or process parameters[4,7,8] have been conducted, the influence of the formulation on protein aggregation during peristaltic pumping has not been fully characterized.

Her and Carpenter observed a relationship between protein formulation and particle formation during peristaltic pumping, attributing it to altered colloidal stability.[6] But also, a similar total particle concentration during pumping despite different colloidal stabilities of the formulations has been reported.[4] Furthermore, the formulation impacts the protein mass adsorbed onto the tubing but with only minor effects on particle formation.[9] Additionally, particle formation upon transfer of an antibody solution with a chemically modified stainless-steel piston pump is related to electrostatic interactions.[10] Recently, using one monoclonal antibody and three different anions, Västberg et al. attributed the effects of ions on particle formation during peristaltic pumping to a combination of colloidal and interfacial stability; yet they did not differentiate the effects.[11] Regardless, the specific mechanisms by which formulation parameters influence protein aggregation at interfaces are not fully understood.

In the past, computational methods such as Molecular Dynamics (MD) have become highly valuable tools in formulation and process development. To reduce the computational demand, high-resolution coarse-grained approaches such as the popular Martini 3 are of great importance. In this coarse-grained force field on average four heavy atoms together with their hydrogens are grouped into one bead based on thermodynamic partitioning data. Water molecules are represented explicitly.[12] We recently published an MD model to gain mechanistic insights into the dynamics of protein aggregation at moving interfaces, such as tubing during peristaltic pumping.[13] It allowed for a semiquantitative assessment of protein aggregation and was validated experimentally, as simulated cluster sizes corresponded to subvisible particle (SVP) formation and turbidity in protein solutions. Building on our previous work, we now adapted the model to investigate the effects of pH, ionic strength,

and type of protein on aggregation. Using computational as well as experimental methods, we wanted to unravel the specific points of action by which formulation parameters influence particle formation. We improved our model by implementing a potential at the interface, matching experimentally determined values and allowing us to correctly represent interactions with and at the interface. We studied our model protein, human growth hormone (hGH), at three pH values and variable ionic strength. In addition, we included lysozyme as a different low-molecular-weight protein. MD results for aggregation propensity at the interface and during the transfer of aggregates into the bulk were compared to experimental data on particle formation, protein–protein interactions and adsorbed mass. Additionally, our model allowed for a semiquantitative estimation of protein particle formation *in silico*, potentially saving time, cost and labor in formulation and process development.

3. Materials and Methods

3.1 Computational Details

Simulations were performed as previously described.[13] For the steered MD simulations the GROMACS simulation package version 2020.4 and the open-source PLUMED library version 2.8.0 were used, whereas for all other simulations GROMACS 2021.4 was utilized.[14–18] A reparametrized version of the Martini 3 coarse-grained force field was used. As the original Martini 3 force field tends to overestimate protein–protein interactions, the improved version shows better agreement with experimental data on second virial coefficient and diffusion coefficient of low-molecular-weight proteins such as lysozyme.[19] Coarse-grained models of the proteins were built from the atomistic structure using the martinize2 script,[20] with a Go-like model being employed to allow for some flexibility while still conserving the molecules' native structure.[21] PROPKA 3[22,23] was used to assign the protonation states.

A polymer slab imitating the properties of PDMS[24] was generated. As protein adsorption to PDMS is mediated by both hydrophobic and electrostatic interactions,[9,25,26] we applied charged beads onto the interface to provide a simplified model imitating the known charge of the material. The bead type TQ5 was selected, representing a tiny bead of the Martini ion block. For simulations at pH 3 a charge of +1 was assigned, whereas for pH 5 and 7 a charge of -1 was chosen (**Table S1**).

The Verlet cutoff scheme with a buffer tolerance of 0.005 kJ/mol was used for all simulations. Coulomb interactions were treated with the Particle mesh Ewald algorithm[27,28] and a cutoff of 1.1 nm, and Van-der-Waals interactions were handled with the cutoff scheme using the same cutoff distance of 1.1 nm as previously suggested.[12,29] The system size of 86x35x18 nm was selected to balance a sufficiently large sample of a tubing section with computational resources, while preventing self-interaction with periodic images. 100 protein monomers were inserted around the polymer layer. Counterions were added to neutralize the system. For hGH at pH 7 and pH 5, 700 and 130 sodium ions were added, respectively. For hGH at pH 3, 2330 chloride ions were necessary, whereas for simulations of 50 lysozyme molecules 100 chlorides were added. The system was solvated using approximately 350,000 explicit water molecules. After all structures were energy minimized, the system was equilibrated under NPT conditions for temperature, pressure, density, and root mean square deviation of hGH C_α atoms to stabilize. The temperature was controlled by the stochastic velocity rescaling thermostat[30] at 298 K. During pre-studies, a significant amount of

simulation time was required until the protein molecules came into initial contact with the interface. To save computational resources, we applied harmonic restraints to minimize the x-dimensional distance between the center of mass of the individual protein monomers and that of the polymer slab, forcing the molecules toward the interface. This artificial step was followed by an actual adsorption step of 400 ns. During this adsorption stage, proteins were allowed to move freely without constraints to interact with the interface and one another, to reorient, and for initial cluster formation to converge.

The simulation box was compressed with a velocity of 0.04 m/s, equivalent to a strain rate of $-4.7 \cdot 10^5\ s^{-1}$. To keep the volume constant, the simulation box was expanded perpendicular to the interface. Positional restraints on the interface imitated the restoring forces of the elastic polymer. 30 independent simulations per condition were performed.

For detachment studies, harmonic restraints were applied to increase the x-dimensional distance between the center of mass of the protein monomers and that of the polymer slab. Ten monomers were pulled in each of ten different fully compressed systems. Formed aggregates were simulated in equilibrium for 400 ns after detachment. For cluster analysis, the average number of monomers per cluster was calculated using a cutoff distance of 0.53 nm. While other cutoff distances yielded comparable trends (**Figure S1**), this value represents twice the van der Waals radius of a standard Martini bead[12] and therefore represents a just contact between two hard spheres.

3.2 Experimental Details

3.2.1 Materials

hGH (22 kDa, PDB: 1HGU) and lysozyme (14 kDa, PDB: 1DPX) in 10 mM sodium phosphate buffer were used as model proteins. hGH solutions at pH 3 and 5 were obtained by spiking 9 g/L hGH stock solution (10 mM sodium phosphate, pH 7) into respective buffers with a lower pH value to reach the final concentration and pH. pH 7 formulations were obtained by diluting the hGH stock solution with 10 mM sodium phosphate buffer pH 7 and by dissolving lysozyme in the same buffer. Buffers were filtered through 0.2 µm cellulose acetate filters (47 mm diameter, Sartorius Stedim Biotech GmbH), whereas the protein solutions were filtered through 0.22 µm poly(ether sulfone) membrane syringe filters (VWR, Darmstadt, Germany). The final concentrations were verified via the extinction coefficient using a Nanodrop 2000 photometer (Thermo Fisher Scientific, Wilmington,

USA). Disodium hydrogen phosphate, sodium dihydrogen phosphate and phosphoric acid were obtained from Merck KGaA (Darmstadt, Germany). Lysozyme was obtained as a lyophilized powder from Sigma-Aldrich (Darmstadt, Germany).

3.2.2 Stretching Studies

Stretching studies were conducted in triplicates as previously described.[13] Accusil silicone tubing pieces (Watson-Marlow, Falmouth, United Kingdom) of 6.0 mm inner diameter were filled with protein solution and sealed with stoppers. Stretching was carried out using a TA.Xtplus Texture Analyser (Stable Micro Systems, Surrey, United Kingdom) at a speed of 5 mm/s for a total of 500 cycles, while compression factor was defined as the ratio of the maximum and minimum length of the tubing piece. Afterward, the protein solution was removed and analyzed for particles. Analysis of the control samples was conducted following a 1-hour incubation period in tubing.

3.2.3 Particle Analysis

Subvisible particle (SVP) is a broad term that usually describes a micrometer-sized particle below the visibility limit of the eye. The origin of these particles can be exogenous but can also result from protein aggregates.[3] SVP analysis was performed using light obscuration with a PAMAS SVSS particle counter (PAMAS Partikelmess- und Analysesysteme, Rutesheim, Germany), in accordance with Ph. Eur. 2.9.19 guidelines. After pre-rinse with 0.3 mL sample, three separate analyses using 0.4 mL of the sample for each measurement were performed.

Turbidity is the result of light scattering caused by submicroscopic particles in a solution.[31] As many factors such as protein concentration and particle size influence the opalescence of a protein solution, turbidity measurement is usually used to evaluate unspecific protein aggregation in comparative measurements.[3] For turbidity analysis, samples were measured using a TL2360 turbidimeter (Hach Lange, Duesseldorf, Germany), with data reported in formazine nephelometric units (FNU).

3.2.4 High-Performance Size-Exclusion Chromatography (HP-SEC)

The amount of adsorbed protein was quantified by HP-SEC.[4,32] Six tubing pieces per formulation were filled to the top with 1 mL of 1 mg/mL protein solution and incubated overnight. The pieces were washed with formulation buffer, filled with 1 mL desorption buffer (10 mM phosphate buffer pH 7.0 with 145 mM NaCl and 0.05% sodium dodecyl sulfate), and incubated overnight. Samples were analyzed using an Agilent 1100 device

(Agilent Technologies, Boeblingen, Germany) equipped with a G1314A UV detector. The injection volume was set to 400 µL, and the flow rate was maintained at 0.7 ml/min using the desorption buffer as mobile phase. The amount of desorbed protein was quantified by HP-SEC with a 7.8 x 300 mm TSK Gel G3000 SWXL column (Tosoh Bioscience, Stuttgart, Germany) at 210 nm using protein-specific calibration curves ($R^2 > 0.9995$).

3.2.5 DLS

Protein samples with concentrations between 1 and 8 mg/ml were used except for hGH at pH 5, which was analyzed between 0.8 and 1.6 mg/ml due to solubility limitations. 25 µL of protein solution were filled into the wells of a 384 microwell plate (Corning, New York, United States), the plate was centrifuged for 2 min at 2,000 rpm, and measurements were performed in triplicates at 25 °C using a DynaPro plate reader III (Wyatt Technology, Santa Barbara, USA) with 20 acquisitions of 5 s each. The interaction parameter k_D was derived from the concentration dependence of the protein mutual diffusion coefficient:

$$k_D = \frac{\frac{D}{D_0} - 1}{c}$$

with D = mutual diffusion coefficient, D_0 = diffusion coefficient at infinite dilution, c = protein concentration.

3.2.6 Circular Dichroism (CD) Spectroscopy

Samples were incubated in their respective buffer for 6 hours to assess conformational stability for the duration of a typical stretching study. Near- and far-UV CD spectra were obtained using a Jasco J-810 spectropolarimeter (JASCO Deutschland, Pfungstadt, Germany). For near-UV spectra, a cuvette with 10 mm wavelength path and a protein concentration of 1 g/L was used, whereas for far-UV spectra a cuvette with 1 mm wavelength path and a protein concentration of 0.4 g/L was used. Five accumulations each were recorded at a speed of 20 nm/min. After subtraction of the buffer spectrums and smoothing using the Savitzky-Golay algorithm with 9 smoothing points, the mean residue ellipticity (MRE) of the protein at each wavelength was determined.[33]

3.2.7 Differential Scanning Fluorimetry (nanoDSF)

To determine the thermal stability of hGH formulations, capillaries were filled with 1 g/L protein solutions. A 1 °C/min temperature ramp from 20 to 95 °C was applied and the intrinsic protein fluorescence intensity at 330 and 350 nm, following excitation at 280 nm, was measured using the Prometheus NT.48 system (NanoTemper Technologies, Munich, Germany). The apparent protein melting temperature T_m was determined from the maxima of the first derivative of the fluorescence intensity ratio curves.

4. Results and Discussion

4.1 Improving the MD Model

We recently proposed an MD model to investigate protein aggregation at moving interfaces. This model accounted for the structural and interactive properties of the protein molecules, including their mutual interactions as well as their interactions with the interface. However, some shortcomings needed to be addressed to accurately depict the influence of formulation parameters on protein aggregation. These specifically included more realistic electrostatic interactions between the protein molecules themselves as well as with the polymer interface. To this end, we treated Coulomb interactions with the PME algorithm.[27,28] Although the reaction field method used previously is more computationally efficient, the PME algorithm reduces artifacts and allows for more accurate electrostatic interactions.[34,35]

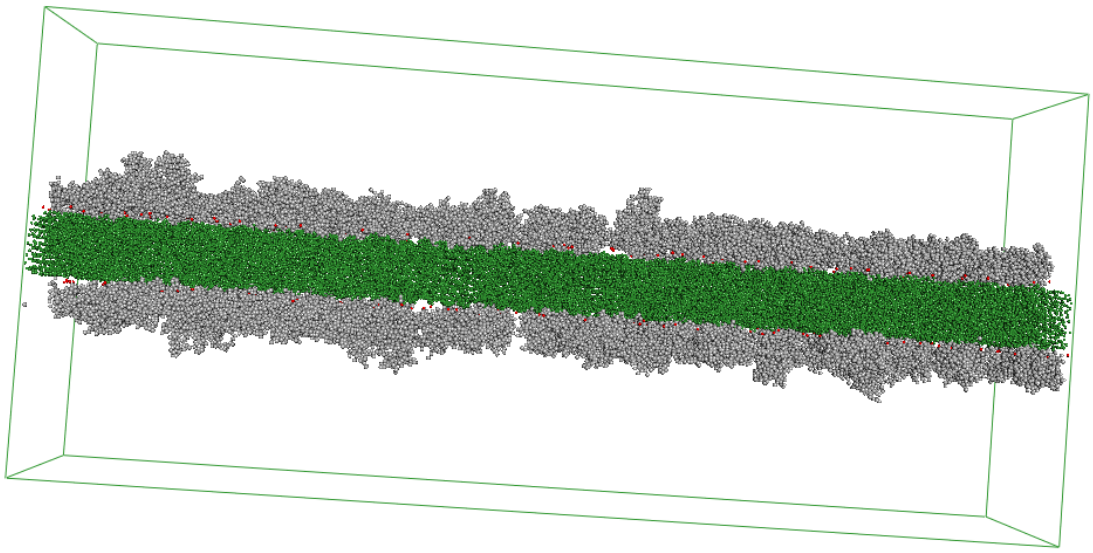

Figure 1: MD setup to investigate protein aggregation at moving interfaces. Protein molecules (grey) are adsorbed onto the polymer layer (dark green), which has charged beads (red) anchored to it.

Furthermore, a zeta potential at silicone tubing interfaces has been observed and quantified experimentally.[9] This potential is likely caused by the adsorption of ions, such as hydroxide, to the tubing interface.[36,37] As the adsorption of protein molecules to PDMS is driven by hydrophobic as well as electrostatic interactions,[9,25,26] we incorporated charged beads on top of the interface to introduce a formal charge (**Figure 1**). The number of beads reflects the

proportions of the experimentally determined potential values (**Table S1**) rather than absolute values.

The implementation of the PME algorithm and a zeta potential allowed for a more realistic representation of the phenomena occurring in a protein solution at a polymer interface. This adaptation then enabled the use of our MD model for investigating the influence of formulation parameters on protein aggregation.

4.2 Influence of pH Value on hGH Particle Formation

To assess the influence of pH value on particle formation, hGH solutions at pH 3, 5, and 7 were filled into tubing pieces and subjected to compression–relaxation cycles at compression factors ranging from 1.1 to 1.4. As has been observed previously, higher compression factors resulted in an increase in turbidity and SVP count for all formulations.[13,38–40] The pH 3 solution showed by far the least particle formation, which has also been observed for other types of proteins such as BSA[41] or mAbs.[42] The pH 5 and pH 7 solutions behaved similarly, with slightly more particles observed at pH 5 (**Figure 2**).

a)

b)

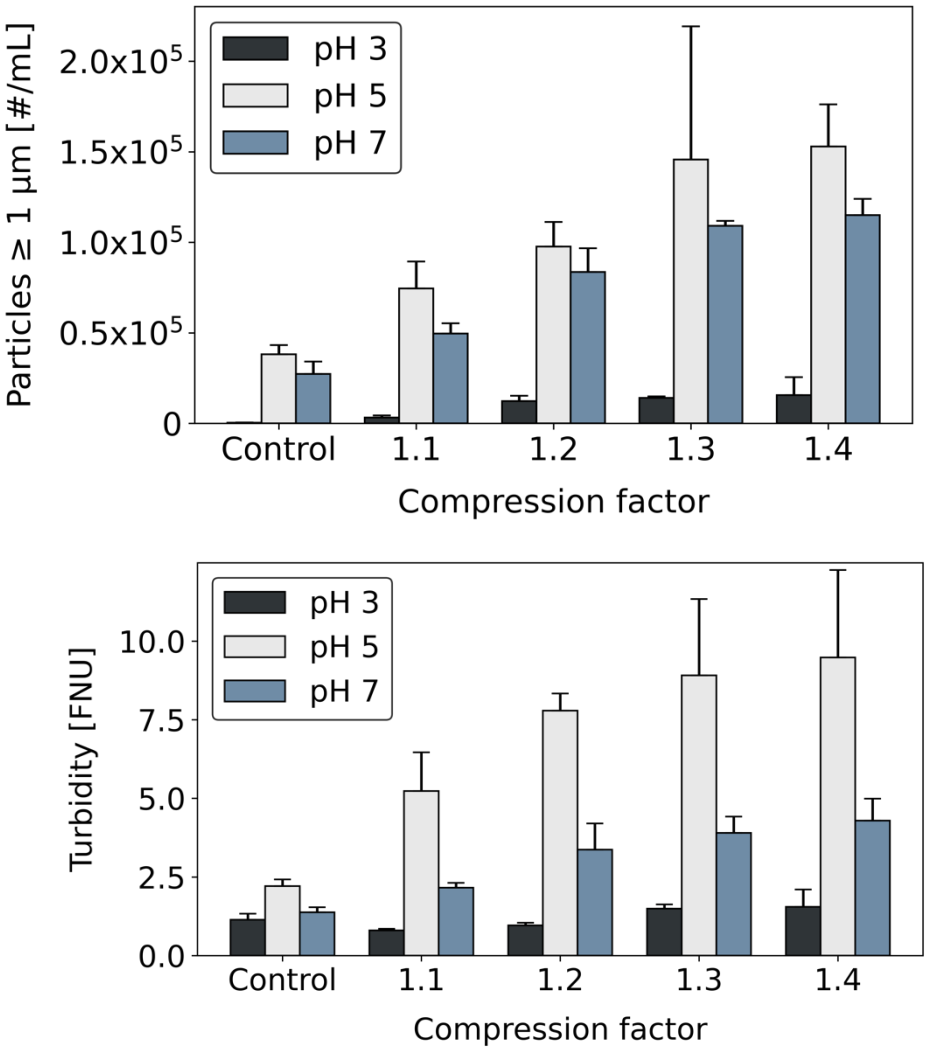

Figure 2: SVPs (a) and turbidity (b) for hGH at pH 3, 5, and 7 determined in stretch-relax experiments with compression factors ranging from 1.1 to 1.4.

Table 1 Amount of protein adsorbed to the tubing interface and k_D values (Mean ± SD).

Formulation	Adsorbed protein [mg/m^2]	k_D [mL/g]
hGH pH 3	4.4 ± 0.9	+41.5 ± 3.2
hGH pH 5	5.1 ± 0.9	-84.0 ± 8.3
hGH pH 7	4.9 ± 0.5	-8.6 ± 0.9
hGH pH 3 + NaCl	6.5 ± 1.3	-12.4 ± 1.0
Lysozyme pH 7	1.7 ± 0.1	+17.7 ± 1.0

Next, we aimed to replicate this setup *in silico* to elucidate the roots of the differences in particle formation and to see if MD is a suitable tool for ranking and to aid understanding the aggregation propensity of formulations differing in pH value. Our coarse-grained approach employs protein molecules in the native state. Unfolding can take place at interfaces and may additionally contribute to aggregate formation. It has been observed that adsorption to solid interfaces does not necessarily cause protein unfolding[43,44] and particles formed under mechanical interfacial stress contain protein molecules with native-like (meaning potential higher order structural changes below the limit of detection of the analytical method) conformation.[40,45,46] Overall, the mechanisms identified in our study should apply to native and slightly structurally changed protein molecules.

First, the amount of protein adsorbed to the tubing was determined experimentally by SEC followed by UV detection. As no significant differences could be observed (**Table 1**), the amount of protein loaded onto the interface was not responsible for the differences in particle formation of hGH solutions at different pH values. Furthermore, the results suggested that our MD simulations should be set up with the same number of protein molecules for hGH at pH values 3, 5, and 7. The final amount of protein molecules adsorbed to the interface in the model was in the range of the experimentally determined amount. Mathes et al. observed a pH-dependency of the amount of protein adsorbed to an interface, which was attributed to the interplay between protein–protein and protein–polymer interactions.[32] This work, however, was performed with a monoclonal antibody on a glass surface over a wider pH range. Depending on the protein used and the ionic strength of the solution, other studies could only see a limited impact of pH on antibody adsorption to a hydrophobic surface.[9,47]

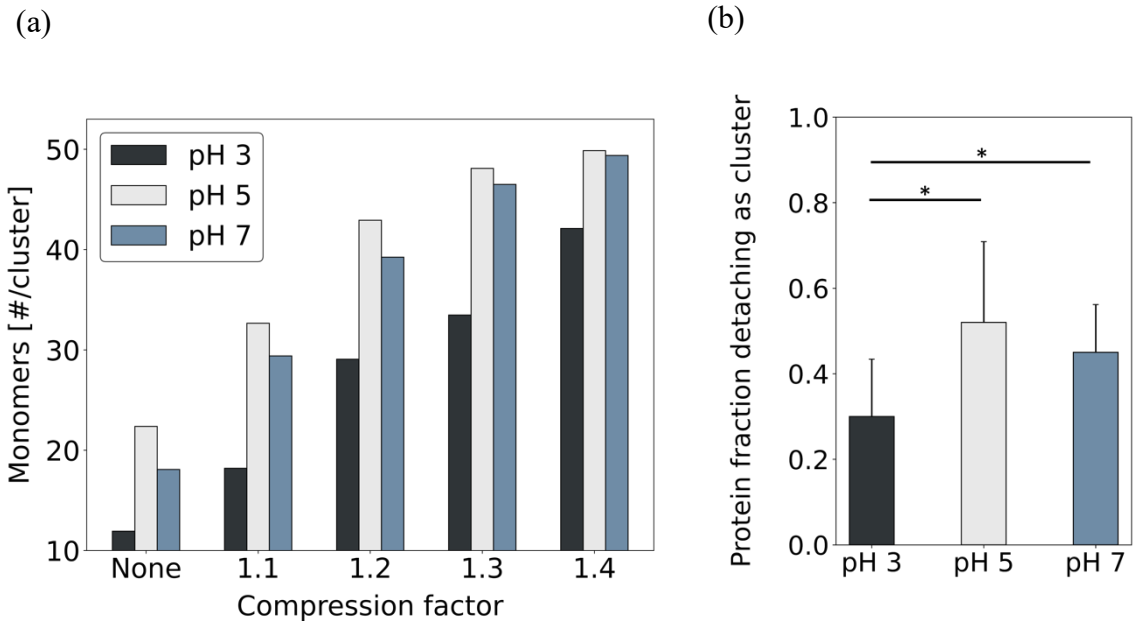

Figure 3: (a) Average number of monomers per cluster for hGH at pH 3, 5, and 7 determined in MD simulations with compression factors ranging from 1.1 to 1.4. (b) Fraction of protein molecules detaching as clusters rather than as isolated monomers in ten simulated systems for hGH at pH 3, 5, and 7 at a compression factor of 1.4. A t-test was performed with * for $p \leq 0.05$.

After setting up the MD simulations, we compressed the interface loaded with protein molecules and performed a cluster analysis (**Figure 3a**). The extent of cluster formation in the model was previously shown to correlate with turbidity and SVP formation for an hGH solution at pH 7.[13] Our simulations indicated the lowest cluster formation for the pH 3 formulation. pH 5 and pH 7 showed comparable cluster formation, with slightly larger clusters at pH 5. In addition, we checked whether the pH value also influenced the transfer of the protein aggregates formed at the interface into the bulk. As desorption did not occur within our limited simulation time, we induced protein detachment by Steered MD (SMD) simulations. Compared to the other formulations, hGH molecules desorbed significantly less often as clusters at pH 3, and rather as individual monomers (**Figure 3b**). Again, the pH 5 and the pH 7 formulations behaved similarly, with a slightly higher tendency to detach in a clustered state at pH 5. Formed aggregates did not show signs of disintegration over 400 ns of additional simulation time. This indicates persistence and illustrates correspondence with the experimental aggregate analysis conducted after several hours.

The trends for cluster formation at the interface as well as desorption of aggregates found in MD simulations corresponded to the experimental results. Thus, MD is a suitable tool to estimate the aggregation propensity of an hGH formulation at different pH values. Our results further indicate that the pH value influences particle formation directly at the interface as well as during the transfer of the aggregates into the bulk.

4.3 Underlying Causes of pH-Dependent Particle Formation

Following this, we aimed to determine the exact mechanism by which the pH value influences particle formation. As the pH value did not affect the protein load at the tubing interface, the cause of the differing particle formation must lie somewhere else. The stability of hGH against the mild heat exposure encountered during mechanical stressing of tubing[4,8] was confirmed by nanoDSF with T_m values of 70.5 ± 0.1 and 77 ± 1.2 °C at pH 3 and 7, respectively. Protein aggregation is often associated with unfolding,[48,49] to which proteins are especially prone to at acidic pH values.[41,50] We therefore assessed the conformational stability of the pH 3 formulation for the duration of our experiments by CD. When compared to a pH 7 solution and a denatured reference incubated at pH 1, secondary and tertiary structure remained intact at pH 3 (**Figure S2**).

One likely cause for the varying particle formation is the strength of the protein–protein interactions that changes with pH value.[3,48,49,51] We therefore determined the interaction parameter k_D of our three formulations experimentally (**Table 1**). The interaction parameter k_D is related to the second virial coefficient A_2 and indicates the tendency of self-interaction. Although, unlike A_2, the sign does not provide direct information about the net nature of the interactions, a highly positive k_D suggests net repulsive, whereas a highly negative k_D suggests net attractive protein self-interaction.[52,53] Furthermore, trends of k_D were found to correspond with those of A_2.[54]

As expected, due to the highly positive net charge at pH 3, repulsive interactions dominated as indicated by a k_D value of +41.5 ± 3.2 mL/g. At pH 5, close to the isoelectric point,[55] attractive interactions prevailed (k_D = -84.0 ± 8.3 mL/g). With a k_D of -8.6 ± 0.9 mL/g, the protein–protein interactions at pH 7 were weaker with a slight tendency toward attractive interactions. Therefore, more attractive protein–protein interactions correlated with more SVPs as well as higher turbidity in our interfacial stress testing. Whereas this has been shown previously,[51,56,57] the exact point of action of protein self-interaction is not fully understood. Sorret et al. suggested that attractive protein–protein interactions lead to stronger interfacial gels at the air–liquid interface, which are then more likely to remain aggregated in the bulk.[58]

It was further proposed that, in any case, protein associates form at the interface and are transferred into the bulk. The protein–protein interactions then determine whether these associates dissolve or persist in solution and can be detected as particles.[42,56] Our MD results, however, indicate that protein–protein interactions influence aggregate formation during both the compression step of the highly crowded interface as well as during the transfer of the aggregates from the interface into the bulk.

4.4 Influence of Ionic Strength on Particle Formation

So far, only the pH value of our formulation was varied. We next aimed to examine the particle formation of a protein solution at pH 3 at high ionic strength by addition of 145 mM NaCl. Compared to the pH 3 formulation with low ionic strength, which showed marked repulsive protein self-interactions, a lower colloidal stability due to charge shielding was to be expected.[51,52,59] Indeed, the addition of salt reduced the k_D value from +41.5 ± 3.2 g/mL to -12.4 ± 1.0 g/mL, indicating more attractive protein–protein interactions, comparable to the pH 7 formulation (**Table 1**). If solely the protein self-interactions were key for particle formation, as was the case for the hGH formulations with different pH value, a particle count similar to hGH solution at pH 7 could be expected. However, although the k_D value was similar, the high ionic strength pH 3 formulation showed significantly higher particle formation than the pH 7 solution (**Figure 4**).

a)

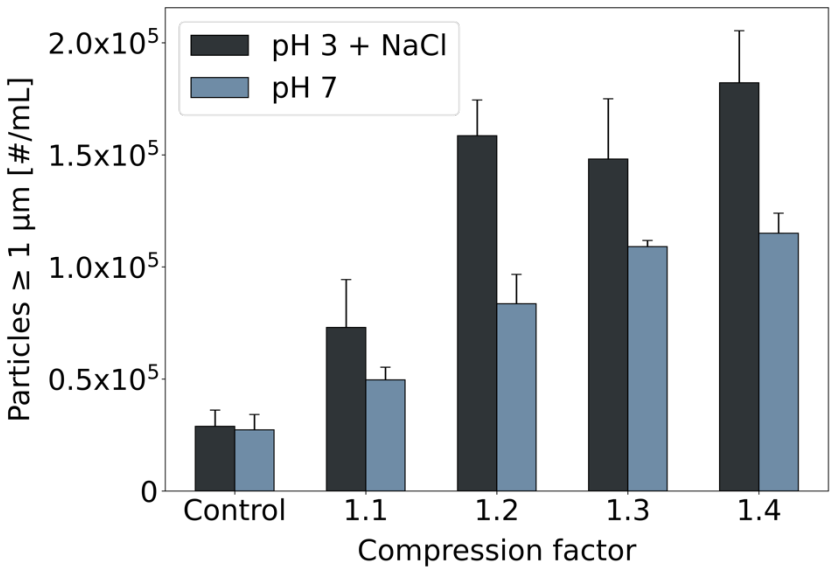

b)

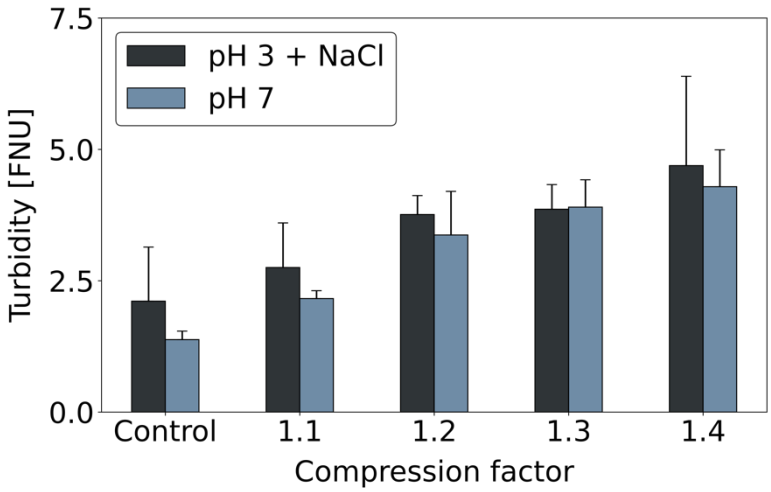

Figure 4: SVPs (a) and turbidity (b) for hGH at pH 3 + 145 mM NaCl and pH 7 determined in stretch-relax experiments with compression factors ranging from 1.1 to 1.4.

SEC data revealed a significantly (p=0.03) higher amount of adsorbed protein molecules in the high ionic strength pH 3 formulation, exceeding the amount at pH 7 by approximately a factor of 1.3 (**Table 1**). This higher surface adsorption at high ionic strength corresponds to findings for tubing,[4,9] glass,[32] and the air-water interface.[60] We therefore performed MD simulations with a 1.3-fold higher number of protein monomers in the simulation box. The trends in MD reflected those observed in SVP formation and turbidity (**Figure 5**). The results indicate that at a comparable level of self-interaction, the amount of protein adsorbed to the tubing interface can be the prevailing mechanism for protein particle formation. Thus, MD can not only provide a prognosis for the aggregation propensity of formulations differing in pH values, as shown before, but also after NaCl is added as an excipient. MD also provides highly valuable insights regarding the dependence of aggregate formation on both self- and surface-interaction.

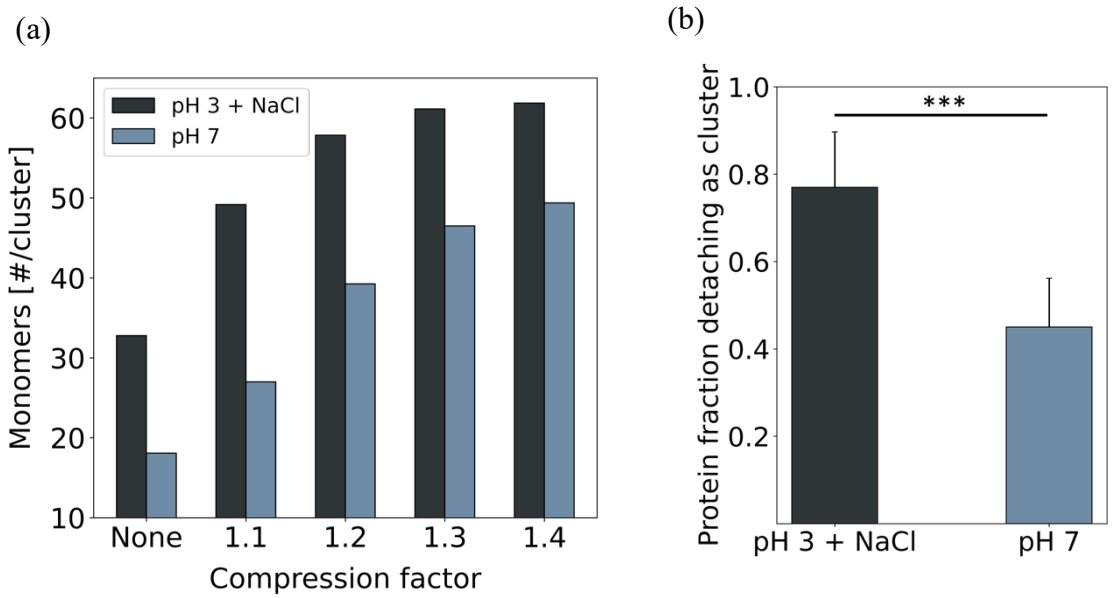

Figure 5: (a) Average number of monomers per cluster for hGH at pH 3 + 145 mM NaCl and pH 7 determined in MD simulations with compression factors ranging from 1.1 to 1.4. (b) Fraction of protein molecules detaching as clusters rather than as isolated monomers in ten simulated systems for hGH at pH 3 + 145 mM NaCl and pH 7 at a compression factor of 1.4. A t-test was performed with *** for $p \leq 0.001$.

4.5 Influence of the Protein Molecule on Particle Formation

In order to understand whether our observations were hGH-specific or could be generalized to other protein molecules, we performed our experimental and computational analyses with lysozyme at pH 7. SVP formation and turbidity were markedly lower for lysozyme than for hGH at the same pH value, with the SVP count being approximately seven times higher and turbidity twice as high for the stressed hGH samples (**Figure 6**). The adsorbed lysozyme amount was roughly one-third of that of the corresponding hGH formulation (**Table 1**). Considering that the molecular weight of lysozyme is about two-thirds of that of hGH, we conducted our lysozyme simulations with half the number of protein molecules compared to hGH at pH 7 (**Figure 7**). The simulations showed very low cluster formation that only increased marginally with increasing compression factor. SMD simulations indicated that lysozyme molecules preferably detached as isolated monomers rather than clusters. Thus, as with hGH, trends in MD corresponded to the experimental data on particle formation for lysozyme.

Even when increasing the number of monomers in the simulation to the level of hGH at pH 7, aggregate formation for lysozyme was still markedly lower than for hGH (**Figure 7**). This indicated that the level of protein loading at the interface was only one factor explaining the differences in particle formation between hGH and lysozyme at pH 7. Protein self-interaction analysis revealed net repulsive interactions for lysozyme, in contrast to the more attractive interactions for hGH at the same pH value (**Table 1**). Protein–protein interactions therefore seem to be the most dominant mechanism influencing protein aggregation at interfaces. Furthermore, our findings are valid not only for hGH but also for another type of protein.

a)

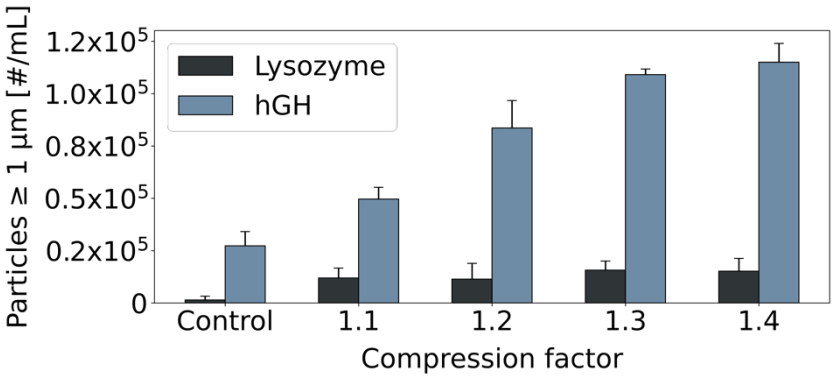

b)

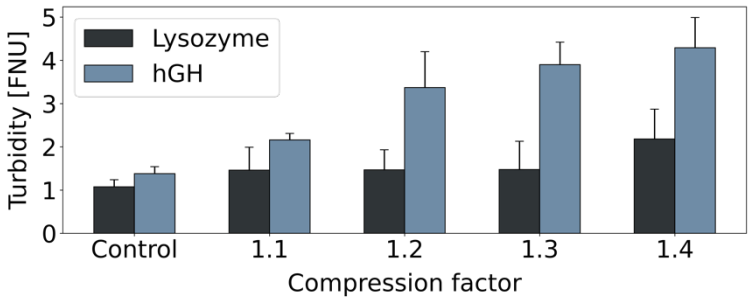

Figure 6: SVPs (a) and turbidity (b) for hGH and lysozyme at pH 7 determined in stretch-relax experiments with compression factors ranging from 1.1 to 1.4.

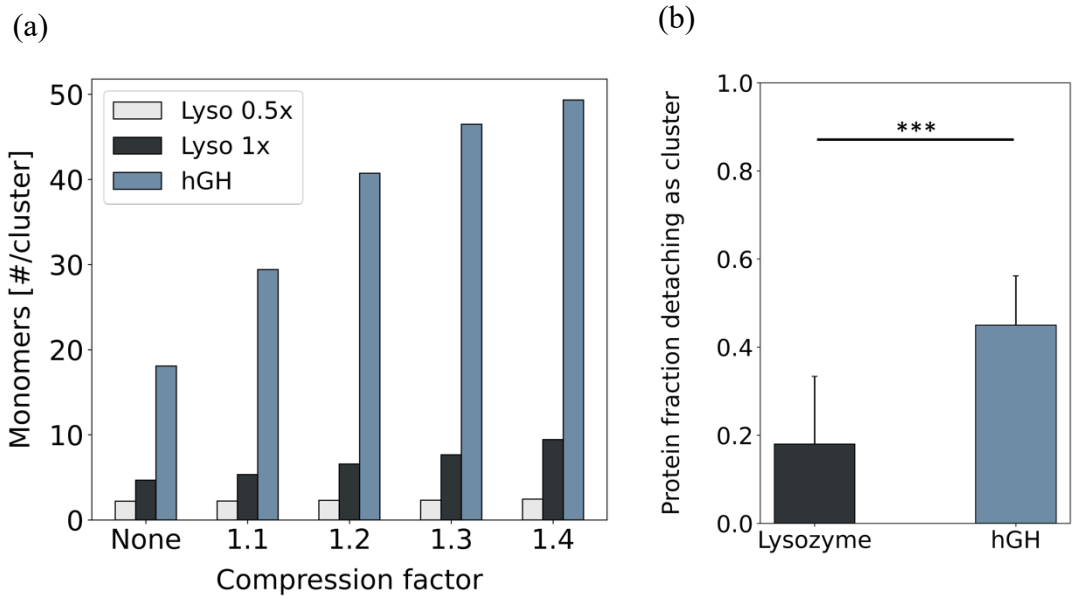

Figure 7: (a) Average number of monomers per cluster for hGH and lysozyme at pH 7, with either half (0.5x) or the same number (1x) of protein molecules for lysozyme as for hGH, determined in MD simulations with compression factors ranging from 1.0 to 1.4. (b) Fraction of protein molecules detaching as clusters rather than as isolated monomers in ten simulated systems for hGH and lysozyme (0.5x) at pH 7 at a compression factor of 1.4. A t-test was performed with *** for $p \leq 0.001$.

5. Conclusions

In this study, we investigated the impact of the protein formulation on particle formation at a moving, solid interface using MD and experimental techniques. Previous work could not pinpoint the exact mechanisms involved. To address this, we improved our recently published MD model on protein aggregation at interfaces by incorporating an interfacial potential and improved electrostatic interactions. Our MD results for hGH at different pH values matched experimental data, indicating that pH influences aggregate formation both directly at the interface and during the transfer of aggregates into the bulk. Both steps are influenced by protein–protein interactions, which are therefore relevant not only in the bulk but also in earlier stages. Notably, the pH value did not affect the adsorbed mass. A high ionic strength formulation showed that at a comparable level of self-interaction, the amount of protein adsorbed to the tubing interface can be the predominant mechanism for protein particle formation. Therefore, protein–protein interactions appear to be the most dominant mechanism influencing protein aggregation at the interface, but they need to be considered together with the amount of protein adsorbed onto the interface. Our findings are valid not only for hGH but can be generalized to other proteins as shown for lysozyme.

Hence, our study helps to determine the exact role of formulation parameters in interfacial protein aggregation. We further showed that MD is a suitable tool for estimating the aggregation propensity of formulations varying in pH, ionic strength, or type of protein. Consequently, MD can potentially be used to save time, cost, and labor in formulation and process development. In future studies, the impact of the interface type (e.g. air–liquid interface) could be investigated. Furthermore, additional research is necessary to assess the impact of structural changes on protein particle formation at moving interfaces, as in reality the particles formed at the interface can include at least a fraction of at least partially unfolded molecules which in not reflected in our coarse-grained model.

6. Acknowledgments

The authors gratefully acknowledge the Gauss Centre for Supercomputing e.V. (www.gauss-centre.eu) for funding this project by providing computing time on the GCS Supercomputer SuperMUC at Leibniz Supercomputing Centre (www.lrz.de). Furthermore, the authors gratefully acknowledge the Leibniz Supercomputing Centre for funding this project by providing computing time on its Linux-Cluster.

7. References

(1) Schellekens, H. Immunogenicity of Therapeutic Proteins: Clinical Implications and Future Prospects. *Clin. Ther.* **2002**, *24* (11), 1720–1740.

(2) Rosenberg, A. S. Effects of Protein Aggregates: An Immunologic Perspective. *AAPS J.* **2006**, *8* (3), E501–E507.

(3) Mahler, H.; Friess, W.; Grauschopf, U.; Kiese, S. Protein Aggregation: Pathways, Induction Factors and Analysis. *J. Pharm. Sci.* **2009**, *98* (9), 2909–2934.

(4) Deiringer, N.; Friess, W. Proteins on the Rack: Mechanistic Studies on Protein Particle Formation during Peristaltic Pumping. *J. Pharm. Sci* **2022**, *111* (5), 1370–1378.

(5) Deiringer, N.; Aleshkevich, S.; Müller, C.; Friess, W. Modification of Tubings for Peristaltic Pumping of Biopharmaceutics. *J. Pharm. Sci.* **2022**, *111* (12), 3251–3260.

(6) Her, C.; Carpenter, J. F. Effects of Tubing Type, Formulation, and Postpumping Agitation on Nanoparticle and Microparticle Formation in Intravenous Immunoglobulin Solutions Processed With a Peristaltic Filling Pump. *J. Pharm. Sci* **2020**, *109* (1), 739–749.

(7) Her, C.; Tanenbaum, L. M.; Bandi, S.; Randolph, T. W.; Thirumangalathu, R.; Mallela, K. M. G.; Carpenter, J. F.; Elias, Y. Effects of Tubing Type, Operating Parameters, and Surfactants on Particle Formation During Peristaltic Filling Pump Processing of a MAb Formulation. *J. Pharm. Sci.* **2020**, *109* (4), 1439–1448.

(8) Fanthom, T. B.; Wilson, C.; Gruber, D.; Bracewell, D. G. Solid-Solid Interfacial Contact of Tubing Walls Drives Therapeutic Protein Aggregation During Peristaltic Pumping. *J. Pharm. Sci.* **2023**, *112* (12), 3022–3034.

(9) Deiringer, N.; Rüdiger, D.; Luxbacher, T.; Zahler, S.; Frieß, W. Catching Speedy Gonzales: Driving Forces for Protein Film Formation on Silicone Rubber Tubing during Pumping. *J. Pharm. Sci* **2022**.

(10) Wu, H.; Randolph, T. W. Aggregation and Particle Formation During Pumping of an Antibody Formulation Are Controlled by Electrostatic Interactions Between Pump Surfaces and Protein Molecules. *J. Pharm. Sci* **2020**, *109* (4), 1473–1482.

(11) Västberg, A.; Markova, N.; Nilsson, L.; Nylander, T.; Sivakumar, B.; Wahlgren, M.; Elofsson, U. Particle Formation during Peristaltic Pumping of Therapeutic Proteins: Hofmeister Anions Effect. *J. Pharm. Sci.* **2025**, *114* (4), 103700.

(12) Souza, P. C. T.; Alessandri, R.; Barnoud, J.; Thallmair, S.; Faustino, I.; Grünewald, F.; Patmanidis, I.; Abdizadeh, H.; Bruininks, B. M. H.; Wassenaar, T. A.; et al. Martini 3: A General Purpose Force Field for Coarse-Grained Molecular Dynamics. *Nat. Methods* **2021**, *18* (4), 382–388.

(13) Sarter, T.; Friess, W. Molecular Dynamics Study of Protein Aggregation at Moving Interfaces. *Mol. Pharm.* **2024**, *21* (3), 1214–1221.

(14) Spoel, D. V. D.; Lindahl, E.; Hess, B.; Groenhof, G.; Mark, A. E.; Berendsen, H. J. C. GROMACS: Fast, Flexible, and Free. *J. Comput. Chem.* **2005**, *26* (16), 1701–1718.

(15) Abraham, M. J.; Murtola, T.; Schulz, R.; Páll, S.; Smith, J. C.; Hess, B.; Lindahl, E. GROMACS: High Performance Molecular Simulations through Multi-Level Parallelism from Laptops to Supercomputers. *SoftwareX* **2015**, *1*, 19–25.

(16) Lindahl, E.; Hess, B.; Spoel, D. van der. GROMACS 3.0: A Package for Molecular Simulation and Trajectory Analysis. *Mol. Model. Annu.* **2001**, *7* (8), 306–317.

(17) Bonomi, M.; Bussi, G.; Camilloni, C.; Tribello, G. A.; Banáš, P.; Barducci, A.; Bernetti, M.; Bolhuis, P. G.; Bottaro, S.; Branduardi, D.; et al. Promoting Transparency and Reproducibility in Enhanced Molecular Simulations. *Nat. Methods* **2019**, *16* (8), 670–673.

(18) Tribello, G. A.; Bonomi, M.; Branduardi, D.; Camilloni, C.; Bussi, G. PLUMED 2: New Feathers for an Old Bird. *Comput. Phys. Commun.* **2014**, *185* (2), 604–613.

(19) Binder, J.; Zalar, M.; Huelsmeyer, M.; Siedler, M.; Curtis, R.; Friess, W. Enhancing Martini3 for Protein Self-Interaction Simulations. *Eur. J. Pharm. Sci.* **2025**, 107068.

(20) Kroon, P. C.; Grünewald, F.; Barnoud, J.; Tilburg, M. van; Souza, P. C.; Wassenaar, T. A.; Marrink, S.-J. Martinize2 and Vermouth: Unified Framework for Topology Generation. *arXiv preprint arXiv:2212.01191* **2022**.

(21) Poma, A. B.; Cieplak, M.; Theodorakis, P. E. Combining the MARTINI and Structure-Based Coarse-Grained Approaches for the Molecular Dynamics Studies of Conformational Transitions in Proteins. *J. Chem. Theory Comput.* **2017**, *13* (3), 1366–1374.

(22) Søndergaard, C. R.; Olsson, M. H. M.; Rostkowski, M.; Jensen, J. H. Improved Treatment of Ligands and Coupling Effects in Empirical Calculation and Rationalization of PK a Values. *J. Chem. Theory Comput.* **2011**, *7* (7), 2284–2295.

(23) Olsson, M. H. M.; Søndergaard, C. R.; Rostkowski, M.; Jensen, J. H. PROPKA3: Consistent Treatment of Internal and Surface Residues in Empirical PK a Predictions. *J. Chem. Theory Comput.* **2011**, *7* (2), 525–537.

(24) Cambiaso, S.; Rasera, F.; Rossi, G.; Bochicchio, D. Development of a Transferable Coarse-Grained Model of Polydimethylsiloxane. *Soft Matter* **2022**, *18* (40), 7887–7896.

(25) Yu, X.; Xiao, J.; Dang, F. Surface Modification of Poly(Dimethylsiloxane) Using Ionic Complementary Peptides to Minimize Nonspecific Protein Adsorption. *Langmuir* **2015**, *31* (21), 5891–5898.

(26) Höger, K.; Mathes, J.; Frieß, W. IgG1 Adsorption to Siliconized Glass Vials—Influence of PH, Ionic Strength, and Nonionic Surfactants. *J. Pharm. Sci.* **2015**, *104* (1), 34–43.

(27) Essmann, U.; Perera, L.; Berkowitz, M. L.; Darden, T.; Lee, H.; Pedersen, L. G. A Smooth Particle Mesh Ewald Method. *J. Chem. Phys.* **1995**, *103* (19), 8577–8593.

(28) Darden, T.; York, D.; Pedersen, L. Particle Mesh Ewald: An N ·log(N) Method for Ewald Sums in Large Systems. *J. Chem. Phys.* **1993**, *98* (12), 10089–10092.

(29) Jong, D. H. de; Baoukina, S.; Ingólfsson, H. I.; Marrink, S. J. Martini Straight: Boosting Performance Using a Shorter Cutoff and GPUs. *Comput. Phys. Commun.* **2016**, *199*, 1–7.

(30) Bussi, G.; Donadio, D.; Parrinello, M. Canonical Sampling through Velocity Rescaling. *J. Chem. Phys.* **2007**, *126* (1), 014101.

(31) (EDQM), E. D. for the Q. of M. & H. *European Pharmacopoeia*, 11th ed.; Council of Europe: Strasbourg, France.

(32) Mathes, J.; Friess, W. Influence of PH and Ionic Strength on IgG Adsorption to Vials. *Eur. J. Pharm. Biopharm.* **2011**, *78* (2), 239–247.

(33) Kelly, S. M.; Jess, T. J.; Price, N. C. How to Study Proteins by Circular Dichroism. *Biochimica Et Biophysica Acta Bba - Proteins Proteom* **2005**, *1751* (2), 119–139.

(34) Karttunen, M.; Rottler, J.; Vattulainen, I.; Sagui, C. Chapter 2 Electrostatics in Biomolecular Simulations: Where Are We Now and Where Are We Heading? *Curr. Top. Membr.* **2008**, *60*, 49–89.

(35) Wong-ekkabut, J.; Karttunen, M. Assessment of Common Simulation Protocols for Simulations of Nanopores, Membrane Proteins, and Channels. *J. Chem. Theory Comput.* **2012**, *8* (8), 2905–2911.

(36) Marinova, K. G.; Alargova, R. G.; Denkov, N. D.; Velev, O. D.; Petsev, D. N.; Ivanov, I. B.; Borwankar, R. P. Charging of Oil−Water Interfaces Due to Spontaneous Adsorption of Hydroxyl Ions. *Langmuir* **1996**, *12* (8), 2045–2051.

(37) Gu, Y.; Li, D. The ζ-Potential of Silicone Oil Droplets Dispersed in Aqueous Solutions. *J. Colloid Interface Sci.* **1998**, *206* (1), 346–349.

(38) Bee, J. S.; Schwartz, D. K.; Trabelsi, S.; Freund, E.; Stevenson, J. L.; Carpenter, J. F.; Randolph, T. W. Production of Particles of Therapeutic Proteins at the Air–Water Interface during Compression/Dilation Cycles. *Soft Matter* **2012**, *8* (40), 10329–10335.

(39) Deiringer, N.; Frieß, W. Reaching the Breaking Point: Effect of Tubing Characteristics on Protein Particle Formation during Peristaltic Pumping. *Int. J. Pharmaceut.* **2022**, *627*, 122216.

(40) Koepf, E.; Eisele, S.; Schroeder, R.; Brezesinski, G.; Friess, W. Notorious but Not Understood: How Liquid-Air Interfacial Stress Triggers Protein Aggregation. *Int. J. Pharmaceut.* **2018**, *537* (1–2), 202–212.

(41) Lan, H.; Liu, H.; Ye, Y.; Yin, Z. The Role of Surface Properties on Protein Aggregation Behavior in Aqueous Solution of Different PH Values. *AAPS PharmSciTech* **2020**, *21* (4), 122.

(42) Koepf, E.; Richert, M.; Braunschweig, B.; Schroeder, R.; Brezesinski, G.; Friess, W. Impact of Formulation PH on Physicochemical Protein Characteristics at the Liquid-Air Interface. *Int. J. Pharm.* **2018**, *541* (1–2), 234–245.

(43) Haynes, C. A.; Norde, W. Structures and Stabilities of Adsorbed Proteins. *J. Colloid Interface Sci.* **1995**, *169* (2), 313–328.

(44) Norde, W.; Favier, J. P. Structure of Adsorbed and Desorbed Proteins. *Colloids Surf.* **1992**, *64* (1), 87–93.

(45) Telikepalli, S. N.; Kumru, O. S.; Kalonia, C.; Esfandiary, R.; Joshi, S. B.; Middaugh, C. R.; Volkin, D. B. Structural Characterization of IgG1 MAb Aggregates and Particles Generated Under Various Stress Conditions. *J. Pharm. Sci.* **2014**, *103* (3), 796–809.

(46) Brych, S. R.; Gokarn, Y. R.; Hultgen, H.; Stevenson, R. J.; Rajan, R.; Matsumura, M. Characterization of Antibody Aggregation: Role of Buried, Unpaired Cysteines in Particle Formation. *J. Pharm. Sci.* **2010**, *99* (2), 764–781.

(47) Buijs, J.; Berg, P. A. W. van den; Lichtenbelt, J. W. Th.; Norde, W.; Lyklema, J. Adsorption Dynamics of IgG and Its F(Ab′)2and Fc Fragments Studied by Reflectometry. *J. Colloid Interface Sci.* **1996**, *178* (2), 594–605.

(48) Chi, E. Y.; Krishnan, S.; Randolph, T. W.; Carpenter, J. F. Physical Stability of Proteins in Aqueous Solution: Mechanism and Driving Forces in Nonnative Protein Aggregation. *Pharm. Res.* **2003**, *20* (9), 1325–1336.

(49) Sahin, E.; Grillo, A. O.; Perkins, M. D.; Roberts, C. J. Comparative Effects of PH and Ionic Strength on Protein–Protein Interactions, Unfolding, and Aggregation for IgG1 Antibodies. *J. Pharm. Sci.* **2010**, *99* (12), 4830–4848.

(50) Dill, K. A. Dominant Forces in Protein Folding. *Biochemistry* **1990**, *29* (31), 7133–7155.

(51) Chou, D. K.; Krishnamurthy, R.; Manning, M. C.; Randolph, T. W.; Carpenter, J. F. Physical Stability of Albinterferon-α2b in Aqueous Solution: Effects of Conformational Stability and Colloidal Stability on Aggregation. *J. Pharm. Sci.* **2012**, *101* (8), 2702–2719.

(52) Menzen, T.; Friess, W. Temperature-Ramped Studies on the Aggregation, Unfolding, and Interaction of a Therapeutic Monoclonal Antibody. *J. Pharm. Sci.* **2014**, *103* (2), 445–455.

(53) Yadav, S.; Shire, S. J.; Kalonia, D. S. Factors Affecting the Viscosity in High Concentration Solutions of Different Monoclonal Antibodies. *J. Pharm. Sci.* **2010**, *99* (12), 4812–4829.

(54) Lehermayr, C.; Mahler, H.; Mäder, K.; Fischer, S. Assessment of Net Charge and Protein–Protein Interactions of Different Monoclonal Antibodies. *J. Pharm. Sci.* **2011**, *100* (7), 2551–2562.

(55) Ettori, C.; Righetti, P. G.; Chiesa, C.; Frigerio, F.; Galli, G.; Grandi, G. Purification of Recombinant Human Growth Hormone by Isoelectric Focusing in a Multicompartment Electrolyzer with Immobiline Membranes. *J. Biotechnol.* **1992**, *25* (3), 307–318.

(56) Koepf, E.; Schroeder, R.; Brezesinski, G.; Friess, W. The Missing Piece in the Puzzle: Prediction of Aggregation via the Protein-Protein Interaction Parameter A∗ 2. *Eur. J. Pharm. Biopharm.* **2018**, *128*, 200–209.

(57) Thirumangalathu, R.; Krishnan, S.; Ricci, M. S.; Brems, D. N.; Randolph, T. W.; Carpenter, J. F. Silicone Oil- and Agitation-induced Aggregation of a Monoclonal Antibody in Aqueous Solution. *J. Pharm. Sci.* **2009**, *98* (9), 3167–3181.

(58) Sorret, L. L.; DeWinter, M. A.; Schwartz, D. K.; Randolph, T. W. Protein–Protein Interactions Controlling Interfacial Aggregation of RhIL-1ra Are Not Described by Simple Colloid Models. *Protein Sci.* **2018**, *27* (7), 1191–1204.

(59) Zhang, F.; Skoda, M. W. A.; Jacobs, R. M. J.; Martin, R. A.; Martin, C. M.; Schreiber, F. Protein Interactions Studied by SAXS: Effect of Ionic Strength and Protein Concentration for BSA in Aqueous Solutions. *J. Phys. Chem. B* **2007**, *111* (1), 251–259.

(60) Raikos, V.; Campbell, L.; Euston, S. R. Effects of Sucrose and Sodium Chloride on Foaming Properties of Egg White Proteins. *Food Res. Int.* **2007**, *40* (3), 347–355.

8. Supporting Information

Table S1 Interfacial potentials determined experimentally, and charge and number of beads fixed on top of the interface in simulations for pH 3, 5, and 7.

pH	Exp. potential [mV][11]	Charge and number of fixed beads
3	+15	+130
5	-15	-130
7	-35	-300

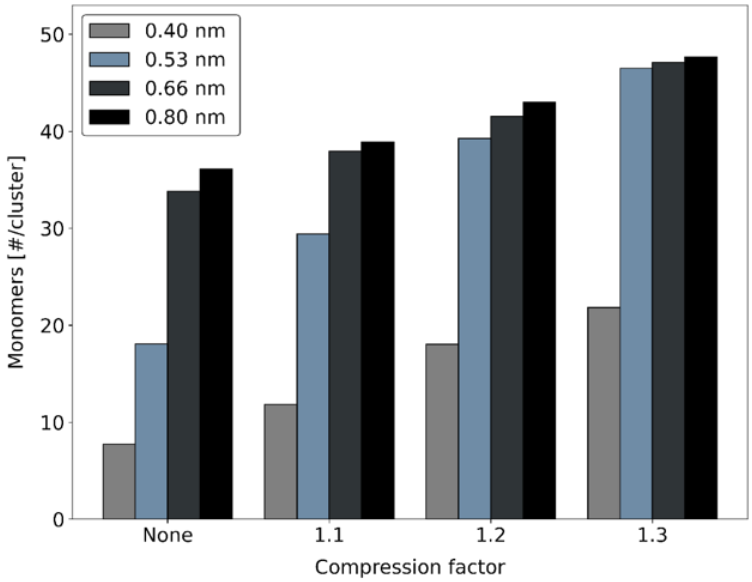

Figure S1 Contact analysis for hGH pH 7 simulations using different cutoff values.

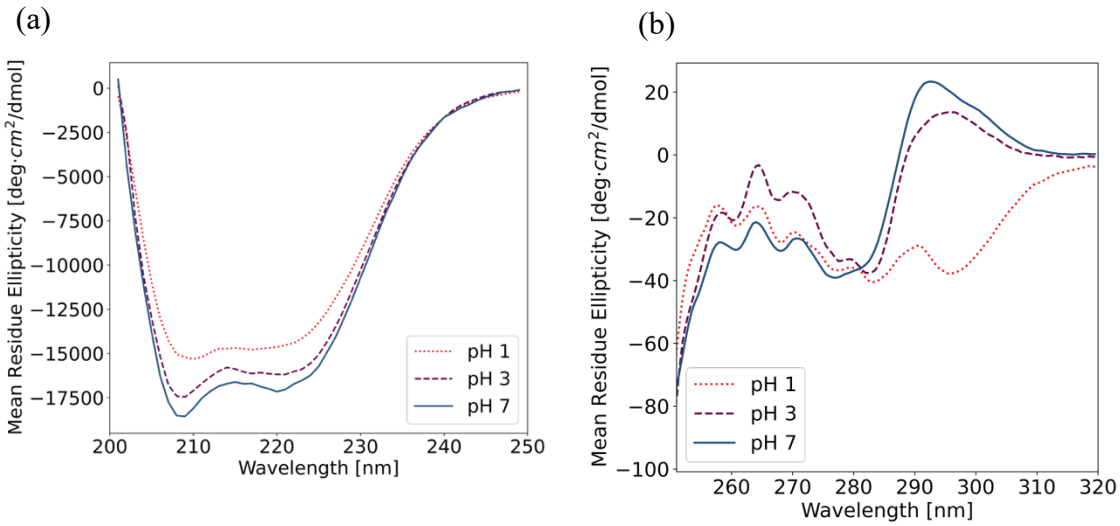

Figure S2 Far (a) and near UV CD spectra (b) of hGH formulations at pH 1, pH 3 and pH 7 after incubation for 6 hours.

Chapter V: Elucidating the Mechanism of Protein Particle Formation under Mechanical Stress at Different Compressible Interfaces by Molecular Dynamics and Experiments

This chapter is published as:

Sarter, T.[a], Karavalasi, A.[b], & Friess, W.[a]

Elucidating the Mechanism of Protein Particle Formation under Mechanical Stress at Different Compressible Interfaces by Molecular Dynamics and Experiments

Molecular Pharmaceutics, 2026.

[a]Department of Pharmacy, Pharmaceutical Technology and Biopharmaceutics, Ludwig-Maximilians-Universität München, 81377 Munich, Germany

[b]School of Pharmacy; Aristotle University of Thessaloniki; 54124 Thessaloniki, Greece

Note from the authors:

The version included in this thesis is identical with the published article apart from minor changes.

The published article can be assessed online via:

https://doi.org/10.1021/acs.molpharmaceut.5c01525

Keywords:

Molecular Dynamics; Protein Aggregation; Interface; Air–Liquid Interface; Mechanical Stress; Shaking; Formulation

1. Abstract

Mechanical stress of protein solutions in contact with a compressible interface can cause protein aggregation. This is a known problem for air-liquid and silicone-liquid interfaces which occur during processing and handling of biopharmaceuticals. A systematic study comparing and unraveling the mechanism of particle formation at different compressible interfaces is lacking. To this end, we combined novel molecular dynamics simulations and established experimental setups that isolate and precisely define compression-decompression stress to elucidate and compare the mechanism of protein particle formation at the silicone-liquid interface, reflecting tubing used in pumping, and air-liquid interface. Simulations revealed that protein molecules bind rather loosely to the air-liquid interface and show high mobility. During interfacial compression, protein molecules therefore move from the air-liquid interface toward the bulk, reducing protein aggregation. At the silicone-liquid interface, strongly bound protein molecules are forced together upon compression of the adsorbed protein film, promoting particle formation already at little compression. Aggregates detach easily from the air-liquid interface and compression further facilitates detachment. This enhanced detachment from the air-liquid interface renders similar particle counts in the bulk for both interface types at high interfacial compression, although simulations indicate less aggregate formation directly at the air-liquid interface. Clusters at the silicone-liquid interface break up during relaxation, whereas clusters at the air-liquid interface persist. This, in combination with more easy detachment leads to the formation of smaller particles at the air-liquid interface compared to the silicone-liquid interface. The simulations indicate that at high compression speed the highly mobile protein molecules at the air-liquid interface do not have sufficient time to interact during compression and form fewer particles. Additionally, strong repulsive protein self-interaction resulting from high charge at low pH values reduced particle formation at the air-liquid interface more strongly due to the high molecular mobility at this interface as compared to the silicone-liquid interface. Our findings provide insights into the mechanisms of protein aggregation at different compressible interfaces, which is essential for developing strategies to mitigate particle formation in biopharmaceutical manufacturing and handling.

Graphical Abstract

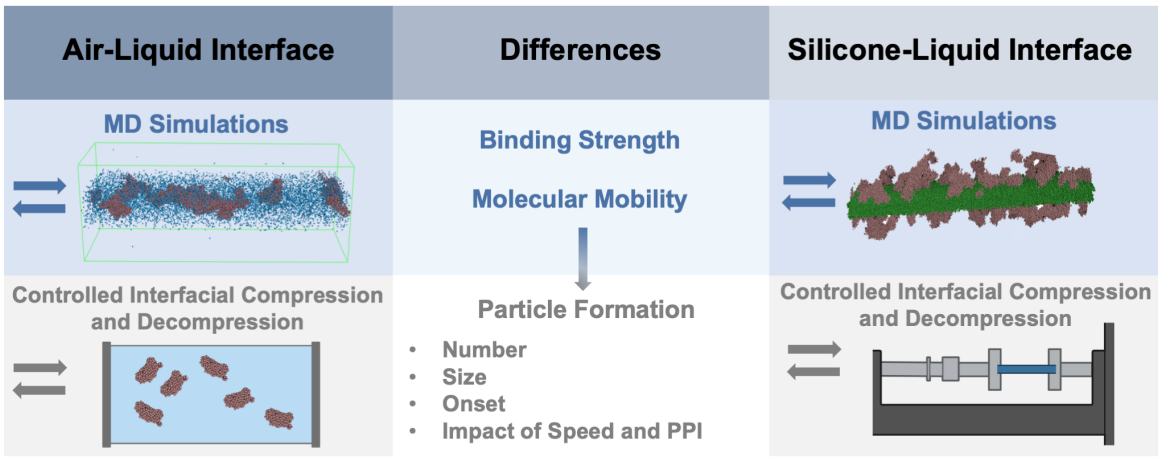

2. Introduction

Protein particle formation can lead to loss of activity, failure to meet regulatory requirements, and a higher risk of immunogenicity in biopharmaceuticals. Compressible interfaces, such as silicone-liquid interfaces (SLI) in the form of tubing during pumping, or the air-liquid interface (ALI) upon shaking, are a major root cause for protein particles.[1] Initially, protein molecules adsorb to the interface, forming a film. Already its viscoelasticity and the surface pressure indicate the aggregation propensity of the protein molecules.[2,3] Mechanical movement then causes interface compression, thereby additionally compacting the already highly concentrated phase of protein molecules and causing network formation.[4–6] The extent of network formation is, among others, dependent on the specific structure and rigidity of the protein molecule.[7] Subsequently, the interface expands. During this whole process protein film fragments transfer as particles into the bulk solution.[8–10] The underlying mechanistic details of particle formation at moving interfaces, especially the role of the type of interface, are, however, still not fully understood.

The ALI is a transitional zone between the gaseous and aqueous phases, with a thickness of approximately 6-8 Å.[11] The fluid nature of air leads to a “softer” character of the interface compared to rigid solid phases.[12] Consequently, monolayers at the ALI are susceptible to buckling upon lateral compression.[13–15] Protein molecules adsorb to the ALI through diffusion and advection, a process that is driven by evaporation.[16] However, the strength of this adsorption varies significantly between interfaces, as does their hydrophobicity. As highlighted by all-atom simulations and experiments, proteins attach more strongly and are less mobile at a tetradecane-water interface or a hydrophilic silica-water interface compared to the ALI, although a solid silicone-liquid interface was not considered.[17,18]

These studies, unfortunately, did not explicitly consider the impact on protein particle formation. Particle formation in protein solutions at the ALI has previously been investigated simply by shaking or under more controlled conditions of interface changes using rotating vials[4] or a trough with moving barriers.[8,19] Both latter methods underline a compression-relaxation-based mechanism for protein particle formation and showed a dependence of particle number on compression factor and speed. Particle formation upon peristaltic pumping of protein solutions follows this mechanism as well, as studies under controlled interfacial stress could show.[6,10,20] However, differences in experimental conditions regarding protein type, formulation, extent of mechanical stress, and analytical readout make a comparison of these studies investigating the mobile ALI and the stable SLI impossible.

Currently, a systematic approach elucidating similarities and contrasts in the mechanism of particle formation at different compressible interfaces is lacking.

In addition to experiments, molecular dynamics (MD) has emerged as a powerful tool in formulation and process development. We recently published a coarse-grained MD model that allowed for mechanistic insights into protein aggregation at moving silicone interfaces under well-defined process and formulation conditions on a molecular level.[21,22] In this present study we combined MD simulations with suitable experimental setups that isolate and precisely define interfacial compression-decompression stress, although adjacent fluid layers may also be affected. We aim to conduct a systematic, comparative study of protein aggregation at different interfaces, which is highly relevant for the processing and handling of protein drugs.

3. Materials and Methods

3.1 Computational Details

The GROMACS simulation package version 2024.3[23–25] was used in combination with a reparametrized version of the Martini 3 coarse-grained force field that utilizes the same four-to-one mapping scheme. The force field was designed to accurately represent bulk self-interactions of low-molecular-weight proteins and verified against experimental data on second virial and diffusion coefficients of protein molecules.[26] Coulomb interactions were calculated with the particle mesh Ewald algorithm[27,28] and a cutoff of 1.1 nm, while Van-der-Waals interactions were handled with the cutoff scheme using the same cutoff distance as previously suggested.[29,30] If not stated otherwise, 30 independent simulations per condition were performed.

Human growth hormone (hGH, PDB: 1HGU) was chosen as a model protein. With 191 amino acids and a molecular weight of 22 kDa, the protein has a characteristic four-helix bundle structure and two binding domains to its receptor.[31,32] The coarse-grained model of hGH was built via the martinize2 script.[33] Only the native structure can be accurately depicted, which was conserved by a Go-like approach.[34] The protonation states were assigned by Propka 3.[35] Fifty protein monomers and the respective number of sodium counterions for neutralization were inserted into a box. We selected the system size of 87 x 27 x 17 nm to ensure a sufficiently large interface sample and prevent periodic image interactions. The simulation box was then filled with water molecules. For ALI simulations, the box was extended in the z-dimension to create a vacuum layer mimicking the gas phase, as suggested before[13,29,36,37]. After energy minimization using a steepest descent algorithm, the system was equilibrated in a canonical ensemble until temperature and root mean square deviation of hGH C_α atoms stabilized. This was followed by an additional equilibration step of 400 ns to allow the protein molecules to reorient and for initial cluster formation to converge. Convergence criteria for cluster formation were defined as a rolling standard deviation below 0.75 monomers/cluster and a slope below 0.075 monomers/cluster per 10 ns over a window size of 8 data points. Afterward, the system was unilaterally compressed in the x-dimension. If not stated otherwise, the simulation box was compressed and decompressed with a velocity of 40 mm/s. This is faster than in corresponding experiments to save computational resources.

As the aggregation state of the protein molecules in MD simulations is determined via a clustering algorithm, we refer to protein aggregates as protein clusters when they are

assessed *in silico.* For protein cluster analysis, the average number of monomers per cluster was determined using a cutoff distance of 0.53 nm, a value equivalent to twice the van der Waals radius of a standard Martini bead.[29] Protein beads within the cutoff across periodic boundaries are assigned to the same cluster, preventing artificial fragmentation of aggregates at box edges. For interfacial contact analysis, the water distribution in the box was assessed. We defined the beginning point of the air layer as the 0.1 nm thick region along the z-coordinate where the number of water molecules did not exceed 200. A contact was defined as a maximum distance of 1 nm between a protein bead and the beginning point of the air layer. The diffusion coefficient was determined using the *gmx_msd* function over a duration of 320 ns. Simulations at polydimethylsiloxane (PDMS), imitating silicone tubing, were performed as described previously.[21] In brief, a polymer slab with properties mimicking PDMS[38] was generated, and charged beads on its surface provide a simplified representation of the known charge of the material. For those beads, the bead type TQ5 with a charge of -1 was selected, representing a tiny bead of the Martini ion block. After equilibration, the box was compressed, and positional restraints were applied to the interface to imitate the restoring forces of the elastic polymer.

3.2 Experimental Details

3.2.1 Materials

Solutions of 1 g/L hGH solution in 10 mM sodium phosphate were used. The pH 3 solution was prepared by adding 9 g/L hGH stock solution (10 mM sodium phosphate, pH 7) to a buffer with a lower pH value to achieve the final concentration and pH. The pH 7 formulation was obtained by diluting the hGH stock solution with the respective buffer. All buffers were filtered through 0.2 µm cellulose acetate filters (47 mm diameter, Sartorius Stedim Biotech GmbH), and protein solutions were filtered using 0.22 µm poly (ether sulfone) membrane syringe filters (VWR, Darmstadt, Germany). Final protein concentrations were verified using a Nanodrop 2000 photometer (Thermo Fisher Scientific, Wilmington, USA). Buffer substances were obtained from Merck KGaA (Darmstadt, Germany).

3.2.2 ALI Stress Studies

Compression-decompression studies at the ALI were performed in a custom-made PTFE mini-trough of 90 x 30 x 5 mm with two barriers moving at the surface as previously described.[8] The trough was washed with ethanol, highly purified water, and filled with 14.5 mL of protein solution. After an incubation period of 30 min, 2.5 mL of the bulk sample

was taken out as a control and replaced. Interfacial stress was applied by the movement of the barriers by a distance corresponding to the desired compression factors. Compression factor c_f is defined as the ratio of maximum and minimum length and is related to compressive strain by $c_f = 1/(1-\varepsilon)$. The samples were stressed for 500 cycles with the two barriers moving at 2.5 mm/s each. The impact of compression speed was evaluated by additional tests at 40 mm/s. Experiments were performed in quadruplicate.

3.2.3 SLI Stress Studies

Stretching studies were conducted in quadruplicate as previously described[22]. Accusil silicone tubing pieces (Watson-Marlow, Falmouth, United Kingdom) with an inner diameter of 6.0 mm were filled with protein solution and sealed. The tubing was subjected to 500 stretching-relaxation cycles at a speed of 5 mm/s using a TA.Xtplus Texture Analyser (Stable Micro Systems, Surrey, United Kingdom). The protein solution was removed and analyzed for particles. For control samples, a 1-hour incubation period in the tubing was conducted prior to analysis.

3.2.4 Particle Analysis

Subvisible particle (SVP) content was determined by light obscuration with a PAMAS SVSS particle counter (PAMAS Partikelmess- und Analysesysteme, Rutesheim, Germany), adhering to Ph. Eur. 2.9.19 guidelines. Following a prerinse with 0.3 mL of the sample, three measurements of 0.4 mL each were performed.

4. Results and Discussion

4.1 Mobility and Interfacial Contacts

First, we assessed the differences in the flexibility of the interfaces. As a fluid-fluid interface, the ALI is softer than the rigid SLI, allowing it to fluctuate.[12] This is also reflected in our model. Without interfacial compression, the silicone beads of the SLI showed only minimal movement in the z-dimension due to positional restraints. In contrast, the positions of the water molecules directly at the ALI varied by more than 1 nm during a 200 ns equilibration phase (**Figure S1**). This highlights the markedly higher propensity of the ALI for fluctuations.

We then compared the adsorption state of the protein molecules at the two interfaces *in silico.* At the end of the equilibration phase, all hGH molecules were in close proximity to the respective interfaces. Additionally, nearly all protein molecules were also in direct contact with the silicone layer and therefore adsorbed to this interface. However, only about 10% of the molecules were in contact with the air as defined by a maximum distance of 1 nm between a protein bead and the air layer (**Table 1**). This was reflected by the 30x higher diffusivity of hGH molecules at the ALI than at the SLI. With the high mobility at the ALI comes a rapid exchange of the protein molecules which are in contact with the interface. Within 100 ns, about 90% of the molecules initially in contact with the ALI were exchanged against others close from the bulk. In contrast, no exchange took place at the SLI within this time frame. Current literature mostly focuses on the differences between the ALI and oil-liquid, not solid silicone-liquid interfaces. Protein molecules are known to attach less strongly to the ALI than to a tetradecane-liquid interface,[17] resulting in higher molecular mobility at the air-liquid interface.[18] Similarly, an all-atom MD study of different protein molecules also observed a stronger coupling and lower lateral diffusion at the oil-liquid interface than at the ALI, with no desorption from the oil-liquid interface within the simulated time frame.[39]

Table 1: hGH Behavior at the ALI and SLI in MD Simulations.

	Air–Liquid	**Silicone–Liquid**
Molecules with Interfacial Contact after 400 ns	10%	100%
D [10^{-7}cm^2/s]	3.77 ± 0.87	0.12 ± 0.04
Molecule Exchange within 100 ns	87%	0%

4.2 Protein Particle Formation at the Air– and Silicone–Liquid Interface and Cluster Formation upon Compression in MD

Next, solutions of hGH at pH 7 were subjected to compression-relaxation events at the ALI and SLI, using setups established previously.[6,8,19,40] We note, however, that in the case of the SLI setup adjacent fluid layers as well as the bulk solution are also affected by the compression-relaxation stress. Previous studies lacked standardized experimental conditions to accurately compare particle formation at both these compressible interfaces. Therefore, we selected the same formulation, compression factors, compression speed, and number of cycles. As was established before, compression-relaxation cycles of interfaces loaded with protein molecules lead to an increase in particle formation.[5,6,8,20,41] SVP measurements in the bulk indicated that the onset of particle formation at the tubing surface occurs at lower compression compared to the ALI (**Figure 1**). A plateau in interfacial particle formation was observed for tubing at a compression factor of 1.3. Notably, at that compression factor, the SVP count ≥ 1 µm in the bulk formed upon compression and decompression at the ALI did not differ from an unstressed control sample. Starting at compression factor 1.5, particles formed at the ALI rose with increasing compression factor without plateau formation. For monoclonal antibodies, this critical compression factor with a substantial increase in particle formation at the ALI has previously been suggested to be at about 3 or 5.[4,8]

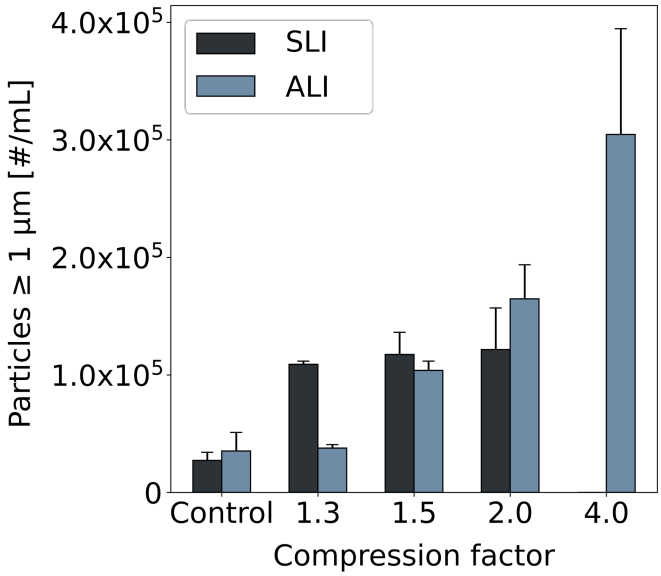

Figure 1: SVP count ≥ 1 µm in hGH bulk solutions pH 7 at different compression factors at the SLI and ALI after 500 compression–relaxation cycles. Rupture of the silicone tubing impeded measurements at compression factors above 2.0.

MD simulations were performed to elucidate the differences in particle formation (**Figure 2**). Already at little compression, marked protein clustering occurred at the SLI. Simulations revealed that protein molecules at the SLI stick to the interface with virtually all protein molecules being in permanent contact with the SLI. Subsequently, protein molecules are forced together, leading to aggregation and particle formation even at little compression. A compression factor as low as 1.1 marked the onset point of protein particle formation in tubing.[20,21] Due to the crowded interface, further increasing the compression level has minimal impact on aggregation and particle formation at the SLI, leading to plateau formation in clustering within the simulated tubing segment. At the ALI, high mobility and weak binding to the interface allow protein molecules to escape toward the bulk phase upon compression. This prevents the aggregation of all monomers in an interfacial region under little compression. However, enough protein molecules remain near the interface, which then accumulate and aggregate upon further compression. While we could not observe a plateau in protein particle count in our study, it was suggested that plateau formation at the air-liquid interface occurs later at a rather high compression factor of about 8, which we did not study.[8]

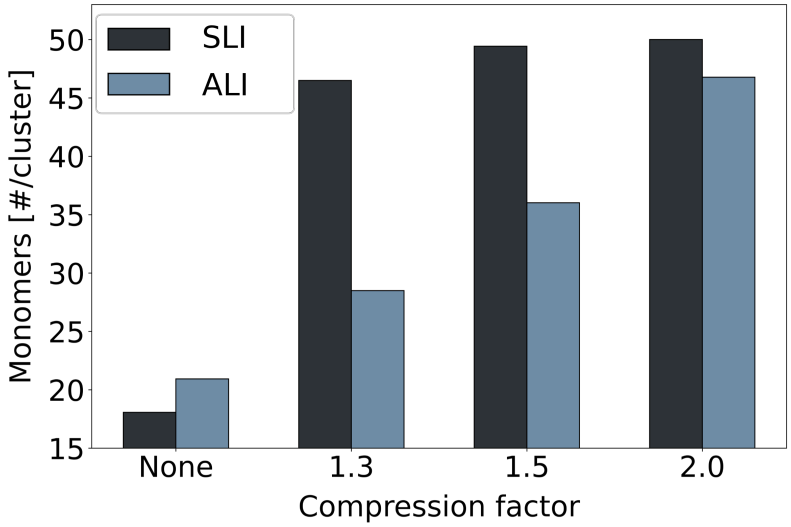

Figure 2: Average number of monomers per cluster for hGH pH 7 determined in MD simulations at different compression factors at the SLI and ALI.

The extent of clustering in MD simulations was previously shown to correlate with SVP formation in an hGH solution upon compression stress.[22] As MD data on protein cluster formation aligned well with SVP formation at little compression, the extent of aggregation at the interface is the primary factor for particle formation. At higher compression, MD

simulations at the ALI showed less cluster formation than at the SLI, whereas there was no significant difference in particle formation experimentally. Therefore, other factors than the extent of aggregation at the interface must contribute to SVP formation.

Protein molecules detach easily from the ALI (**Table 1**). Interfacial contact analysis during the compression step revealed that at factors 1.3 and 2, 53% and 18% respectively of the formed clusters had contact with the interface. Thus, with increasing compression, the clusters formed at the ALI have an increasing tendency to detach from the interface and move toward the bulk phase. Similarly, Murray observed a substantial increase in β-lactoglobulin desorption rate from an air-liquid and oil-liquid interface when the surface pressure was increased by slow compression of the protein film.[17] This pronounced desorption from the ALI at high compression could lead to similar particle numbers in the bulk, even when the simulated extent of cluster formation at the ALI is lower than at the SLI.

Interestingly, differences in protein particle size were detected (**Figure 3**). At a compression factor of 1.5, the number of SVPs ≥ 1 µm formed at both interfaces is similar. However, significantly more large SVPs form at the SLI than at the ALI. MD simulations revealed that protein clusters detach easily from the ALI, leading to their detachment before forming larger particles. Therefore, at the same SVP count ≥ 1 µm, compression-decompression cycles at the SLI induce the formation of larger SVPs. Similarly, the share of SVPs ≥ 10 µm in a mAb solution stressed at the ALI was well below 1% of the SVP count ≥ 1 µm[42] or ≥ 2 µm.[43] In comparison, when pumping formulations of a mAb, the share of particles ≥ 10 µm relative to the SVP count ≥ 1 µm was up to 10% depending on the type of tubing.[20] A different study on peristaltic pumping of a mAb solution showed that only about 1% of the total SVPs were ≥ 10 µm, however, the formulation contained surfactant.[44] Competitive adsorption between surfactant and protein molecules leads to lower absolute particle numbers.[45]

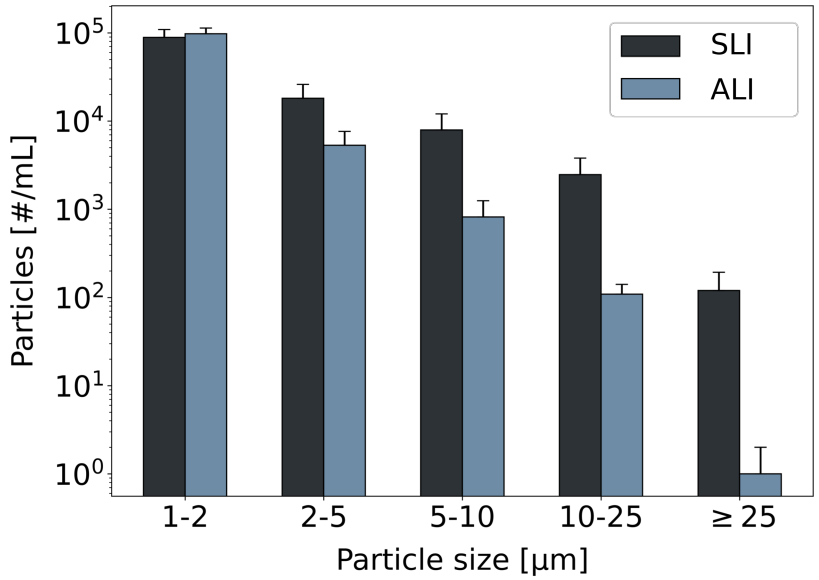

Figure 3: Particle size distribution for hGH pH 7 at the SLI and ALI after 500 compression–relaxation cycles at a compression factor of 1.5.

4.3 MD Compression–Relaxation Cycles

For further understanding, three compression and relaxation sequences were simulated to investigate the impact of multiple interfacial stress cycles on protein cluster formation. We note, however, that no additional protein molecules were added to the simulation box, whereas in experiments new molecules could diffuse from the bulk toward the interface. At the SLI, the protein clusters which had formed during compression were torn apart upon subsequent relaxation and the average cluster size returned to the initial level with clusters not coming loose (**Figure 4a**).

a)

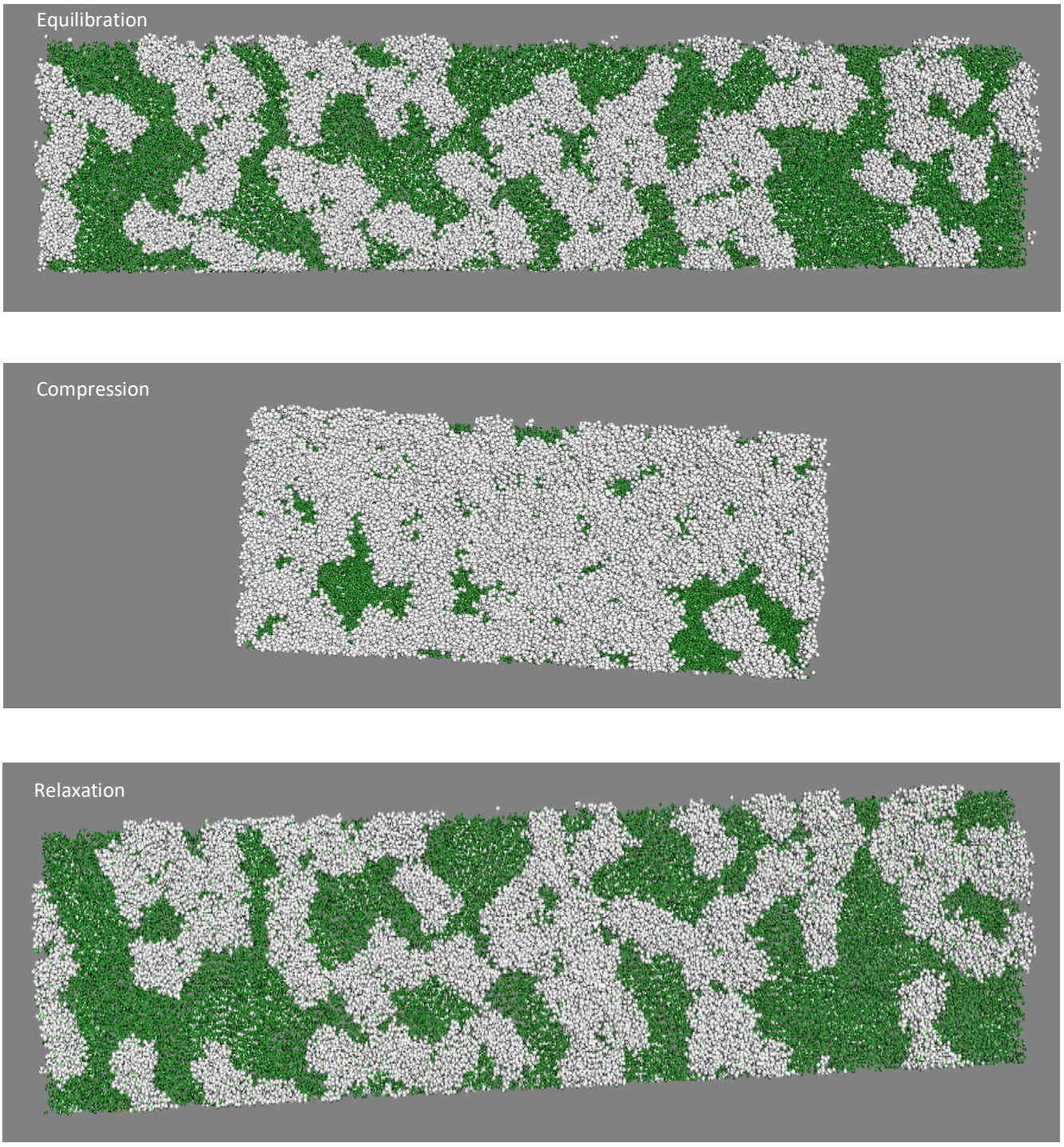

b)

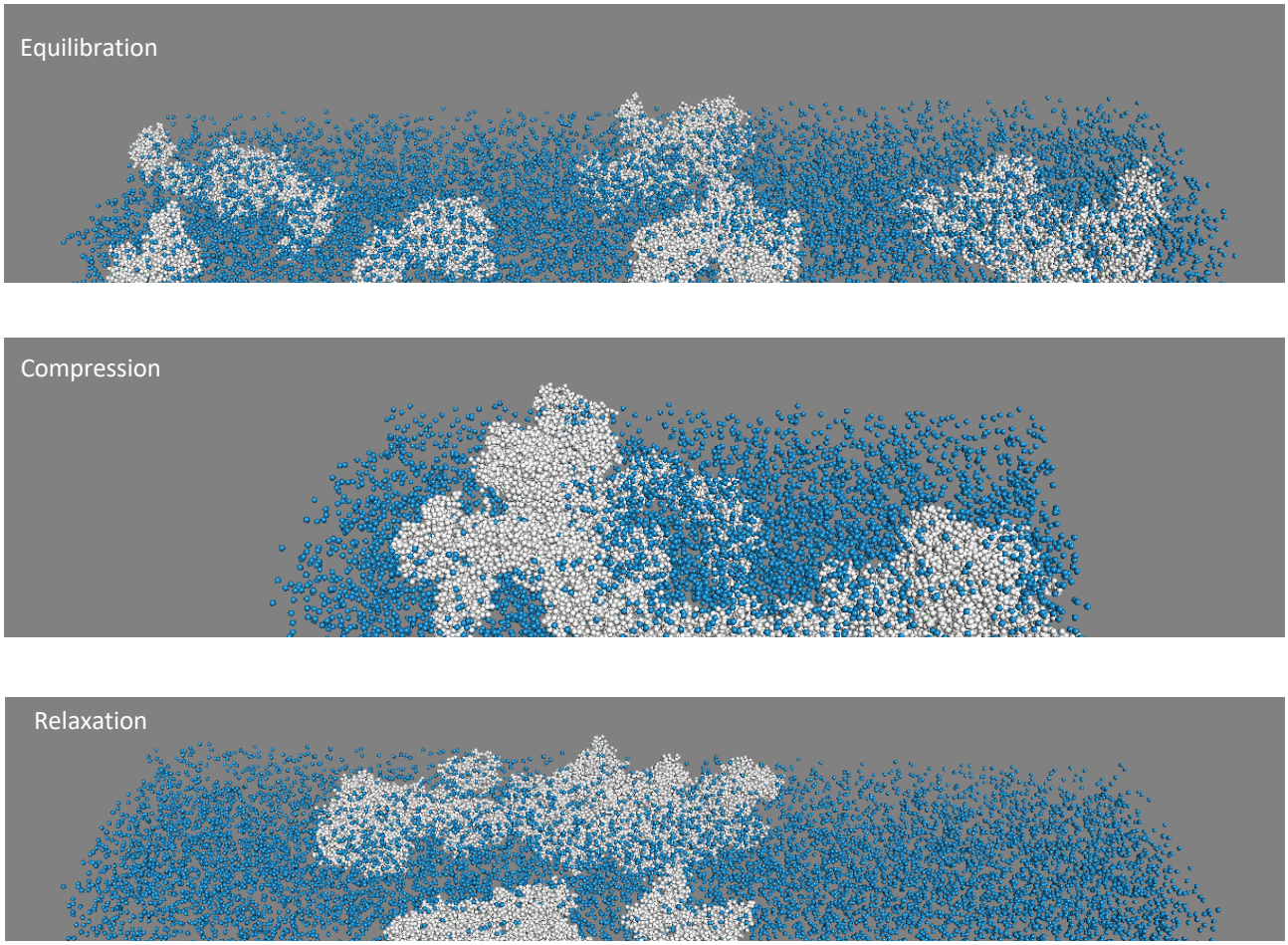

Figure 4: Protein molecules (white) after equilibration, compression, and subsequent relaxation at the SLI (green) (a) and ALI with water beads in blue (b). The SLI is shown as two-dimensional projection, while the ALI is shown in a three-dimensional perspective. To better visualize the ALI, 95% of water beads in the simulation box were randomly removed.

At the ALI, protein molecules also formed clusters during the compression phase. These clusters persisted during the subsequent relaxation (**Figure 4b**). Two additional compression-relaxation cycles did not cause any further changes in cluster number or average cluster size compared to a single compression step. While the strong silicone-protein interactions overcome the protein-protein interactions and tear apart the protein clusters during stretching of the interface in the relaxation phase, the weaker air-protein interactions do not overcome the protein-protein interactions which stabilize the clusters. In addition, since spontaneous desorption of the clusters into the bulk phase is far more likely at the ALI, most clusters are not even present at the interface anymore.

While MD simulations of cluster formation at the interfaces showed smaller clusters formed at the ALI than at the SLI for high compression factors, experimental results revealed a similar total SVP count ≥ 1 µm for both. The high stability of the protein aggregates formed at the ALI could contribute to the unexpectedly high SVP count. During the relaxation phase, these clusters persist, allowing for more time to spontaneously desorb into the bulk solution than for clusters formed at the SLI.

4.4 Impact of Compression Speed on Protein Aggregation

The shaking speed of vials containing protein solution directly determines the interfacial compression speed and affects aggregation. To evaluate the impact of compression speed on particle formation, the protein solution at the ALI was additionally stressed at a 4-fold higher speed of 20 mm/s. At high compression speed, significantly less particle formation was observed (**Figure 5a)**. To reduce computational cost, the corresponding MD simulations employed higher absolute speeds while maintaining the same 4-fold difference between compression speeds. A slight trend toward smaller clusters at higher compression speed could be observed (**Figure 5b).** Interestingly, compression speed did not influence the cluster size in SLI simulations.[22] The stronger interface-protein interactions at the SLI force the protein molecules together even at high compression speed. At the ALI, faster compression leaves less time for the highly mobile protein molecules to arrange and interact, leading to less aggregation.

This is supported by data on the protein film formation process at the two different interfaces during the equilibration phase of the MD simulations (**Figure S2)**. After placing the protein molecules at the interface, it took twice as long for the initial cluster formation to converge at the ALI compared to the SLI. The higher mobility counteracts the aggregation. A study

employing markedly lower compression speeds found more SVPs at higher compression speeds at the ALI[8]. Others also observed an increased particle count at a higher compression rate, which, however, can be attributed to the 15-fold increased cycle number compared to the lower compression rate.[19] Similar findings to ours have been observed for silicone.[6,20]

Equilibration of surface pressure upon β-casein adsorption took longer at the air-water compared to a tetradecane-water interface,[46] yet an inverse trend was observed for β-lactoglobulin.[17] However, unfolding could have affected the surface pressure.

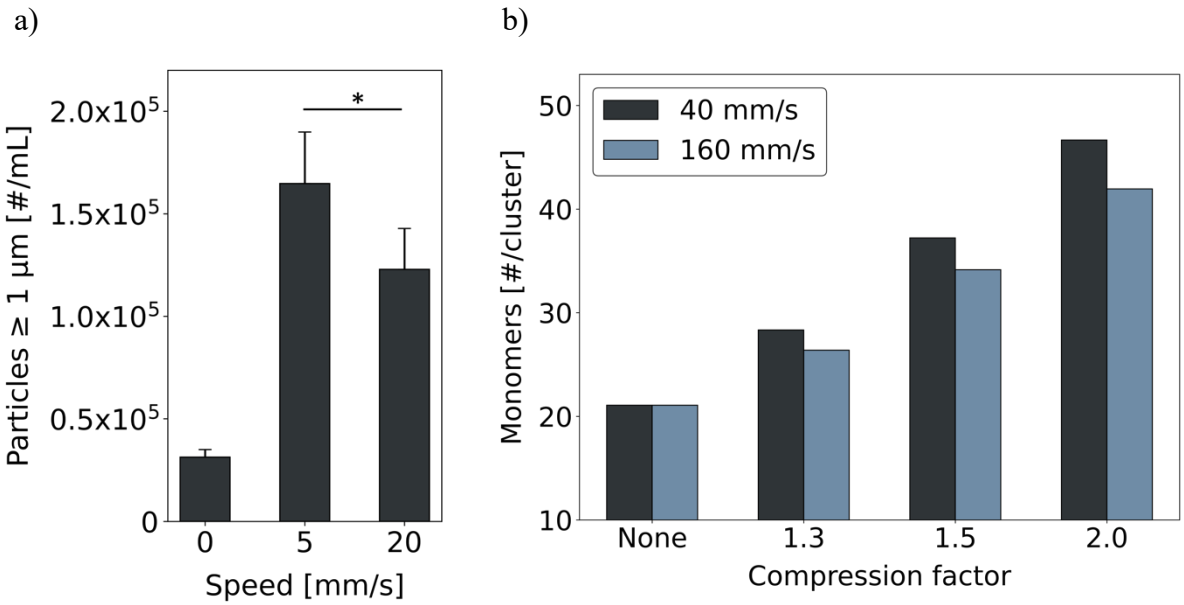

Figure 5: SVP formation at compression factor 2.0 (a) and average number of monomers per cluster determined in MD simulations (b) at the ALI for different compression speeds. A t-test was performed with * for $p \leq 0.05$.

4.5 Impact of pH Value on Protein Aggregation

The pH value is key for the charge state of protein molecules and thereby modulates protein–protein interaction (PPI) as well as protein–interface interaction. Repulsive PPI lead to reduced particle formation during shaking and pumping.[42,47–51] To better understand the impact of PPI, modulated by formulation pH, compression at pH 3 was studied in addition to the tests at pH 7. At pH 3, hGH shows repulsive PPI, whereas at pH 7 the interactions are

neutral or slightly attractive.[21] The results at the ALI were compared to previously published SLI data (**Figure 6**).

At both SLI and ALI, fewer particles formed at pH 3 compared to pH 7. At the ALI, compression did not increase the SVP count in pH 3 formulations compared to an unstressed control sample. In contrast, at the SLI, compression at pH 3 led to significant SVP formation. Others saw less particle formation at the ALI for a pH 4.5 PBS formulation of a mAb, not a low-molecular-weight protein, compared to a formulation at pH 7.4.[19] In addition to differences in formulation, more pronounced unfolding of the mAb at pH 4.5 could be responsible for increased particle formation.[52]

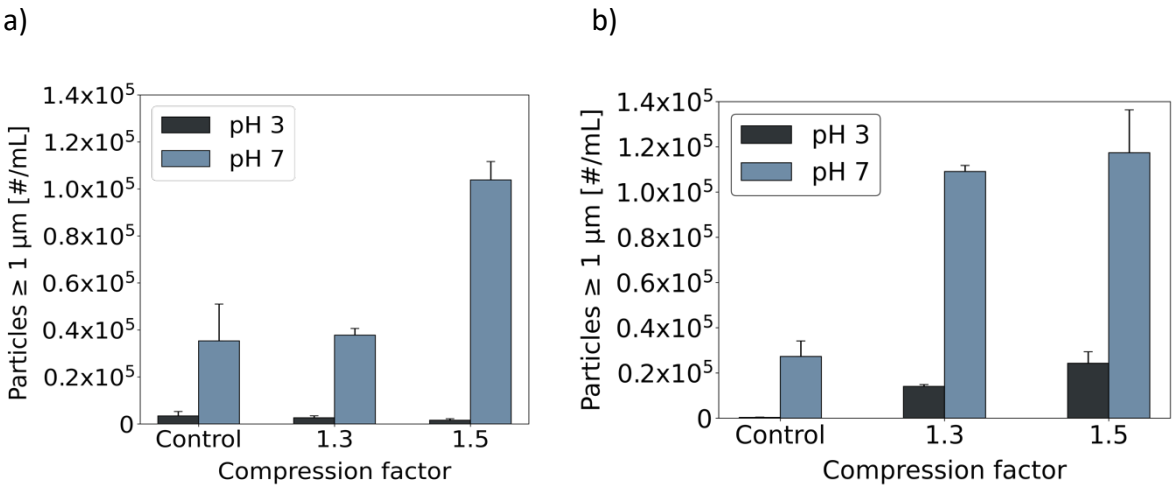

Figure 6: SVP formation at the ALI (a) and SLI (b) at compression factors 1.3 and 1.5 for hGH at pH 3 and 7. SLI data from Sarter and Friess, 2025.[14]

This is in line with the MD simulation results. Smaller clusters formed upon compression of the ALI compared to the SLI systems at both pH values (**Figure 7**). At both interfaces, clusters formed at pH 3 were smaller than at pH 7. ALI simulations showed only a minor increase in cluster size with rising compression at pH 3. In contrast, SLI simulations revealed a marked increase in cluster size from a compression factor of 1.3 onward. Despite the pronounced impact on PPI,[21] the pH value did not significantly influence protein-interface interactions, as the number of molecules with interfacial contact at both the ALI and the SLI after 400 ns of simulation time did not significantly differ between pH 3 and pH 7. The pH 3 formulation was less prone to aggregation at the ALI than at the SLI in both MD simulations and experiments. This suggests that repulsive interactions, which are known to

reduce protein aggregation, have a stronger effect at the ALI, where the molecules are highly mobile. At the SLI, the tightly bound molecules are forced together during compression and pulled apart during relaxation, allowing for less impact of the PPI on aggregation.

a) b)

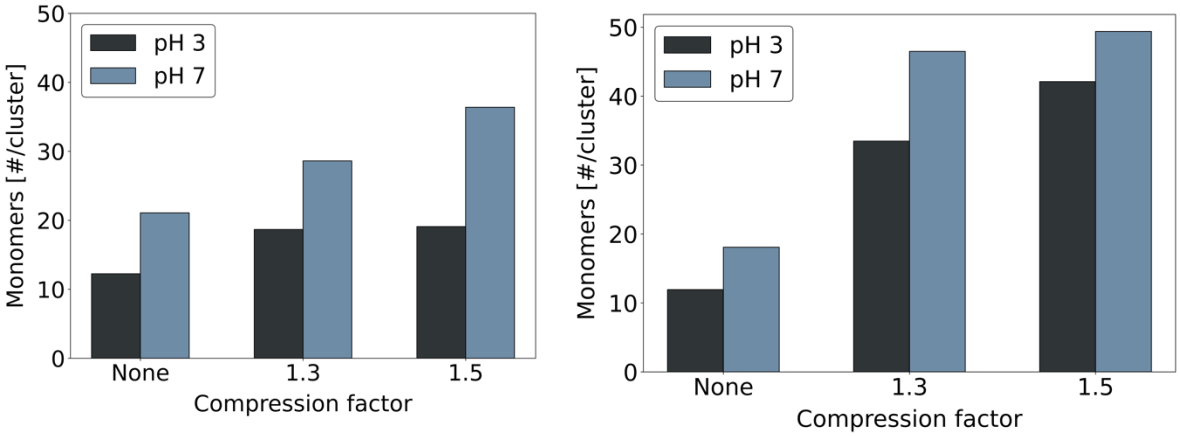

Figure 7: Average number of monomers per cluster at the ALI (a) and SLI (b) at compression factors 1.3 and 1.5 for hGH formulations pH 3 and 7 determined in MD simulations. SLI data from Sarter and Friess, 2025.[14]

5. Conclusion

Compressible interfaces, such as the SLI or ALI, contribute to particle formation during the manufacturing and handling of protein therapeutics. For a better mechanistic understanding, we studied the impact of compression of the protein film adsorbed to the ALI and SLI on protein aggregation by MD and experimentally under well-defined compression and decompression conditions. Weaker binding of the hGH molecules to the ALI than to the SLI results in higher mobility and a rapid exchange with bulk molecules. This allows molecules to escape from the ALI into the bulk, impeding aggregation upon little compression at this interface. Also, clusters formed upon compression in simulations detach from the ALI. With increasing compression, detachment becomes more pronounced, which overall favors the formation of smaller particles. In contrast, protein molecules bind strongly to the SLI. Therefore, compression of the SLI forces hGH molecules together, promoting the buildup of larger clusters and aggregates. During the relaxation phase, clusters formed at the SLI are torn apart again due to the rigorous attachment of the protein molecules to the interface. In contrast, clusters formed at the ALI persist during the relaxation phase, increasing the likelihood of small clusters detaching into the bulk. The simulations showed that higher compression speed hindered the self-interaction of hGH molecules at the ALI, thereby reducing protein clustering. In contrast, the strong interactions between the SLI and the protein molecules force the molecules together, even at high compression speeds. For the same reason, repulsive PPIs in an hGH formulation at pH 3 have less effect on particle formation at this interface. At the ALI, the effects of repulsive PPIs are more pronounced due to the higher molecular mobility, leading to fewer particles than at the SLI for the same formulation.

In summary, weak binding and high mobility of hGH molecules at the ALI delay the onset of protein particle formation upon compression and favor the formation of smaller protein particles. Furthermore, the high molecular mobility amplifies the effects of faster compression and repulsive PPI, leading to reduced particle formation. In contrast, at the SLI, the strong interface-protein interactions cause protein particle formation even at little compression and result in a tendency toward larger particles. Protein aggregation is also less affected by high compression speed or repulsive PPI.

Our combined approach of MD simulations and precisely controlled interfacial-stress experiments provides deeper insight into the mechanisms of protein aggregation at different compressible interfaces. Future work should extend the MD model to other proteins and

excipients, ultimately aiming to estimate and possibly mitigate interfacial particle formation in therapeutic protein formulations. Additionally, as protein adsorption can lead to protein unfolding and thus particle formation, structural changes should be depicted in the model.

6. Acknowledgments

The authors gratefully acknowledge the Gauss Centre for Supercomputing e.V. (www.gauss-centre.eu) for funding this project by providing computing time on the GCS Supercomputer SuperMUC at Leibniz Supercomputing Centre (www.lrz.de). Furthermore, the authors gratefully acknowledge the Leibniz Supercomputing Centre for funding this project by providing computing time on its Linux-Cluster.

7. References

(1) Li, J.; Krause, M. E.; Chen, X.; Cheng, Y.; Dai, W.; Hill, J. J.; Huang, M.; Jordan, S.; LaCasse, D.; Narhi, L.; Shalaev, E.; Shieh, I. C.; Thomas, J. C.; Tu, R.; Zheng, S.; Zhu, L. Interfacial Stress in the Development of Biologics: Fundamental Understanding, Current Practice, and Future Perspective. *Aaps J* **2019**, *21* (3), 44.

(2) Kannan, A.; Shieh, I. C.; Negulescu, P. G.; Suja, V. C.; Fuller, G. G. Adsorption and Aggregation of Monoclonal Antibodies at Silicone Oil–Water Interfaces. *Mol. Pharm.* **2021**, *18* (4), 1656–1665.

(3) Pham, K. G.; Thompson, B. R.; Wang, T.; Samaddar, S.; Qian, K. K.; Liu, Y.; Wagner, N. J. Interfacial Pressure and Viscoelasticity of Antibodies and Their Correlation to Long-Term Stability in Formulation. *J. Phys. Chem. B* **2023**.

(4) Bee, J. S.; Schwartz, D. K.; Trabelsi, S.; Freund, E.; Stevenson, J. L.; Carpenter, J. F.; Randolph, T. W. Production of Particles of Therapeutic Proteins at the Air–Water Interface during Compression/Dilation Cycles. *Soft Matter* **2012**, *8* (40), 10329–10335.

(5) Lin, G. L.; Pathak, J. A.; Kim, D. H.; Carlson, M.; Riguero, V.; Kim, Y. J.; Buff, J. S.; Fuller, G. G. Interfacial Dilatational Deformation Accelerates Particle Formation in Monoclonal Antibody Solutions. *Soft Matter* **2016**, *12* (14), 3293–3302.

(6) Deiringer, N.; Friess, W. Proteins on the Rack: Mechanistic Studies on Protein Particle Formation during Peristaltic Pumping. *J Pharm Sci* **2022**, *111* (5), 1370–1378.

(7) Freer, E. M.; Yim, K. S.; Fuller, G. G.; Radke, C. J. Interfacial Rheology of Globular and Flexible Proteins at the Hexadecane/Water Interface: Comparison of Shear and Dilatation Deformation. *J. Phys. Chem. B* **2004**, *108* (12), 3835–3844.

(8) Koepf, E.; Eisele, S.; Schroeder, R.; Brezesinski, G.; Friess, W. Notorious but Not Understood: How Liquid-Air Interfacial Stress Triggers Protein Aggregation. *Int J Pharmaceut* **2018**, *537* (1–2), 202–212.

(9) Koepf, E.; Schroeder, R.; Brezesinski, G.; Friess, W. The Film Tells the Story: Physical-Chemical Characteristics of IgG at the Liquid-Air Interface. *Eur. J. Pharm. Biopharm.* **2017**, *119*, 396–407.

(10) Deiringer, N.; Rüdiger, D.; Luxbacher, T.; Zahler, S.; Frieß, W. Catching Speedy Gonzales: Driving Forces for Protein Film Formation on Silicone Rubber Tubing during Pumping. *J Pharm Sci* **2022**.

(11) Fellows, A. P.; Duque, A. D.; Balos, V.; Lehmann, L.; Netz, R. R.; Wolf, M.; Thämer, M. How Thick Is the Air–Water Interface?□A Direct Experimental Measurement of the Decay Length of the Interfacial Structural Anisotropy. *Langmuir* **2024**, *40* (35), 18760–18772.

(12) Vácha, R.; Zangi, R.; Engberts, J. B. F. N.; Jungwirth, P. Water Structuring and Hydroxide Ion Binding at the Interface between Water and Hydrophobic Walls of Varying Rigidity and van Der Waals Interactions. *J. Phys. Chem. C* **2008**, *112* (20), 7689–7692.

(13) Baoukina, S.; Monticelli, L.; Risselada, H. J.; Marrink, S. J.; Tieleman, D. P. The Molecular Mechanism of Lipid Monolayer Collapse. *Proc National Acad Sci* **2008**, *105* (31), 10803–10808.

(14) Prakash, S.; Perrin, H.; Botto, L. Buckling of a Monolayer of Platelike Particles Trapped at a Fluid-Fluid Interface. *Phys. Rev. E* **2024**, *109* (1), 014801.

(15) Razavi, S.; Cao, K. D.; Lin, B.; Lee, K. Y. C.; Tu, R. S.; Kretzschmar, I. Collapse of Particle-Laden Interfaces under Compression: Buckling vs Particle Expulsion. *Langmuir* **2015**, *31* (28), 7764–7775.

(16) Pasquier, C.; Pezennec, S.; Bouchoux, A.; Cabane, B.; Lechevalier, V.; Floch-Fouéré, C. L.; Paboeuf, G.; Pasco, M.; Dollet, B.; Lee, L.-T.; Beaufils, S. Protein Transport upon Advection at the Air/Water Interface: When Charge Matters. *Langmuir* **2021**, *37* (42), 12278–12289.

(17) Murray, B. S. Dynamics of Proteins at Air-Water and Oil-Water Interfaces Using Novel Langmuir Trough Methods; Steinkopff, 1997; pp 41–50.

(18) Ley, K.; Christofferson, A.; Penna, M.; Winkler, D.; Maclaughlin, S.; Yarovsky, I. Surface-Water Interface Induces Conformational Changes Critical for Protein Adsorption: Implications for Monolayer Formation of EAS Hydrophobin. *Front. Mol. Biosci.* **2015**, *2*, 64.

(19) Ghazvini, S.; Kalonia, C.; Volkin, D. B.; Dhar, P. Evaluating the Role of the Air-Solution Interface on the Mechanism of Subvisible Particle Formation Caused by Mechanical Agitation for an IgG1 mAb. *J Pharm Sci* **2016**, *105* (5), 1643–1656.

(20) Deiringer, N.; Frieß, W. Reaching the Breaking Point: Effect of Tubing Characteristics on Protein Particle Formation during Peristaltic Pumping. *Int J Pharmaceut* **2022**, *627*, 122216.

(21) Sarter, T.; Friess, W. Unraveling the Role of Formulation Parameters in Protein Particle Formation at Moving Interfaces Using Molecular Dynamics and Experiments. *Mol. Pharm.* **2025**.

(22) Sarter, T.; Friess, W. Molecular Dynamics Study of Protein Aggregation at Moving Interfaces. *Mol. Pharm.* **2024**, *21* (3), 1214–1221.

(23) Spoel, D. V. D.; Lindahl, E.; Hess, B.; Groenhof, G.; Mark, A. E.; Berendsen, H. J. C. GROMACS: Fast, Flexible, and Free. *J. Comput. Chem.* **2005**, *26* (16), 1701–1718.

(24) Abraham, M. J.; Murtola, T.; Schulz, R.; Páll, S.; Smith, J. C.; Hess, B.; Lindahl, E. GROMACS: High Performance Molecular Simulations through Multi-Level Parallelism from Laptops to Supercomputers. *SoftwareX* **2015**, *1*, 19–25.

(25) Lindahl, E.; Hess, B.; Spoel, D. van der. GROMACS 3.0: A Package for Molecular Simulation and Trajectory Analysis. *Mol. Model. Annu.* **2001**, *7* (8), 306–317.

(26) Binder, J.; Zalar, M.; Huelsmeyer, M.; Siedler, M.; Curtis, R.; Friess, W. Enhancing Martini3 for Protein Self-Interaction Simulations. *Eur. J. Pharm. Sci.* **2025**, 107068.

(27) Essmann, U.; Perera, L.; Berkowitz, M. L.; Darden, T.; Lee, H.; Pedersen, L. G. A Smooth Particle Mesh Ewald Method. *J. Chem. Phys.* **1995**, *103* (19), 8577–8593.

(28) Darden, T.; York, D.; Pedersen, L. Particle Mesh Ewald: An N ·log(N) Method for Ewald Sums in Large Systems. *J. Chem. Phys.* **1993**, *98* (12), 10089–10092.

(29) Souza, P. C. T.; Alessandri, R.; Barnoud, J.; Thallmair, S.; Faustino, I.; Grünewald, F.; Patmanidis, I.; Abdizadeh, H.; Bruininks, B. M. H.; Wassenaar, T. A.; Kroon, P. C.; Melcr, J.; Nieto, V.; Corradi, V.; Khan, H. M.; Domański, J.; Javanainen, M.; Martinez-Seara, H.; Reuter, N.; Best, R. B.; Vattulainen, I.; Monticelli, L.; Periole, X.; Tieleman, D. P.; Vries, A. H. de; Marrink, S. J. Martini 3: A General Purpose Force Field for Coarse-Grained Molecular Dynamics. *Nat Methods* **2021**, *18* (4), 382–388.

(30) Jong, D. H. de; Baoukina, S.; Ingólfsson, H. I.; Marrink, S. J. Martini Straight: Boosting Performance Using a Shorter Cutoff and GPUs. *Comput. Phys. Commun.* **2016**, *199*, 1–7.

(31) Vos, A. M. D.; Ultsch, M.; Kossiakoff, A. A. Human Growth Hormone and Extracellular Domain of Its Receptor: Crystal Structure of the Complex. *Science* **1992**, *255* (5042), 306–312.

(32) Chantalat, L.; Jones, N.; Korber, F.; Navaza, J.; Pavlovsky, A. The Crystal Structure of Wild-Type Growth Hormone at 2.5 A Resolution. *Protein Pept Lett* **1995**, *2*, 333–340.

(33) Kroon, P. C.; Grünewald, F.; Barnoud, J.; Tilburg, M. van; Souza, P. C.; Wassenaar, T. A.; Marrink, S.-J. Martinize2 and Vermouth: Unified Framework for Topology Generation. **2023**.

(34) Poma, A. B.; Cieplak, M.; Theodorakis, P. E. Combining the MARTINI and Structure-Based Coarse-Grained Approaches for the Molecular Dynamics Studies of Conformational Transitions in Proteins. *J Chem Theory Comput* **2017**, *13* (3), 1366–1374.

(35) Olsson, M. H. M.; Søndergaard, C. R.; Rostkowski, M.; Jensen, J. H. PROPKA3: Consistent Treatment of Internal and Surface Residues in Empirical pK a Predictions. *J. Chem. Theory Comput.* **2011**, *7* (2), 525–537.

(36) Nielsen, S. O.; Lopez, C. F.; Moore, P. B.; Shelley, J. C.; Klein, M. L. Molecular Dynamics Investigations of Lipid Langmuir Monolayers Using a Coarse-Grain Model. *J Phys Chem B* **2003**, *107* (50), 13911–13917.

(37) Wizert, A.; Iskander, D. R.; Cwiklik, L. Interaction of Lysozyme with a Tear Film Lipid Layer Model: A Molecular Dynamics Simulation Study. *Biochimica Et Biophysica Acta Bba - Biomembr* **2017**, *1859* (12), 2289–2296.

(38) Cambiaso, S.; Rasera, F.; Rossi, G.; Bochicchio, D. Development of a Transferable Coarse-Grained Model of Polydimethylsiloxane. *Soft Matter* **2022**, *18* (40), 7887–7896.

(39) Zhao, Y.; Cieplak, M. Proteins at Air–Water and Oil–Water Interfaces in an All-Atom Model. *Phys. Chem. Chem. Phys.* **2017**, *19* (36), 25197–25206.

(40) Griffin, V. P.; Merritt, K.; Vaclaw, C.; Whitaker, N.; Volkin, D. B.; Ogunyankin, M. O.; Pace, S.; Dhar, P. Evaluating the Combined Impact of Temperature and Application of Interfacial Dilatational Stresses on Surface-Mediated Protein Particle Formation in Monoclonal Antibody Formulations. *J Pharm Sci* **2022**, *111* (3), 680–689.

(41) Fanthom, T. B.; Wilson, C.; Gruber, D.; Bracewell, D. G. Solid-Solid Interfacial Contact of Tubing Walls Drives Therapeutic Protein Aggregation During Peristaltic Pumping. *J. Pharm. Sci.* **2023**, *112* (12), 3022–3034.

(42) Koepf, E.; Schroeder, R.; Brezesinski, G.; Friess, W. The Missing Piece in the Puzzle: Prediction of Aggregation via the Protein-Protein Interaction Parameter A∗ 2. *Eur. J. Pharm. Biopharm.* **2018**, *128*, 200–209.

(43) Thite, N. G.; Ghazvini, S.; Wallace, N.; Feldman, N.; Calderon, C. P.; Randolph, T. W. Machine Learning Analysis Provides Insight into Mechanisms of Protein Particle Formation inside Containers during Mechanical Agitation. *J Pharm Sci* **2022**.

(44) Nayak, A.; Colandene, J.; Bradford, V.; Perkins, M. Characterization of Subvisible Particle Formation during the Filling Pump Operation of a Monoclonal Antibody Solution. *J. Pharm. Sci.* **2011**, *100* (10), 4198–4204.

(45) Kanthe, A. D.; Krause, M.; Zheng, S.; Ilott, A.; Li, J.; Bu, W.; Bera, M. K.; Lin, B.; Maldarelli, C.; Tu, R. S. Armoring the Interface with Surfactants to Prevent the Adsorption of Monoclonal Antibodies. *ACS Appl. Mater. Interfaces* **2020**, *12* (8), 9977–9988.

(46) Maldonado-Valderrama, J.; Martín-Molina, A.; Gálvez-Ruiz, M. J.; Martín-Rodríguez, A.; Cabrerizo-Vílchez, M. Á. β-Casein Adsorption at Liquid Interfaces: Theory and Experiment. *J. Phys. Chem. B* **2004**, *108* (34), 12940–12945.

(47) Her, C.; Carpenter, J. F. Effects of Tubing Type, Formulation, and Postpumping Agitation on Nanoparticle and Microparticle Formation in Intravenous Immunoglobulin Solutions Processed With a Peristaltic Filling Pump. *J Pharm Sci* **2020**, *109* (1), 739–749.

(48) Lan, H.; Liu, H.; Ye, Y.; Yin, Z. The Role of Surface Properties on Protein Aggregation Behavior in Aqueous Solution of Different pH Values. *AAPS PharmSciTech* **2020**, *21* (4), 122.

(49) Koepf, E.; Richert, M.; Braunschweig, B.; Schroeder, R.; Brezesinski, G.; Friess, W. Impact of Formulation pH on Physicochemical Protein Characteristics at the Liquid-Air Interface. *Int. J. Pharm.* **2018**, *541* (1–2), 234–245.

(50) Chou, D. K.; Krishnamurthy, R.; Manning, M. C.; Randolph, T. W.; Carpenter, J. F. Physical Stability of Albinterferon-α2b in Aqueous Solution: Effects of Conformational Stability and Colloidal Stability on Aggregation. *J. Pharm. Sci.* **2012**, *101* (8), 2702–2719.

(51) Thirumangalathu, R.; Krishnan, S.; Ricci, M. S.; Brems, D. N.; Randolph, T. W.; Carpenter, J. F. Silicone Oil- and Agitation-induced Aggregation of a Monoclonal Antibody in Aqueous Solution. *J. Pharm. Sci.* **2009**, *98* (9), 3167–3181.

(52) Kalonia, C.; Toprani, V.; Toth, R.; Wahome, N.; Gabel, I.; Middaugh, C. R.; Volkin, D. B. Effects of Protein Conformation, Apparent Solubility, and Protein–Protein Interactions on the Rates and Mechanisms of Aggregation for an IgG1Monoclonal Antibody. *J. Phys. Chem. B* **2016**, *120* (29), 7062–7075.

8. Supporting Information

a)

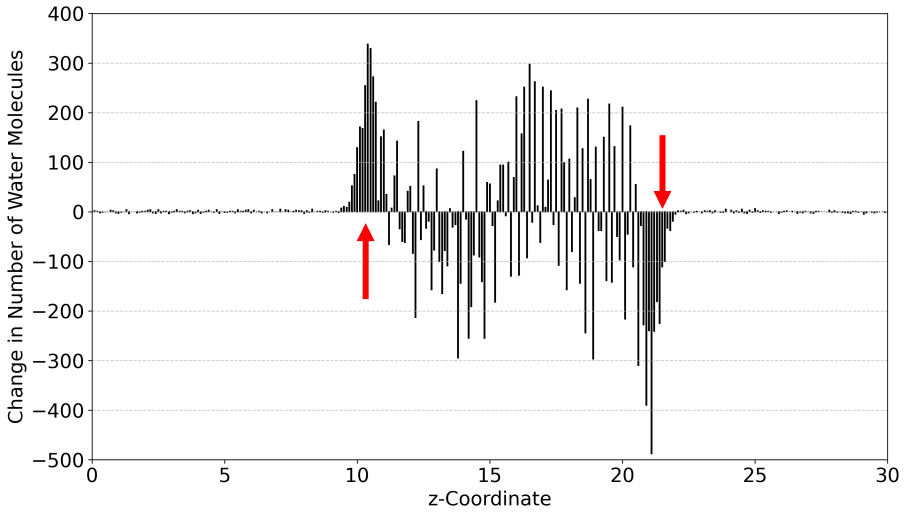

b)

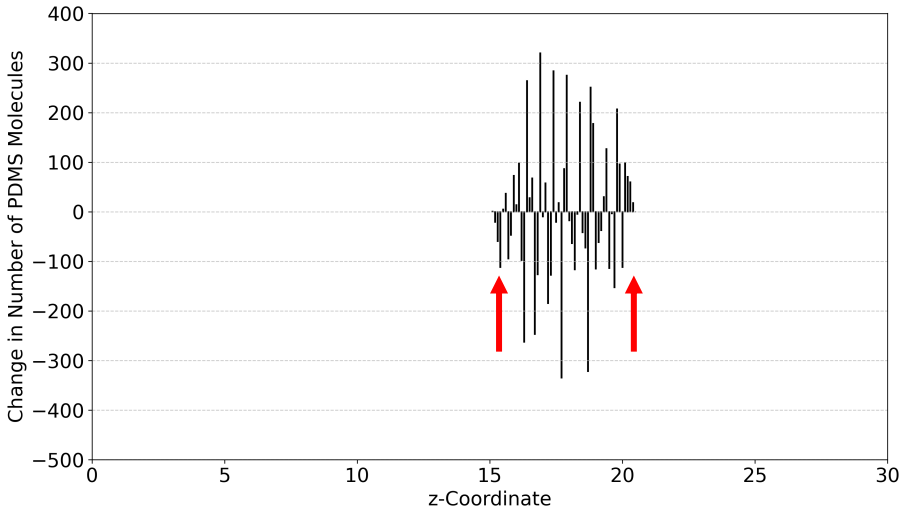

Figure S1: Changes in amount of water (a) and PDMS (b) beads located at each z-coordinate after 200 ns of equilibration time. Whereas in the PDMS layer mostly inner beads move with no effect on the interface, water beads at the boundary to the vacuum phase fluctuate heavily, indicating a wobbling motion of the ALI in the z-direction. Arrows indicate the approximate location of the interface.

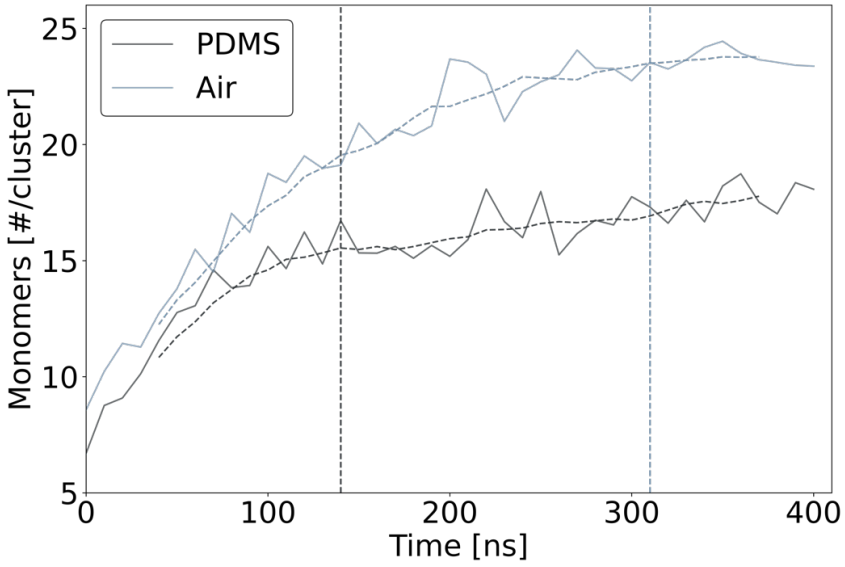

Figure S2: Convergence time of cluster formation during equilibration of hGH molecules at the SLI and ALI.

Chapter VI: Estimating the Aggregation Propensity of Monoclonal Antibody Formulations by Molecular Dynamics Simulations

Sarter, T., & Friess, W.

Department of Pharmacy, Pharmaceutical Technology and Biopharmaceutics, Ludwig-Maximilians-Universität München, 81377 Munich, Germany

1. Introduction

Monoclonal antibodies (mAbs) have become a major class of therapeutics, with at least 212 currently approved worldwide.[1] A key challenge in their development is aggregation, which can be triggered, e.g., by heat, freezing and thawing, or formulation conditions that render highly attractive protein self-interactions. Another important pathway promoting protein particle formation is adsorption to interfaces[2–4] in combination with interfacial compression and decompression, which can occur, e.g., at the air–liquid interface.[5,6]

As protein particle formation can lead to a loss of active protein, non-compliance with regulatory standards, and was linked to an increased risk of immunogenicity,[2,7,8] the physical colloidal instability reflected in the aggregation propensity is routinely assessed in early developability studies of novel mAb drug candidates.[9–11] A standard procedure is agitation on a shaker followed by assessment of the monomer content, higher molecular weight species, subvisible particles (SVPs), and visible particles.[2,3] However, shaking conditions are arbitrary and poorly reproducible, as they depend on factors such as the container type, filling volume, and shaker design, highlighting the need for more controlled testing conditions. Additionally, stress studies consume large amounts of material, which may not be readily available in early stages of formulation and process development.

New computational methods, which require no material at all, are researched and increasingly explored for evaluation of mAb drug candidates and to gain mechanistic understanding of their behavior. The commonly used static computational descriptors like AGGRESCAN,[12] TANGO,[13] or AggScore[14] are generally designed to identify aggregation prone regions and suggest respective point mutations in the protein primary sequence rather than changes in the formulation. In contrast, Lai et al. applied machine learning to different readout parameters from all-atom Molecular Dynamics (MD) simulations and found decent correlation with the aggregation rate of 21 mAbs; all mAbs were formulated in histidine buffer at pH 6.0.[15] Recently, Wang et al. achieved a good correlation between all-atom MD simulations of a mAb fragment and the aggregation kinetics of this fragment in various formulations using a range of molecular features as input.[16] These studies, however, were limited to a single mAb fragment or formulation and did not include an interface. Others investigated the aggregation behavior of a low-molecular-weight protein at a static air–liquid interface by all-atom and coarse-grained (CG) MD simulations without quantitative experimental validation.[17]

Here, we present CG MD simulations of full mAb molecules at the compressible air–liquid interface, generalizing our approach across multiple mAbs and formulations. Compared to other CG forcefields, our mapping of one bead per amino acid provides a relatively high resolution for mAb MD simulations. Our non-equilibrium simulations mimic controlled interfacial compression–decompression. The average cluster size at the end of the simulation served as the sole *in silico* readout parameter and was correlated with the experimental SVP count in protein solutions after shaking stress. This correlation exceeded that between SVP formation and A_2, a parameter commonly used to assess the colloidal stability of mAb formulations.

2. Materials and Methods

2.1 Computational Details

The GROMACS simulation package version 2024.3[18–20] was used in combination with a CG forcefield designed in-house to accurately represent mAb–mAb interactions.[21] Coulomb interactions were calculated with the Particle mesh Ewald algorithm,[22,23] and Van der Waals interactions were treated with the cutoff scheme using the same cutoff distance of 1.15 nm. The crystal structures of the mAbs were prepared via Schrödinger BioLuminate. The mAbs were coarse-grained and respective charges were assigned using a custom python script. 10 independent simulations per condition were performed.

20 protein monomers and the respective number of ions were inserted into a box of 15 x 26 x 85 nm. The simulation box was filled with water molecules and extended in one dimension to generate a vacuum layer, imitating the gas phase, as suggested before.[24–27]

Following energy minimization via a steepest descent algorithm, the system was equilibrated in a canonical ensemble until the temperature stabilized. During a 400 ns equilibration step, the protein molecules were allowed to reorient and initial cluster formation converged. Afterward, the system was compressed at 0.04 m/s up to a compression factor of 2. Protein cluster analysis was performed by determining the average number of monomers per cluster using a cutoff distance of 1.0 nm.

2.2 Experimental Details

2.2.1 Agitation Stress Study

Three monoclonal IgG1 antibodies formulated at 1 g/L in 20 mM histidine buffer at pH 5.5 and pH 7.0 were studied. mAb C was also investigated in formulations with an additional 140 mM NaCl. Buffers were filtered through 0.2 µm cellulose acetate filters (47 mm diameter, Sartorius Stedim Biotech GmbH), and the protein solutions were filtered through 0.22 µm poly(ether sulfone) membrane syringe filters (VWR, Darmstadt, Germany). The final concentrations were checked via their extinction coefficient using a Nanodrop photometer (Thermo Fisher Scientific, Wilmington, USA). L-Histidine, L-histidine hydrochloride monohydrate, and sodium chloride were obtained from Sigma Aldrich (Steinheim, Germany).

4.5 mL of each protein solution was filled into 6R vials under laminar airflow, sealed with rubber stoppers, and placed onto an HS 260 basic shaker (IKA®-Werke, Staufen, Germany).

Samples were subjected to reciprocal shaking at 200 rpm for 48 h. The protein solution did not come into contact with the stoppers. Each formulation was tested in eight replicates.

2.2.2 Particle Analysis

Subvisible particles were analyzed via light obscuration with a PAMAS SVSS particle counter (PAMAS Partikelmess- und Analysesysteme, Rutesheim, Germany) according to Ph. Eur. 2.9.19 guidelines. 0.3 mL of sample was used to pre-rinse, followed by three separate analyses using 0.4 mL of sample.

2.2.3 DLS

25 µL of mAb solutions between 1 and 6 mg/mL were analyzed in a 384 microwell plate (Corning, New York, United States) in triplicates at 25 °C using a DynaPro plate reader III (Wyatt Technology, Santa Barbara, USA) with 20 acquisitions of 5 s each. The interaction parameter k_D was derived from the concentration dependence of the protein mutual diffusion coefficient and then converted into the A_2 value using the TIM equation.[28]

3. Results and Discussion

The SVP formation of the three different mAbs upon agitation was dependent on both molecule and formulation (**Figure 1**). All control samples showed similarly low particle counts ≥ 1 µm below 1000/mL. mAb A formed the fewest particles in both formulations. At low ionic strength, fewer particles were observed at pH 5.5 compared to pH 7.0 for all three mAbs. Particle counts of mAb C were higher in the presence of NaCl — with the pH impact eliminated — likely due to charge shielding effects.[28–30] The CG MD simulations of controlled interfacial compression (**Figure 2**) corresponded to the experimental results. At low ionic strength, cluster formation was less pronounced at pH 5.5 compared to pH 7.0.

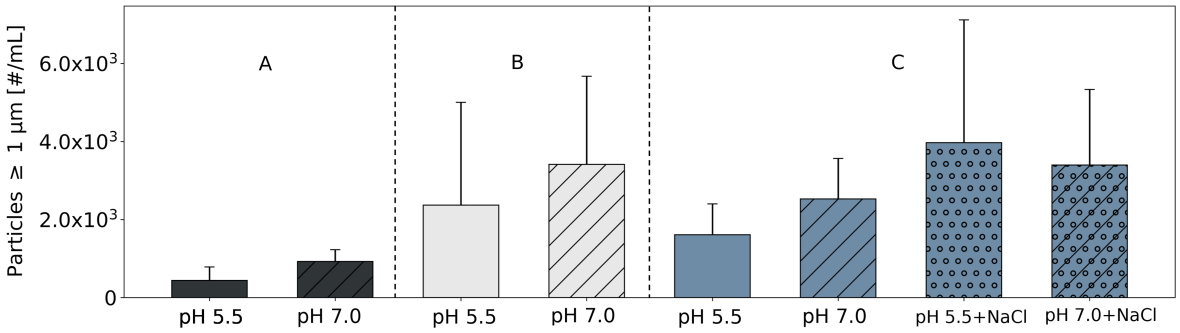

Figure 1: SVP formation of mAb A, B, and C in different formulations upon agitation.

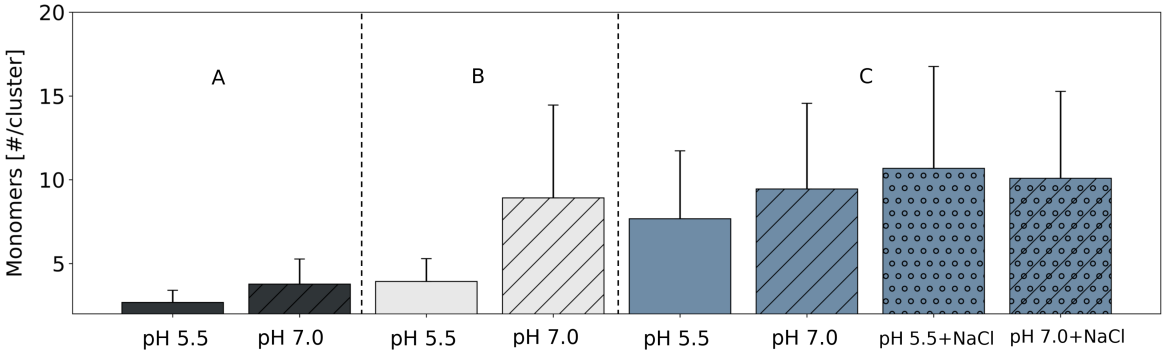

Figure 2: Cluster formation in CG MD simulations of mAb A, B, and C.

Overall, similar trends were observed in experiments and simulations. To evaluate the potential of MD as a predictor of aggregation propensity and enable direct comparison with experiments, we determined the Pearson correlation coefficient (r) between simulated cluster size and experimental particle count ≥ 1 µm (**Figure 3**). The r = 0.85 indicated adequate

correlation, similar to other MD studies assessing the aggregation propensity of mAbs in solution without an interface present.[15,16]

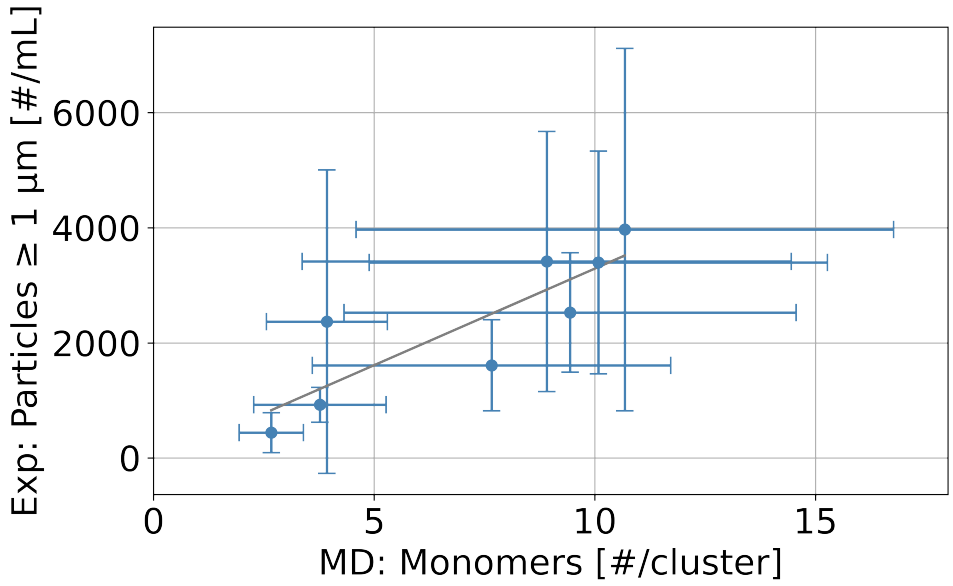

Figure 3: Correlation between number of monomers per cluster from MD simulations and experimental SVP formation with r = 0.85.

In addition to agitation studies, characterization of the mAb self-interaction by k_D and A_2 can be employed in early development.[9,31] To evaluate our MD protocol in comparison to this established approach, the A_2 values of the formulations were determined (**Table 1**).[28] mAb A showed positive A_2 values, indicating net repulsive interactions at the tested pH values. mAb C consistently showed negative A_2 values, suggesting net attractive interactions, and the behavior of mAb B switched between pH 5.5 and pH 7.0. In high ionic strength formulations of mAb C, attractive forces were partially screened, resulting in less negative A_2 values. Although the isoelectric point is around 8 to 9 for all mAbs, the total charge and charge distribution differs between mAb A, B, and C.

Table 1: A_2 values of mAb A, B, and C in the tested formulations.

Formulation	A_2 [10^{-5}·mol·mL/g^2]
A pH 5.5	13.1 ± 0.7
A pH 7.0	21.0 ± 1.3
B pH 5.5	7.1 ± 1.7
B pH 7.0	-3.4 ± 0.4
C pH 5.5	-19.3 ± 1.8
C pH 7.0	-16.7 ± 2.1
C pH 5.5 + NaCl	-8.1 ± 1.7
C pH 7.0 + NaCl	-9.8 ± 1.4

The experimental SVP formation was correlated with A_2, yielding a Pearson correlation coefficient of -0.56 (**Figure 4**). With a more negative A_2 value indicating stronger attractive interactions, the mAbs tend to show increased particle formation. The result is consistent with previous studies that achieved a Spearman correlation of 0.2 between the interaction parameter k_D and the SVP formation for different mAb formulations.[32] Other studies could only observe a qualitative relationship between A_2/k_D and the formation of high molecular weight species[33] or no relationship at all.[34] In contrast, our MD simulations achieved a correlation with an r-value of 0.85, demonstrating substantially higher predictive power for SVP formation than A_2.

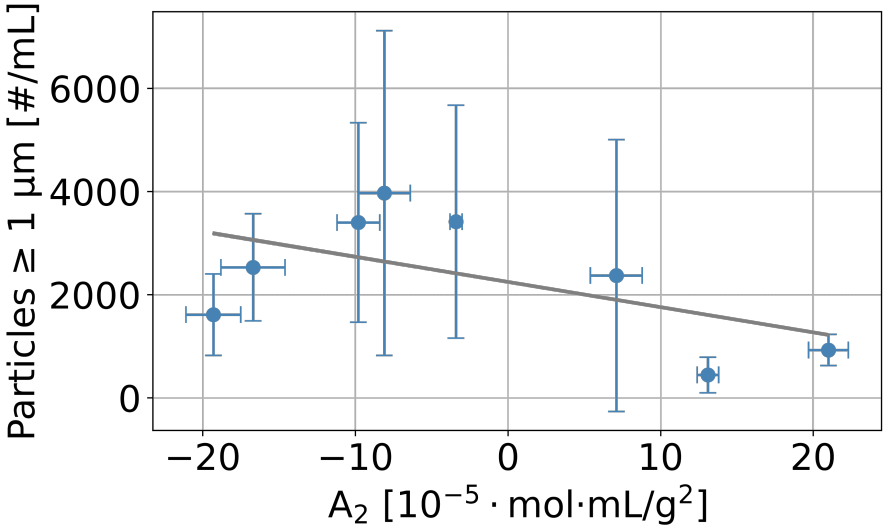

Figure 4: Correlation between experimental SVP formation and A_2 values with r = -0.56.

The better performance of the MD model can likely be attributed to its ability to, albeit in a simplified manner, represent the stress occurring at the air–liquid interface, including adsorption and compression. In contrast, A_2 measures the behavior of mAbs in a solution without an interface. Additionally, A_2 represents the net protein–protein interactions. These are, however, highly anisotropic due to the distinct shape and amino acid distribution of mAbs.[35,36] Both these properties can be depicted in our CG MD model. Others suggested that protein unfolding can cause poor correlation between A_2 and aggregation.[33] Our MD model does not account for conformational changes yet correlates well with experimental particle formation.

4. Conclusions

In this study, we present a CG MD protocol to estimate the aggregation propensity of mAbs in different formulations. Previous work in this field was often limited to a single mAb or formulation, or relied on more complex multi-parameter readouts. Our approach directly mimics the physical stress of agitation by simulating controlled interfacial adsorption and compression, using the average cluster size as a single readout parameter. Simulations showed a strong correlation with experimental subvisible particle formation observed in agitation stress studies. The correlation surpassed that of the second osmotic virial coefficient A_2, an established biophysical method assessing the colloidal stability of mAb formulations. We attribute the superior performance of our MD model to its ability to directly replicate the underlying stress mechanism and account for the anisotropic nature of protein–protein interactions. Our findings establish this MD protocol as a simple and material-free tool for assessing the aggregation propensity of mAbs in early-stage development. Additional validation across a broader range of mAbs and formulations, as well as against accelerated stability studies, is advised.

5. Acknowledgments

The authors gratefully acknowledge the Gauss Centre for Supercomputing e.V. (www.gauss-centre.eu) for funding this project by providing computing time on the GCS Supercomputer SuperMUC at Leibniz Supercomputing Centre (www.lrz.de). We further thank Jonas Binder for his support in implementing the forcefield.

6. References

(1) Chan, A. C.; Martyn, G. D.; Carter, P. J. Fifty Years of Monoclonals: The Past, Present and Future of Antibody Therapeutics. *Nat. Rev. Immunol.* **2025**, 1–21.

(2) Li, J.; Krause, M. E.; Chen, X.; Cheng, Y.; Dai, W.; Hill, J. J.; Huang, M.; Jordan, S.; LaCasse, D.; Narhi, L.; Shalaev, E.; Shieh, I. C.; Thomas, J. C.; Tu, R.; Zheng, S.; Zhu, L. Interfacial Stress in the Development of Biologics: Fundamental Understanding, Current Practice, and Future Perspective. *Aaps J* **2019**, *21* (3), 44.

(3) Joubert, M. K.; Luo, Q.; Nashed-Samuel, Y.; Wypych, J.; Narhi, L. O. Classification and Characterization of Therapeutic Antibody Aggregates. *J. Biol. Chem.* **2011**, *286* (28), 25118–25133.

(4) Arakawa, T.; Prestrelski, S. J.; Kenney, W. C.; Carpenter, J. F. Factors Affecting Short-Term and Long-Term Stabilities of Proteins. *Adv. Drug Deliv. Rev.* **2001**, *46* (1–3), 307–326.

(5) Bee, J. S.; Schwartz, D. K.; Trabelsi, S.; Freund, E.; Stevenson, J. L.; Carpenter, J. F.; Randolph, T. W. Production of Particles of Therapeutic Proteins at the Air–Water Interface during Compression/Dilation Cycles. *Soft Matter* **2012**, *8* (40), 10329–10335.

(6) Koepf, E.; Eisele, S.; Schroeder, R.; Brezesinski, G.; Friess, W. Notorious but Not Understood: How Liquid-Air Interfacial Stress Triggers Protein Aggregation. *Int. J. Pharmaceut.* **2018**, *537* (1–2), 202–212.

(7) Rosenberg, A. S. Effects of Protein Aggregates: An Immunologic Perspective. *AAPS J.* **2006**, *8* (3), E501–E507.

(8) Carpenter, J. F.; Randolph, T. W.; Jiskoot, W.; Crommelin, D. J. A.; Middaugh, C. R.; Winter, G.; Fan, Y.-X.; Kirshner, S.; Verthelyi, D.; Kozlowski, S.; Clouse, K. A.; Swann, P. G.; Rosenberg, A.; Cherney, B. Overlooking Subvisible Particles in Therapeutic Protein Products: Gaps That May Compromise Product Quality. *J. Pharm. Sci.* **2009**, *98* (4), 1201–1205.

(9) Jarasch, A.; Koll, H.; Regula, J. T.; Bader, M.; Papadimitriou, A.; Kettenberger, H. Developability Assessment During the Selection of Novel Therapeutic Antibodies. *J. Pharm. Sci.* **2015**, *104* (6), 1885–1898.

(10) Chi, E. Y.; Krishnan, S.; Randolph, T. W.; Carpenter, J. F. Physical Stability of Proteins in Aqueous Solution: Mechanism and Driving Forces in Nonnative Protein Aggregation. *Pharm. Res.* **2003**, *20* (9), 1325–1336.

(11) Geng, S. B.; Cheung, J. K.; Narasimhan, C.; Shameem, M.; Tessier, P. M. Improving Monoclonal Antibody Selection and Engineering Using Measurements of Colloidal Protein Interactions. *J. Pharm. Sci.* **2014**, *103* (11), 3356–3363.

(12) Conchillo-Solé, O.; Groot, N. S. de; Avilés, F. X.; Vendrell, J.; Daura, X.; Ventura, S. AGGRESCAN: A Server for the Prediction and Evaluation of "Hot Spots" of Aggregation in Polypeptides. *BMC Bioinform.* **2007**, *8* (1), 65.

(13) Fernandez-Escamilla, A.-M.; Rousseau, F.; Schymkowitz, J.; Serrano, L. Prediction of Sequence-Dependent and Mutational Effects on the Aggregation of Peptides and Proteins. *Nat. Biotechnol.* **2004**, *22* (10), 1302–1306.

(14) Sankar, K.; Krystek, S. R.; Carl, S. M.; Day, T.; Maier, J. K. X. AggScore: Prediction of Aggregation-prone Regions in Proteins Based on the Distribution of Surface Patches. *Proteins: Struct., Funct., Bioinform.* **2018**, *86* (11), 1147–1156.

(15) Lai, P.-K.; Fernando, A.; Cloutier, T. K.; Kingsbury, J. S.; Gokarn, Y.; Halloran, K. T.; Calero-Rubio, C.; Trout, B. L. Machine Learning Feature Selection for Predicting High Concentration Therapeutic Antibody Aggregation. *J. Pharm. Sci.* **2021**, *110* (4), 1583–1591.

(16) Wang, Y.; Williams, H. D.; Dikicioglu, D.; Dalby, P. A. Predictive Model Building for Aggregation Kinetics Based on Molecular Dynamics Simulations of an Antibody Fragment. *Mol. Pharm.* **2024**, *21* (11), 5827–5841.

(17) Simone, A. D.; Kitchen, C.; Kwan, A. H.; Sunde, M.; Dobson, C. M.; Frenkel, D. Intrinsic Disorder Modulates Protein Self-Assembly and Aggregation. *Proc. Natl. Acad. Sci.* **2012**, *109* (18), 6951–6956.

(18) Spoel, D. V. D.; Lindahl, E.; Hess, B.; Groenhof, G.; Mark, A. E.; Berendsen, H. J. C. GROMACS: Fast, Flexible, and Free. *J. Comput. Chem.* **2005**, *26* (16), 1701–1718.

(19) Abraham, M. J.; Murtola, T.; Schulz, R.; Páll, S.; Smith, J. C.; Hess, B.; Lindahl, E. GROMACS: High Performance Molecular Simulations through Multi-Level Parallelism from Laptops to Supercomputers. *SoftwareX* **2015**, *1*, 19–25.

(20) Lindahl, E.; Hess, B.; Spoel, D. van der. GROMACS 3.0: A Package for Molecular Simulation and Trajectory Analysis. *Mol. Model. Annu.* **2001**, *7* (8), 306–317.

(21) Binder, J.; Friess, W. *To Be Submitted*. **2025**.

(22) Essmann, U.; Perera, L.; Berkowitz, M. L.; Darden, T.; Lee, H.; Pedersen, L. G. A Smooth Particle Mesh Ewald Method. *J. Chem. Phys.* **1995**, *103* (19), 8577–8593.

(23) Darden, T.; York, D.; Pedersen, L. Particle Mesh Ewald: An N ·log(N) Method for Ewald Sums in Large Systems. *J. Chem. Phys.* **1993**, *98* (12), 10089–10092.

(24) Baoukina, S.; Monticelli, L.; Risselada, H. J.; Marrink, S. J.; Tieleman, D. P. The Molecular Mechanism of Lipid Monolayer Collapse. *Proc. National. Acad. Sci.* **2008**, *105* (31), 10803–10808.

(25) Nielsen, S. O.; Lopez, C. F.; Moore, P. B.; Shelley, J. C.; Klein, M. L. Molecular Dynamics Investigations of Lipid Langmuir Monolayers Using a Coarse-Grain Model. *J. Phys. Chem. B* **2003**, *107* (50), 13911–13917.

(26) Wizert, A.; Iskander, D. R.; Cwiklik, L. Interaction of Lysozyme with a Tear Film Lipid Layer Model: A Molecular Dynamics Simulation Study. *Biochimica Et Biophysica Acta Bba – Biomembr.* **2017**, *1859* (12), 2289–2296.

(27) Souza, P. C. T.; Alessandri, R.; Barnoud, J.; Thallmair, S.; Faustino, I.; Grünewald, F.; Patmanidis, I.; Abdizadeh, H.; Bruininks, B. M. H.; Wassenaar, T. A.; Kroon, P. C.; Melcr, J.; Nieto, V.; Corradi, V.; Khan, H. M.; Domański, J.; Javanainen, M.; Martinez-Seara, H.; Reuter, N.; Best, R. B.; Vattulainen, I.; Monticelli, L.; Periole, X.; Tieleman, D. P.; Vries, A. H. de; Marrink, S. J. Martini 3: A General Purpose Force Field for Coarse-Grained Molecular Dynamics. *Nat. Methods* **2021**, *18* (4), 382–388.

(28) Menzen, T.; Friess, W. Temperature-Ramped Studies on the Aggregation, Unfolding, and Interaction of a Therapeutic Monoclonal Antibody. *J. Pharm. Sci.* **2014**, *103* (2), 445–455.

(29) Chou, D. K.; Krishnamurthy, R.; Manning, M. C.; Randolph, T. W.; Carpenter, J. F. Physical Stability of Albinterferon-α2b in Aqueous Solution: Effects of Conformational Stability and Colloidal Stability on Aggregation. *J. Pharm. Sci.* **2012**, *101* (8), 2702–2719.

(30) Zhang, F.; Skoda, M. W. A.; Jacobs, R. M. J.; Martin, R. A.; Martin, C. M.; Schreiber, F. Protein Interactions Studied by SAXS: Effect of Ionic Strength and Protein Concentration for BSA in Aqueous Solutions. *J. Phys. Chem. B* **2007**, *111* (1), 251–259.

(31) Willis, L. F.; Kapur, N.; Radford, S. E.; Brockwell, D. J. Biophysical Analysis of Therapeutic Antibodies in the Early Development Pipeline. *Biol.: Targets Ther.* **2024**, *18* (0), 413–432.

(32) Svilenov, H. L.; Kulakova, A.; Zalar, M.; Golovanov, A. P.; Harris, P.; Winter, G. Orthogonal Techniques to Study the Effect of pH, Sucrose, and Arginine Salts on Monoclonal Antibody Physical Stability and Aggregation During Long-Term Storage. *J. Pharm. Sci.* **2020**, *109* (1), 584–594.

(33) Saito, S.; Hasegawa, J.; Kobayashi, N.; Kishi, N.; Uchiyama, S.; Fukui, K. Behavior of Monoclonal Antibodies: Relation Between the Second Virial Coefficient (B2) at Low Concentrations and Aggregation Propensity and Viscosity at High Concentrations. *Pharm. Res.* **2012**, *29* (2), 397–410.

(34) He, F.; Woods, C. E.; Becker, G. W.; Narhi, L. O.; Razinkov, V. I. High-throughput Assessment of Thermal and Colloidal Stability Parameters for Monoclonal Antibody Formulations. *J. Pharm. Sci.* **2011**, *100* (12), 5126–5141.

(35) Lewus, R. A.; Levy, N. E.; Lenhoff, A. M.; Sandler, S. I. A Comparative Study of Monoclonal Antibodies. 1. Phase Behavior and Protein–Protein Interactions. *Biotechnol. Prog.* **2015**, *31* (1), 268–276.

(36) Arzenšek, D.; Kuzman, D.; Podgornik, R. Hofmeister Effects in Monoclonal Antibody Solution Interactions. *J. Phys. Chem. B* **2015**, *119* (33), 10375–10389.

Chapter VII: Summary

Protein solutions come in contact with various compressible interfaces such as the silicone tubing–liquid interface (SLI) during pumping or the air–liquid interface (ALI) upon vial shaking. This leads to protein aggregation, impairing product integrity. Yet, the underlying mechanisms remain unclear. The aim of this thesis was to gain molecular–level understanding of the impact of process and formulation parameters on the mechanism of protein aggregation at the compressible SLI and ALI by combining coarse-grained molecular dynamics (MD) simulations with experiments.

Therefore, in **Chapter III**, an MD setup was developed to elucidate the mechanism of protein aggregation at the SLI and to lay the groundwork for future studies. This model incorporated realistic representations of human growth hormone (hGH) molecules and a silicone interface and was verified by an experimental setup allowing for controlled, isolated interfacial stress. Increasing compression factors led to higher interfacial aggregation in the model as well as in experiments. Similar plateau formation in both simulations and experiments was observed. Compression speed did not affect the aggregation behavior of a protein film that has already been formed, but rather its replenishment. As formed clusters break up again during relaxation, particles in the bulk solution originate from interfacial detachment in the compressed state. High compression results in a lower monomer content in the bulk solution, showing that the observations at the interface also translate into the bulk phase.

The exact effect of formulation parameters on particle formation at the same type of interface was studied in **Chapter IV**. Our model was first improved to provide a more accurate representation of protein molecules at tubing. The combination of our MD results for hGH at different pH values with experimental data indicated that pH, and thereby protein self-interaction, affects both aggregate formation directly at the interface and aggregate transfer into the bulk, but not the amount of protein adsorbed to the interface. A high ionic strength formulation indicated that, when protein self-interaction is similar, the amount of protein molecules adsorbed to the interface becomes key for protein particle formation. These findings were verified across different low-molecular-weight proteins.

In **Chapter V**, our MD model was extended to the compressible ALI, representing protein solution in a vial during shaking. Well-defined compression and decompression conditions in experiments and simulations allowed for a direct comparison of the protein aggregation

mechanisms at the SLI and the ALI. At the ALI, protein molecules show weaker binding, higher mobility, and faster exchange with bulk molecules than at the SLI. At the SLI, strong interface–protein interactions induce protein particle formation already at little compression, leading to larger particles. In contrast, more compression is needed for particle formation at the ALI, and smaller particles form at this interface. Clusters at the SLI break up during relaxation, whereas clusters at the ALI persist. Faster compression and repulsive PPI lead to lower particle formation at the ALI. At the SLI, protein aggregation is less affected by these factors.

In **Chapter VI,** our simulations were adapted to the highly relevant biopharmaceutical class of monoclonal antibodies. Using a single readout parameter, MD simulations correlated well with particle formation upon agitation stress. The correlation exceeded that of particle formation and the second osmotic virial coefficient, an indicator of colloidal stability. This demonstrates that our MD protocol provides a straightforward approach for assessing the aggregation propensity of mAbs in different formulations *in silico*.

In summary, MD models to reflect the proposed mechanism of protein particle formation at compressible silicone–liquid and air–liquid interfaces were developed and verified by well-controlled interfacial-stress experiments, thereby allowing us to dissect the influence of individual factors on protein aggregation. Our combined approach provides insights into the mechanism of interfacial protein aggregation on a molecular level, thus providing a basis for improving biopharmaceutical process and formulation development.